Evaluation of pyrochemistry in molten salts for recycling Li-ion batteries

Patricia Nathaly Ruiz Onofre

Sorbonne Université

Ecole doctorale de Chimie Physique et Chimie Analytique de Paris Centre

Laboratoire PHENIX / Equipe Electrochimie et Liquides Ioniques

Evaluation of pyrochemical method for the recycling of Li-ion batteries

Présentée Par Patricia Nathaly Ruiz Onofre

Thèse de doctorat de Chimie-Physique

Dirigée par Dr. Anne-Laure Rollet

Présentée et soutenue publiquement le 1 octobre 2019

Devant un jury composé de :

M. Pierre Chamelot	Professeur, Université Paul Sabatier, Toulouse III	Rapporteur
M. Alexandre Chagnes	Professeur, Université de Lorraine	Rapporteur
Mme. Laurence Croguennec	Directrice de Recherche, Université de Bordeaux	Examinatrice
Mme. Delphine Vantelon	Responsable de ligne, Synchrotron SOLEIL	Examinatrice
M. Hubert Perrot	Directeur de Recherche, Sorbonne Université	Examinateur
Mme. Anne-Laure Rollet	Chargée de Recherche, Sorbonne Université	Directrice de thèse
Mme. Virginie Lair	Maitre de Conférences, Chimie Paristech	Co-Encadrante

“El mundo está en manos de aquellos que tienen el coraje de soñar y de correr el riesgo de vivir sus sueños”

Paulo Coelho

‘El Alquimista’

A ma famille, Alexis et mes amis

En mémoire de mon oncle et de ma grand-mère Jaime et Marujita

Remerciements

Je remercie MM. Pierre Chamelot et Alexandre Chagnes pour m'avoir fait l'honneur de rapporter ce présent manuscrit ainsi que l'ensemble des membres du jury.

Ces travaux ont été réalisés au sein du laboratoire PHENIX et de l'Institut de Recherche de Chimie Paris - IRCP. Je remercie MM. Pierre Levitz et Laurent Michot (ancien et actuel directeur du laboratoire PHENIX- UMR 8234), ainsi que M. Michel Mortier (directeur de l'IRCP UMR 8247), qui m'ont accueillie et ont permis la concrétisation de mes recherches pendant ces trois années.

Je tiens également à remercier ma directrice de thèse Mme Anne-Laure Rollet ainsi que tous mes encadrants : Mmes. Virginie Lair et Denise Krulic et MM. Damien Dambournet et Michel Cassir. Chacun, avec ses compétences et ses expertises dans des domaines respectifs, a permis la réalisation de cette étude. La multiplicité d'idées a représenté un réel défi pour aboutir à un seul et unique manuscrit, et nous sommes parvenus ensemble à finaliser cette thèse. J'en tire une grande fierté.

Je remercie aussi toute l'équipe ELI pour son accueil :

MM. Fréderic Lantelme et Nicolas Faturros pour leurs conseils et leur participation active à ce projet. Mme. Sandrine Leclerc de s'être assurée au quotidien que je dispose du nécessaire dans mon espace de travail. Mme. Ana Gabriela Porras pour son aide au cours de mes deux premières années de thèse.

Je voudrais adresser un remerciement spécial à M. François Dardoize pour tous ses encouragements, conseils et idées tout au long de cette thèse et également un immense merci à M. Didier Devilliers pour avoir été un mentor scientifique très présent tout au long de ces trois ans et pour sa précieuse aide en électrochimie.

Un grand merci également à tous les non permanents qui ont participé à ce projet : Arturo Melendez Ceballos (post-doc) et Gabriele Miranda (stagiaire) pour leur implication dans l'étude de composés organiques de batteries présentée dans cette thèse, ainsi qu'aux étudiantes Natacha Wonneberg, Agnieszka Dynowska et Zohreh Safarzadeh Kermani.

Une thèse en sels fondus à haute température est un défi où les contraintes techniques sont présentes au quotidien. Cette entreprise difficile a été rendue possible grâce à la précieuse aide de « bricoleurs » du laboratoire, de l'atelier de verre et du Synchrotron SOLEIL. C'est ainsi que je remercie M. Jean Chevalet et Mme Flori Lopis pour toute leur aide dans la soudure, la réparation, la mise en forme des matériaux et leur bonne humeur toujours présente. Je remercie de manière spéciale M. José Gomes ainsi que Mme Anne-Laure Rollet et toute l'équipe de la ligne ROCK du Synchrotron SOLEIL pour leur implication dans le développement de la cellule présentée dans ce manuscrit. Je ne remercierai jamais assez Mme. Valerie Briois et M. Laurent Barthe pour leur disponibilité et leur dynamisme lors du créneau des mesures à SOLEIL.

La logistique de cette thèse a été faite avec beaucoup d'efficacité grâce à Mmes. Lise Michelot, Brigitte Carrez, Stéphanie Grison et M. Gérard Guillard : un grand merci. Je tiens aussi à citer et à adresser mes vifs remerciements à toutes les personnes qui m'ont permis de mener à bien les multiples caractérisations au cours de cette thèse : Mme. Delphine Talbot, Mme. Aude Michel Tourgis, M. Mohamed Selmane et M. David Montero.

Cette aventure a été marquée de formidables rencontres qui se sont transformées en amitiés profondes. Parmi ces personnes j'ai une pensée spéciale pour Nadia, Lisbeth, Chérazade, Etienne, Kyle, Anastasia et Seongkoo qui ont été là pour me soutenir au jour au jour, surtout dans la période la plus difficile de cette aventure qu'est la rédaction.

Je porte une pensée douce pour toutes les personnes qui m'ont soutenue depuis le début de ma vie : mes parents, ma sœur et mon frère. De plus, une immense reconnaissance à toi, Alexis pour marcher avec moi tout au long de cette aventure et pour ton inconditionnel soutien surtout pendant la rédaction de ce manuscrit. Et enfin, j'adresse un grand merci à tous mes amis pour leurs encouragements indéfectibles et en particulier à : Sophie, Jacques, Christine, Rodolphe, Guillaume, Johanna, Jessica, Julien et Caterina.

Je termine ces remerciements par une pensée pour tous ceux qui sont encore en chemin vers l'obtention de ce diplôme. Sachez que, comme disait Nelson Mandela, *« Cela paraît impossible jusqu'à ce que ce soit fait ».*

Summary

General introduction

The end of the 20th and the beginning of the 21st century have been marked by very significant technological innovations specially in communications and energy fields.

In fact, a digital revolution or third industrial revolution has quickly changed our society with the public access of the internet, the apparition of cell phones, tablets, among others.

Moreover, the continuous increase of global warming produced by the emission of greenhouse gases is one of the biggest concerns of our societies nowadays. The 21st Conference of the Parties (COP21) leads to the adoption of the Paris agreement, which engaged the different nations to reduce their gas emissions and hold the increase of global average temperature below 2°C[a]. As a consequence, investments in the development of renewable energies as alternative to accelerate the decarbonization of energy production and transports are rising.

The energy storage is a crucial aspect for the improvements of the digital revolution and the energetic transition. As a consequence, different energy storage systems have been developed according to the applications, especially Li-ion batteries in the last years. In this way, they have become part of our daily lives. Every year, there is a growth of their production, especially since 2004[b,c] . This trend is expected to continue in the future. Nevertheless, some of the materials present in this kind of batteries are distributed in an inhomogeneous way in the planet and they come from limited resources. Recycling appears as an alternative to face the future shortage of these materials and contributes to the reduction of wastes. Recycling can play an essential role in the lessening of the environmental impacts related to batteries production and disposal at the end of their life [d].

---

[a] https://unfccc.int/process-and-meetings/conferences/past-conferences/paris-climate-change-conference-november-2015/cop-21(consulted in July 2019)

[b] Report ALBERMARLE. *Global Lithium Market Outlook*; 2016

[c] Report Avicenne Energy. *Lithium-Ion Battery Raw Material Supply and Demand 2017-2025*; 2018

[d] Gaines, L.; Richa, K.; Spangenberger, J. Key Issues for Li-Ion Battery Recycling. *MRS Energy Sustain.* 2018, *5*, 1–14. https://doi.org/10.1557/mre.2018.13.

Different methods have been developed for recycling batteries. Hydrometallurgy and pyrometallurgy are the most widely used in industry. They are very efficient for metals recycling. Nevertheless, these methods do not valorize the organic compounds from batteries. Organic compounds are most of the times burned and the volatized products are usually harmful gases and compounds. An important budget must always be planned for the gas treatment [d].

The portion of organic compounds in a battery is significant. For example, a Li-ion battery is constituted of about 15% organic chemicals and 7% plastics, varying slightly with different manufacturers [e]. This statement justifies the need to develop other new methods for recycling, enabling the valorization of both kind of compounds in one system. In this regard, molten salts systems are promising candidates. In fact, this kind of solvents are widely applied as solvents for different metals recovery and manufacturing by electrolysis such as: aluminum, magnesium, sodium, molybdenum, tungsten, niobium, among others [f,g,h,i,j].

Furthermore, some molten salts systems have the capacity of trapping and/or decomposing hazardous organic compounds [k]. This can be an advantage for lessening all the gas treatment processed after the recycling of batteries. Phenix laboratory is historically known for its research in molten salts. Nevertheless, the research on this project started in Phenix Laboratory with this thesis work. We chose to focalize ourselves in Li-ion batteries recycling and especially in cobalt recovery.

---

[e] Al Hossaini Shuva, M.; Kurny, A. S. W. Hydrometallurgical Recovery of Value Metals from Spent Lithium Ion Batteries. *Am. J. Mater. Eng. Technol.* 2013, *1* (1), 8–12.

[f] Beck, T. R. Hall and Héroult and the Discovery of Aluminum Electrolysis. *Electrochem Soc. Interface* 2014, *23* (2), 36–37

[g] Wulandari, W.; Brooks, G.; Rhamdhani, M.; Monaghan, B. Magnesium: Current and Alternative Production Routes. In *Chemeca 2010: Australasian Conference on Chemical Engineering*; 2010.

[h] Dandapani, K. S.; Srinivasan, L. K. Production of Magnesium in 30 A Cells. *Electrometall. Thermics* **1987**, *3* (2), 127–129.

[i] Senderoff, S.; Mellors, G. W. Coherent Coatings of Refractory Metals. *Science (80-.).* **1966**, *153* (3743), 1475–1481.

[j] Sethi, R. S. Electrocoating from Molten Salts. *J. Appl. Electrochem.* **1979**, *9*, 411–426.

[k] Alam, M.; Kamath, S. Cyanide Destruction in Molten Carbonate Bath: Melt and Gas Analyses. *Environ. Sci Technol.* **1998**, *32*, 3986–3992.

This manuscript is divided in four chapters:

The first chapter provides a bibliographic overview of Li-ion batteries recycling and the existing challenges inherent to it. First, generalities and fundamental notions about batteries and their recycling will be introduced. In a second place, molten salts generalities will be presented as well as their principal properties and applications. Especial attention will be paid to the properties of the molten salt families chosen for this study. Finally, the strategy for this research project will be presented to conclude this chapter.

The second chapter is dedicated to the study of cobalt speciation in molten salts by X-ray absorption spectroscopy (XAS). Fundamental notions about this technique will be presented in a first place. The conception of an adapted device for XAS measurements at high temperatures in molten salt systems is then discussed. Cobalt average oxidation state and its speciation as function of temperature will be finally presented.

The third chapter is dedicated to the study of electrochemical behavior of cathode materials from Li-ion batteries in molten carbonates. The dissolution of cobalt from these compounds will be characterized in this molten medium. The results regarding the possibility of recovering metallic cobalt of these cathodes by electrochemical means will be discussed. Finally, preliminary results of the behavior of organic Li-ion battery compounds will be described.

The fourth and last chapter is focused on the study of cathode material $LiCoO_2$ in molten chlorides. The results of the dissolution of cobalt from this material in this medium will be discussed. Then in a second place, the influence of additives on the dissolution will be described. Results will bring new insights on the best protocol to be used to have the optimal results. Finally, evidences of cobalt recovery from cathode materials by electrochemical means will be shown.

Finally, this manuscript will be closed by general conclusions and perspectives of this research.

Chapter I: State of art

"Dans la vie, rien n'est à craindre,
tout est à comprendre."

Marie Curie

1. Introduction

To understand the inherent importance of batteries recycling research and development, it is important to put into perspective the existing developments done until now. Furthermore, it is essential to take into account the economical, societal and environmental issues, which are currently in evolution due to the development of new technologies using these devices. To do it, the basic concepts of batteries, sales projections and recycling are explained and applied to Li-ion battery recycling in molten salts.

2. Batteries generalities

A battery can be defined as a device that is composed of an electrochemical cell or series of electrochemical cells which can convert chemical energy into electrical energy. Each cell is constituted of a positive electrode (cathode), a negative electrode (anode), the electrolyte and a separator.

There are two types of batteries: the primary or non-rechargeable and the secondary or rechargeable batteries. According to their chemistry, four main types of secondary batteries can be distinguished: nickel-cadmium (Ni-Cd), nickel-metal hydride (Ni-MH), lead-acid and Li-ion (Li-ion) batteries. The purpose of our study concerns this last one, so from now on all the attention will be focused only into Li-ion batteries.

2.1. Working principle

As the other batteries, Li-ion ones can convert chemical energy into electrical energy thanks to redox (reduction-oxidation) reactions that take place at both electrodes simultaneously. For secondary batteries, redox reactions should be reversible (with rapid kinetics) and take place several times. By contrast, primary batteries are used only once and their redox reactions are irreversible. Figure 1 shows the functioning of a classical Li-ion battery. In this particular case, the positive electrode is constituted by a lithiated cobalt oxide $LiCoO_2$ and the negative one by graphite. As both electrode constituents are intercalation materials, Li-ion battery operates by a reversible transport of lithium ions from one electrode to the other.

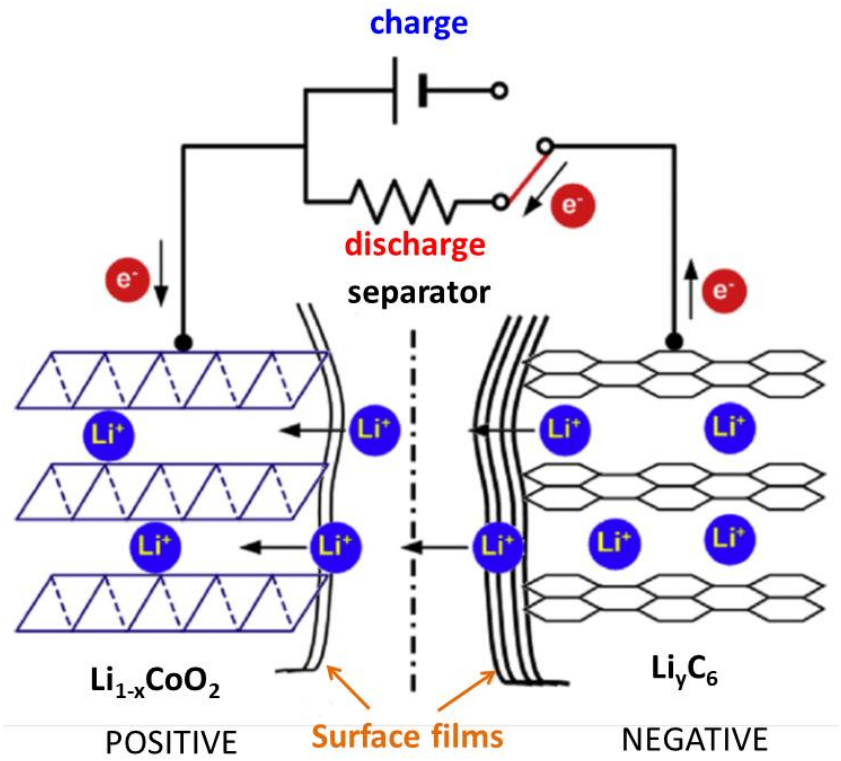

Figure 1 : Scheme of the Li-ion battery functioning, discharge mode [1]

As observed in Figure 1, during the discharge there is a disinsertion of lithium ions from the negative electrode, which works as a hosting structure, to the positive electrode. During this process, electrons are also transferred from the negative electrode to the positive one through an external circuit. This reaction happens spontaneously without any energy supply as its free enthalpy is negative ($\Delta G < 0$). The redox reactions taking place at the electrodes during the discharge is given by the following equations (Eq. 1) and (Eq. 2):

At the negative electrode the oxidation reaction:

$$Li_xC_6 \rightarrow C + xLi^+ + xe^- \qquad \text{(Eq. 1)}$$

At the positive electrode the reduction reaction:

$$Li_{1-x}CoO_2 + xLi^+ + xe^- \rightarrow LiCoO_2 \qquad \text{(Eq. 2)}$$

By contrast during the charge an energy supply is needed, in form of current. This current is provided by an external generator and enables the reverse phenomena to take place, which means the disinsertion of lithium ions at the positive electrode and their insertion at the

negative one. As a consequence, the total equation for the system during charge and discharge process is the following (Eq. 3):

$$Li_xC_6 + Li_{1-x}CoO_2 \leftrightarrow C + LiCoO_2 \quad \text{(Eq. 3)}$$

Once the functioning of the Li-ion battery is discussed, a review of the elements will be presented in the next section.

2.2. The Li-ion battery elements

As it was mentioned before, each electrochemical cell is constituted by four principal components: cathode, anode, electrolyte and separator. The whole battery is protected by a metal casing, covering plastic and electronic control unit[2].

2.2.1. The cathode

The cathode is a composite material deposited on a current collector. An active material, a conductive agent and a binder constitute this composite. The binder is a polymer material that ensures the mechanical resistance of the electrode. The electrons conductivity through the electrode is ensured by a conductive agent. Usually polyvinylidene fluoride (PVDF) is used as binder and black carbon as conductive agent respectively[3,4]. The active material is usually an inorganic oxide compound containing intercalated lithium[3]. There is diversity in the composition of lithium metal oxides materials. The most important in the present market are presented in Figure 2, showing five different lithium oxides: $LiCoO_2$ (LCO), $LiNi_{1/3}Mn_{1/3}Co_{1/3}O_2$ (NMC), $LiNi_{0.8}Co_{0.15}Al_{0.05}O_2$ (NCA), $LiMn_2O_4$ (LMO) and $LiFePO_4$ (LFP). NMC can present several forms according to its composition. There are 3 compositions nowadays in the market: NMC 111, NMC 532, NMC 622 and NMC 811[5]. Table 1 shows in the detail the corresponding transition metals molar composition of each material cathode.

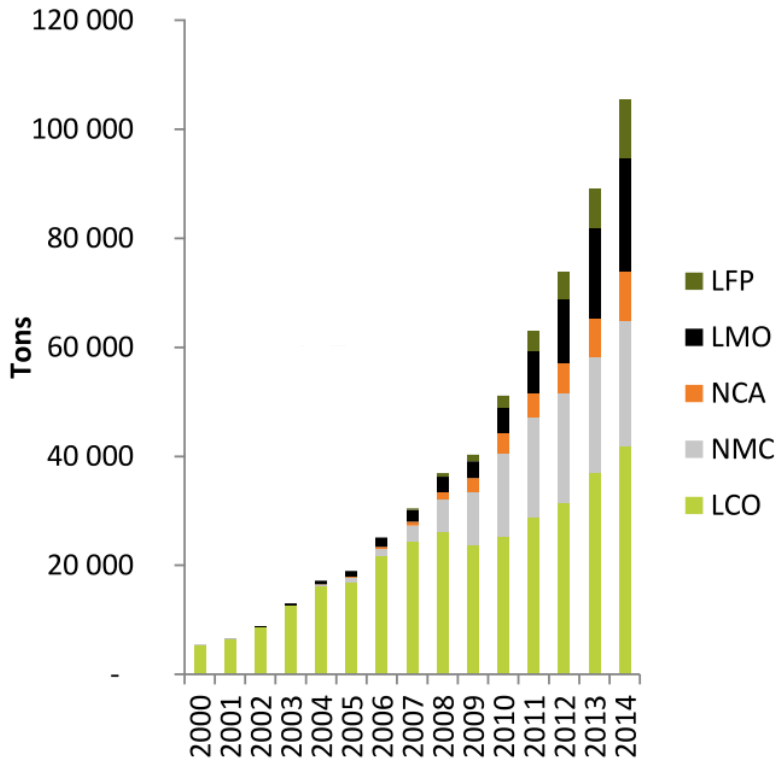

Figure 2 : Li-ion batteries cathode materials demand evolution between 2000 and 2014[6]

Table 1 : Li-ion battery cathode materials composition

Cathode material	Transition metals molar composition	Cobalt molar percentage
LCO	100% Co	100% Co
NCA	80% Ni, 15% Co, 5% Al	15% Co
NMC 111	33.3% Ni, 33.3% Mn, 33.3%Co	33.3% Co
NMC 532	50% Ni, 30% Mn, 20% Co	20% Co
NMC 622	60% Ni, 20% Mn, 20% Co	20% Co
NMC 811	80% Ni, 10% Mn, 10% Co	10% Co
LMO	100% Mn	0% Co
LFP	100% Fe	0% Co

Each material shows advantages and drawbacks, as shown in Figure 3, which can be more or less important according to the application. As observed in Figure 3, LCO shows a good energy density and a low cost. Nevertheless, the high concentration of cobalt makes it an unsuitable candidate for big sizes batteries. NMC shows a higher performance and a lower concentration in cobalt than LCO, and it has a fairly low cost. For these reasons, it is used in electric vehicles and other applications.

In the same way, NCA shows the same advantages as NMC compared to LCO which leads to its use in portable electronics and electric vehicles. In what concerns LMO, it shows a

high safety but a low energy density and high cost compared to other cathode materials. For these reasons, it is no longer used in electric vehicles. Finally, LFP has the advantage of being the safest electrode material on the market and has a high energy density. Nevertheless, it is quite expensive compared to other cathode materials. It is used frequently in electric tools, electric vehicles and buses.

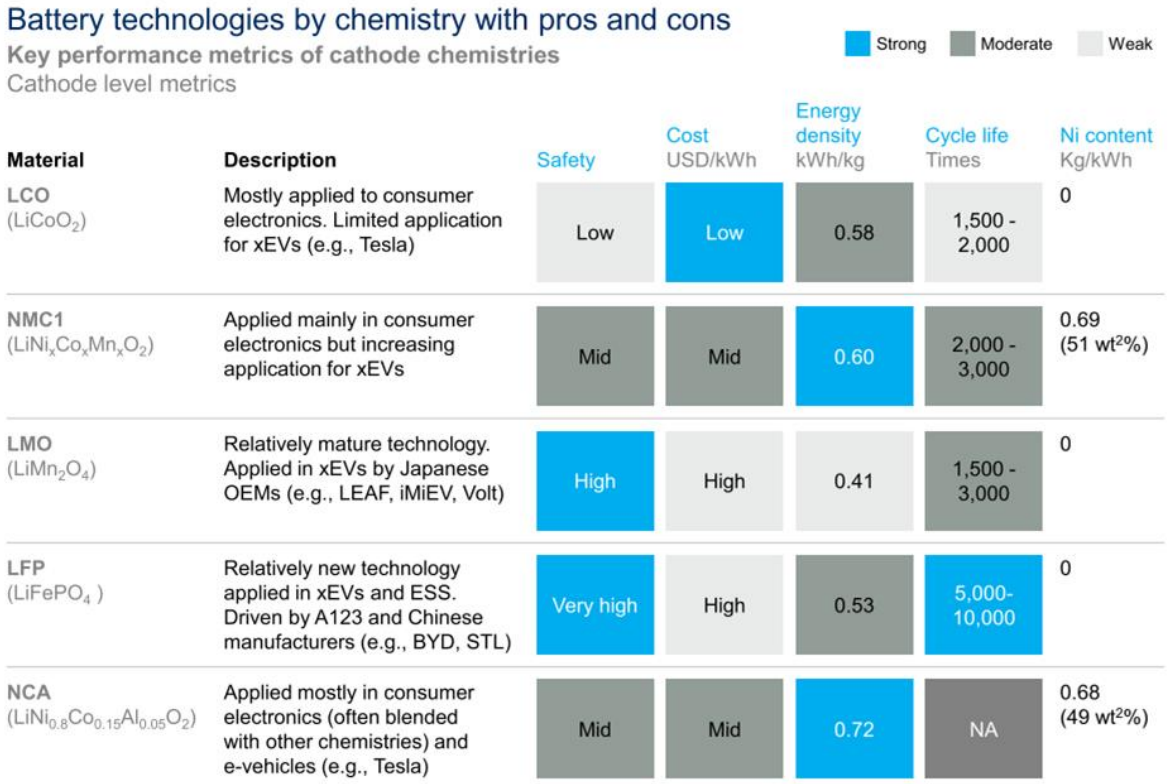

Material	Description	Safety	Cost USD/kWh	Energy density kWh/kg	Cycle life Times	Ni content Kg/kWh
LCO ($LiCoO_2$)	Mostly applied to consumer electronics. Limited application for xEVs (e.g., Tesla)	Low	Low	0.58	1,500 - 2,000	0
NMC1 ($LiNi_xCo_xMn_xO_2$)	Applied mainly in consumer electronics but increasing application for xEVs	Mid	Mid	0.60	2,000 - 3,000	0.69 (51 wt²%)
LMO ($LiMn_2O_4$)	Relatively mature technology. Applied in xEVs by Japanese OEMs (e.g., LEAF, iMiEV, Volt)	High	High	0.41	1,500 - 3,000	0
LFP ($LiFePO_4$)	Relatively new technology applied in xEVs and ESS. Driven by A123 and Chinese manufacturers (e.g., BYD, STL)	Very high	High	0.53	5,000-10,000	0
NCA ($LiNi_{0.8}Co_{0.15}Al_{0.05}O_2$)	Applied mostly in consumer electronics (often blended with other chemistries) and e-vehicles (e.g., Tesla)	Mid	Mid	0.72	NA	0.68 (49 wt²%)

Figure 3 : Advantages and disadvantages of the Li-ion battery cathode materials on the market in 2018[5]

Li-ion batteries cathode development changes really quickly which makes difficult to predict which are the most promising cathode materials[7]. The present trend is essentially developing materials with a lower cobalt quantity: nickel rich materials with diverse compositions and lithium iron phosphates materials[7]. In the future, it is expected that the emergence of new technologies and the development of the electric vehicle will certainly lead to new cathode materials compositions.

2.2.2. The other elements

The anode

The anode is a composite material deposited on a current collector. The current collector is generally a copper plate. The composite is constituted of carbon (most of the times graphite), a binder and a conductive agent. Concerning the conductive agent and the binder, the same materials used for the cathode are present in the anode.

The electrolyte

The electrolyte consists of a lithium salt dissolved in an organic solvent[2,8,9]. Lithium salts most frequently used are $LiPF_6$ or $LiClO_4$, which are dissolved, for example, in propylene carbonate and ethylene carbonate[10]. The function of the electrolyte is to ensure the lithium ions transports between both electrodes.

The separator

The role of the separator is to prevent shorts circuits by separating the anode from the cathode[10]. A polymer membrane such as polyethylene (PE) or polypropylene (PP) constitutes it. This membrane is porous to enable the lithium ions to pass through.

2.3. Importance of Li-ion batteries

Sonny was the pioneer in commercializing Li-ion batteries in 1991. Due to their high energy density, low auto-discharge rate and excellent cycle life, these batteries have substituted Ni-Cd and Ni-MH in many applications[10].

Li-ion batteries have taken part in our daily lives as current devices and dominate nowadays a huge number of applications. Three kinds of applications can be distinguished: consumer electronics and devices, transportation and energy storage as observed in Figure 4 [11,12].The important development in smartphones, tablets and other portable electronic devices has led to a significant increase in Li-ion batteries production since 2004[11]. This trend is expected to continue in the future as shown in Figure 5[13].This trend will be also influenced by the development of electric vehicles. These vehicles, using this kind of batteries, are expected to represent the greatest vehicle market in the near future. Li-ion batteries conceived for this application are estimated to represent the highest demand in the Li-ion market[3].

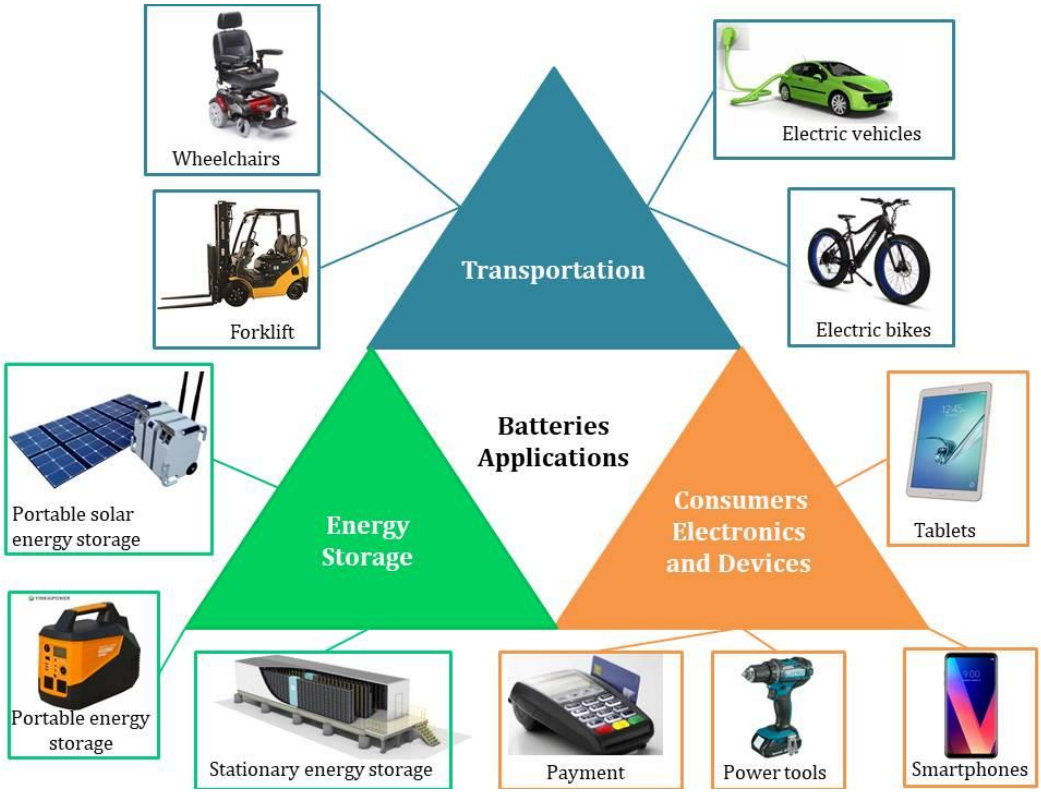

Figure 4 : Li-ion batteries applications adapted from ALBERMARLE report [12]

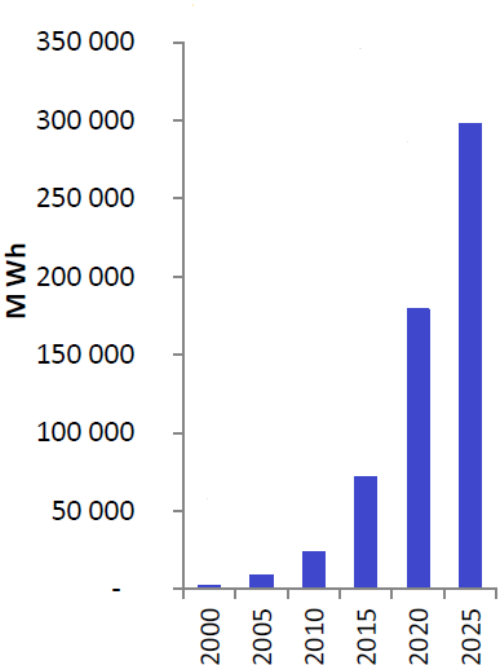

Figure 5 : Li-ion battery worldwide sales predictions 2000-2025[13]

3. Recycling generalities

The most unpredictable aspect about Li-ion batteries future is the increase in prices of the raw materials needed for this type of batteries[11], which constitutes the main concern of the batteries manufacturers. As we have seen in the section above, cathode materials are constituted of several metals. Figure 6 shows the projections for the next years concerning the cathode materials. As observed in Figure 6 it is expected that the cathode materials present on the market, will still be lithium oxides or phosphates (LCO, NMC, NCA, LFP and LMO) containing one or more transition metals. These transition metals are usually nickel, cobalt or manganese.

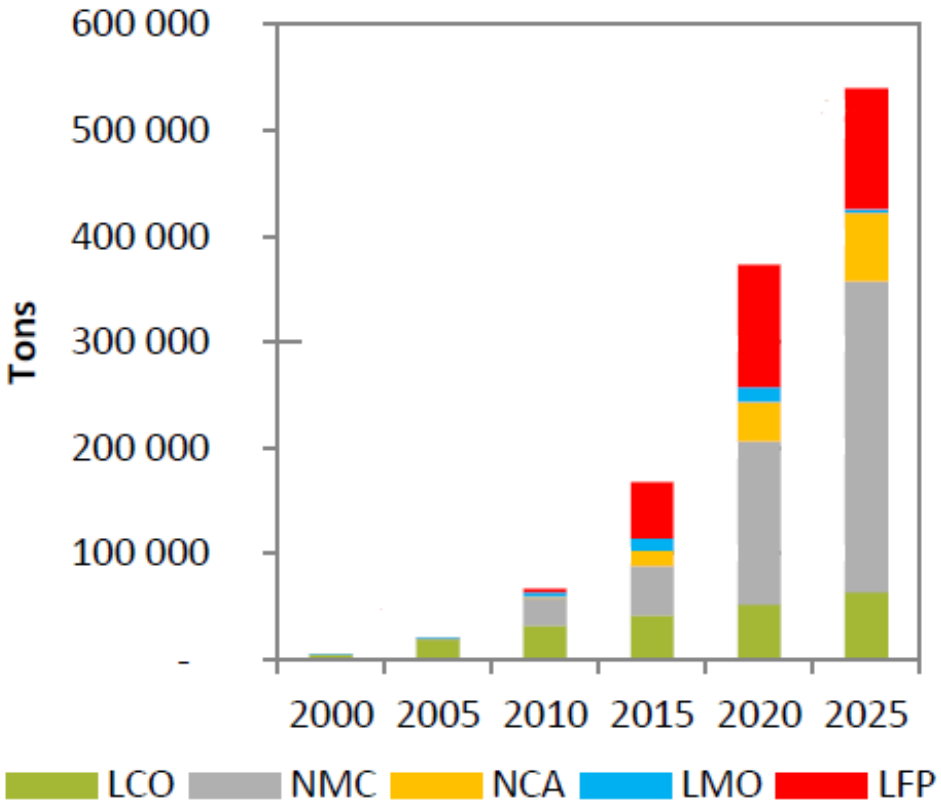

Figure 6 : Cathode active materials forecasts 2000-2025[13]

Projections given in Figure 6 show that the cathode materials demand is expected to exceed 510 000 tons per year by 2025 and its distribution among the different chemistries is observed in Figure 7[13]. Only the quantity of NMC required by 2025 will exceed the total cathode materials demand in 2016, as seen in Figure 7.

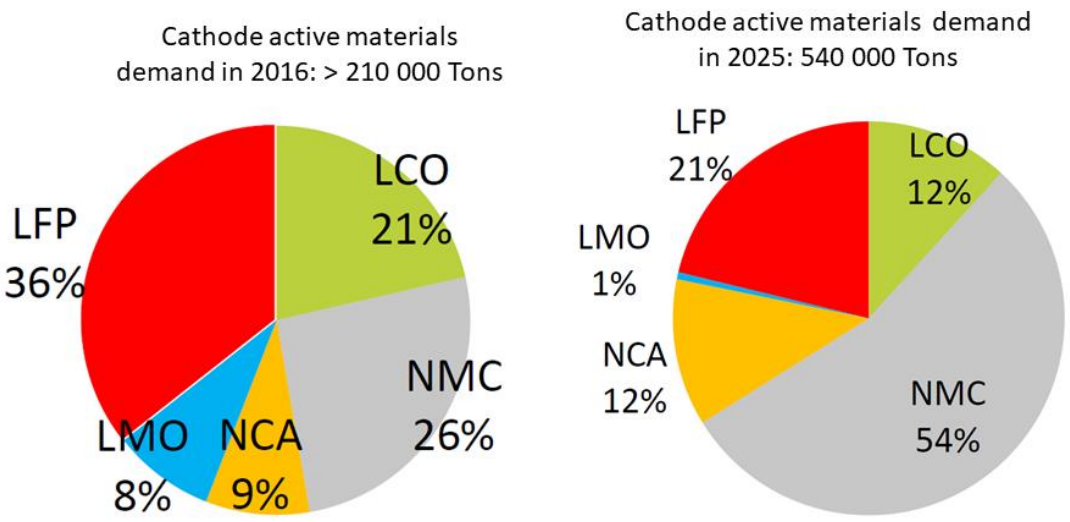

Figure 7 : Cathode active materials demand for 2016 and projections for 2025

Metals needed for Li-ion batteries are distributed in an inhomogeneous way in the planet. Li-ion batteries market could suffer by 2050 because of a supply shortage of key elements: lithium, nickel and cobalt[3,11]. Figure 8 shows some of the principal countries producing these metals. As shown in Figure 8, nickel, cobalt and lithium reserves are not present in Europe[14,15,16].

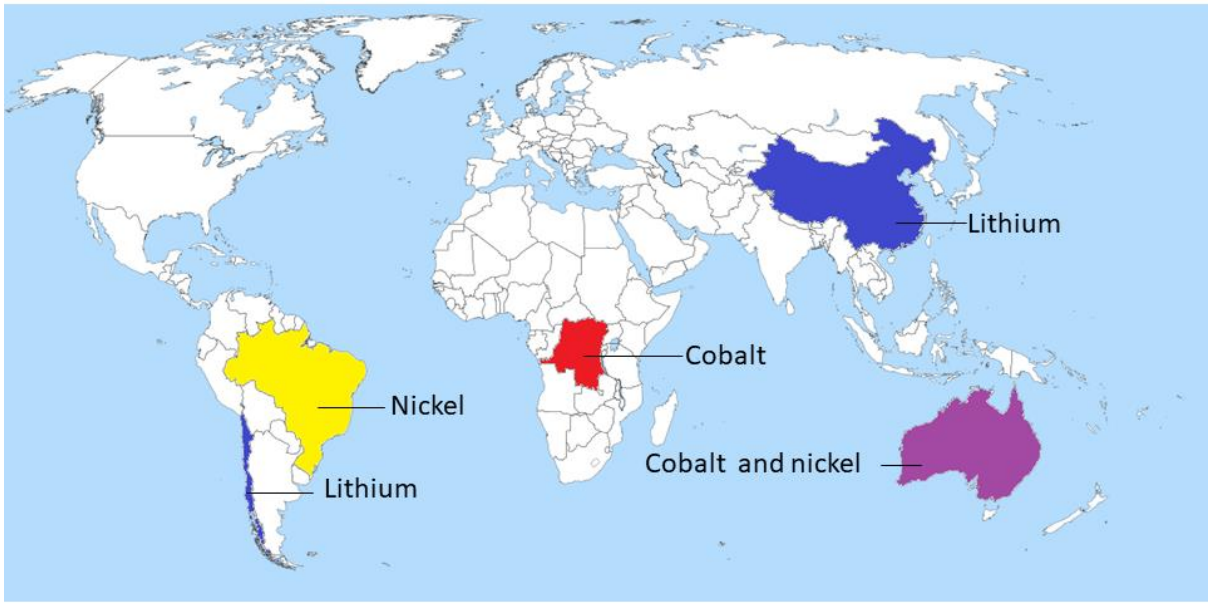

Figure 8 : Worldwide principal producers of nickel, lithium and cobalt[14,15,16]

3.1. Geopolitical and social issues of Li-ion batteries material supply

The concern of the physical availability of the raw materials that constitutes Li-ion batteries has led to apparition of official reports containing the critical raw materials for the different industrial countries. According to the European Commission, "critical raw materials (CRM) are raw materials of high importance to the economy of the European Union (EU) and whose supply is associated with high risk. The two main parameters, economic importance (EI) and supply risk (SR), are used to determine the criticality of the material for the EU"[17].

European Commission has published in 2018 the list concerning European Union critical raw materials[18]. The United States has also set a document containing 35 elements the same year[19]. Both documents include cobalt as critical element which is used in most of the Li-ion batteries compositions. For this reason, our attention will be to cobalt supply situation.

Cobalt is present in several cathode materials. The global reserves of cobalt reported in 2017 are shown in Figure 9 by country[15]. As it can be observed in Figure 9, this transition metal is essentially found in Africa with around 50% of the total reserves. The most important reserve is found in Congo Republic followed by Australia and Cuba. Unfortunately, in Africa practices for extracting this metal are not always responsible. Indeed, there are tens of thousands of young people including children that are working as diggers in dangerous and non-regulated conditions most of the times[20,21]. It represents an important social impact of Cobalt extraction in Democratic Republic of Congo. Around 20-25 % of the total extracted cobalt in Democratic Republic of Congo is extracted in these conditions from artisanal mines.

In the province of Katanga, which is a place of intensive mining in Democratic Republic of Congo, a study has been carried on in order to analyze the impact of human exposure to cobalt. The concentrations of this metal were measured in human urine of residents living close to mines. The results show that the cobalt concentrations were the highest ever reported in this kind of fluid[20]. Cobalt does not only in humans for long periods of time, it is highly toxic for them. In fact, it damages several organs such as : heart, lungs and skin and causes several illness[22].

As a consequence of the mining activities, large quantities of wastes are dispersed, leading to the formation of substrates with a high concentration of metals[23]. This happens because cobalt reacts with the particles around and it finish up in the soils and sediments[24].

Battery manufacturers began to change cathode formulations from cobalt -rich materials to nickel rich-ones due to the extraction conditions of cobalt in Africa[3]. Moreover, this initiative is highly influenced by the instability of cobalt price in the last few years. Cobalt has quadrupled its price in two years[3] as shown in Figure 10.

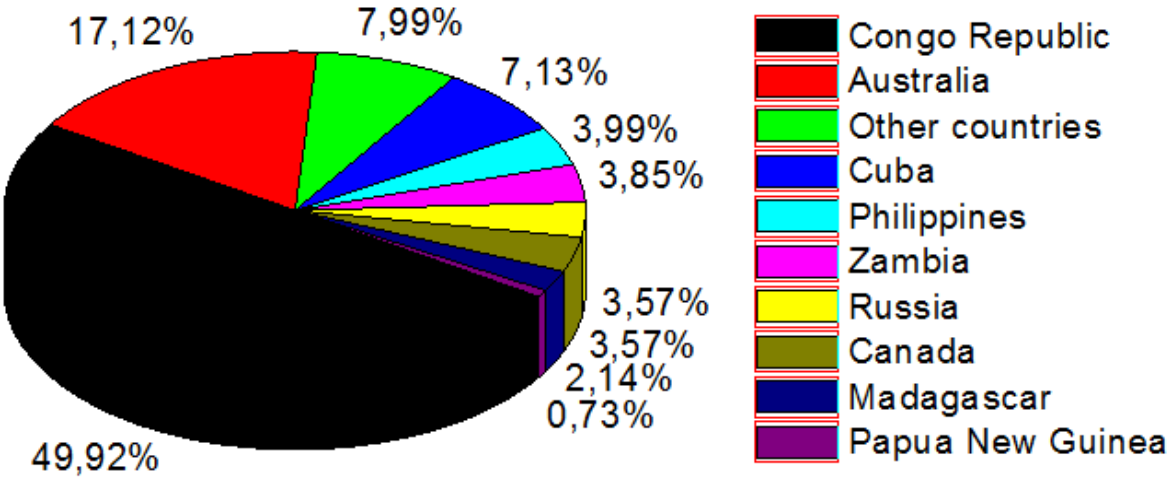

Figure 9 : Cobalt Worldwide reserves reported in 2017

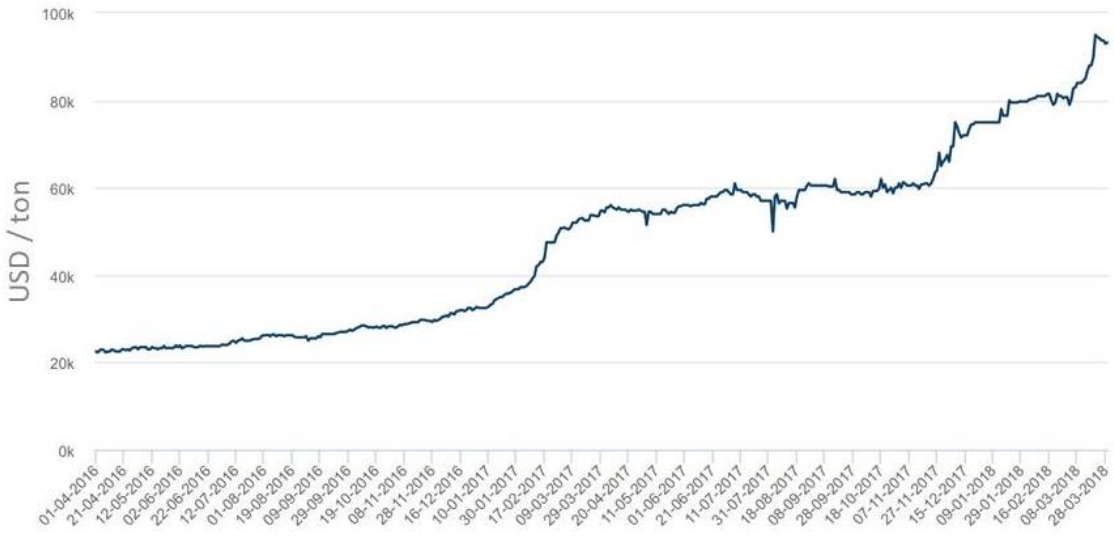

Figure 10 : Recent cobalt price evolution[25]

The increase in Li-ion batteries production has led to an important growth in the demand of cobalt. This demand started to importantly increase in 2005 and this trend continues as shown in Figure 11. By 2050, it is expected that more than 50% of the global cobalt production will be needed only for rechargeable batteries manufacturing. Assuming the scenario in which the actual cathode materials compositions will be present by 2025, only batteries are expected to need more than 10% of global cobalt reserves by 2025 as shown in the Table 2[3].This assumption considers also that all NMC used has the composition: $LiNi_{1/3}Mn_{1/3}Co_{1/3}O_2$. Consequently, there is a real concern about the supply of cobalt in the future.

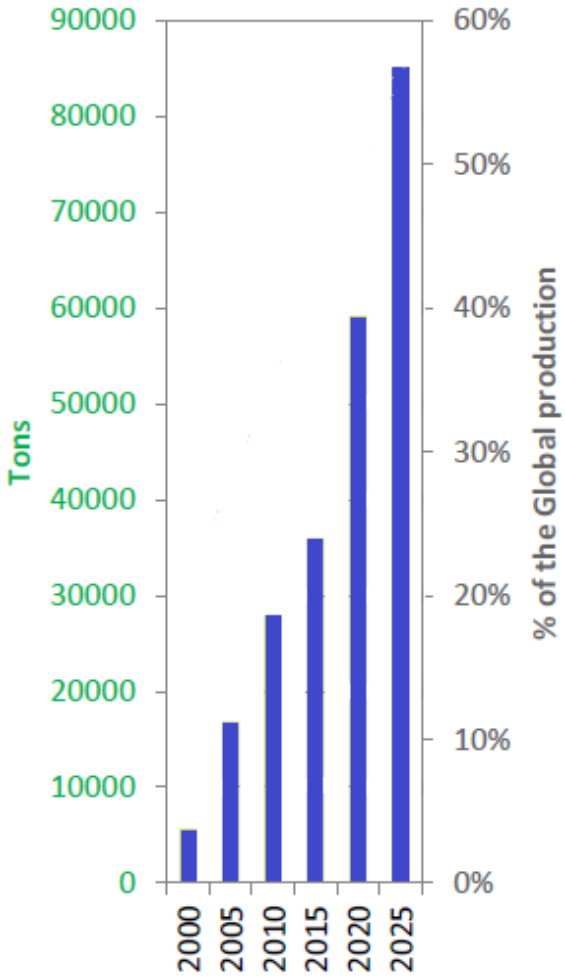

Figure 11 : Cobalt demand projection for the rechargeable batteries 2000-2025[26]

Table 2 : Projection of world battery material demand in 2025[3]

Element	Projected demand (kt)	U.S Geological Survey (USGS) reserves estimations (kt)
Lithium	230	16 000
Cobalt	910	7 100
Nickel	340	74 000

Regardless of the future cathode materials compositions, each year there are millions of used batteries that need to be recycled. Burying them is not a long term viable alternative due to their number and as they constitute a potential source of raw materials.

3.2. Recycling definition and its importance

Recycling has several definitions. It can be defined as making something new from something that has already been used or to use something again. For this project, all the attention will be focused on the waste recycling definition, which consists in any recovery operation by which waste materials are reprocessed into products, materials or substances whether for the original or other purposes.

Recycling of spent Li-ion batteries has become important because of several reasons. Firstly, recycling contributes to reduce the wastes and all stages associated to their disposal. Disposal can be expensive and polluting[27]. Using Li-ion batteries recycled materials contributes to reduce some of the production impacts, including the ones linked to the mining of the ore, the primary processing and the chemical processes of materials[27]. Figure 12 shows the battery manufacturing process steps and how recycled materials can get in it at different stages. It can be observed on Figure 12, that in the first stage the mining of the ore takes place. Once the materials have been extracted, the primary processing takes place. This step is followed by the chemical conversions and the battery fabrication. The manufactured battery is then used in the electric vehicle. At the end of battery lifetime, it is recycled back to one of the manufacturing stages. This happens sometimes directly after being used in electric vehicles. Other times, batteries are reused for energy storage of an electric service before being recycled.

In fact, recycling is a positive alternative to lessen the huge demand for raw materials[11]. Furthermore, recycling will enable to reduce the environmental concerns due to the toxic metals present in this kind of batteries and cope with the depletion of material resources[11]. Having a second resource of critical materials by recycling will enable to maintain market prices of these

elements more or less stable. Unfortunately, today only 5% of Li-ion batteries are recycled[11]. Between 2017-2025, it is expected that the recycling market will raise around 30%[11].

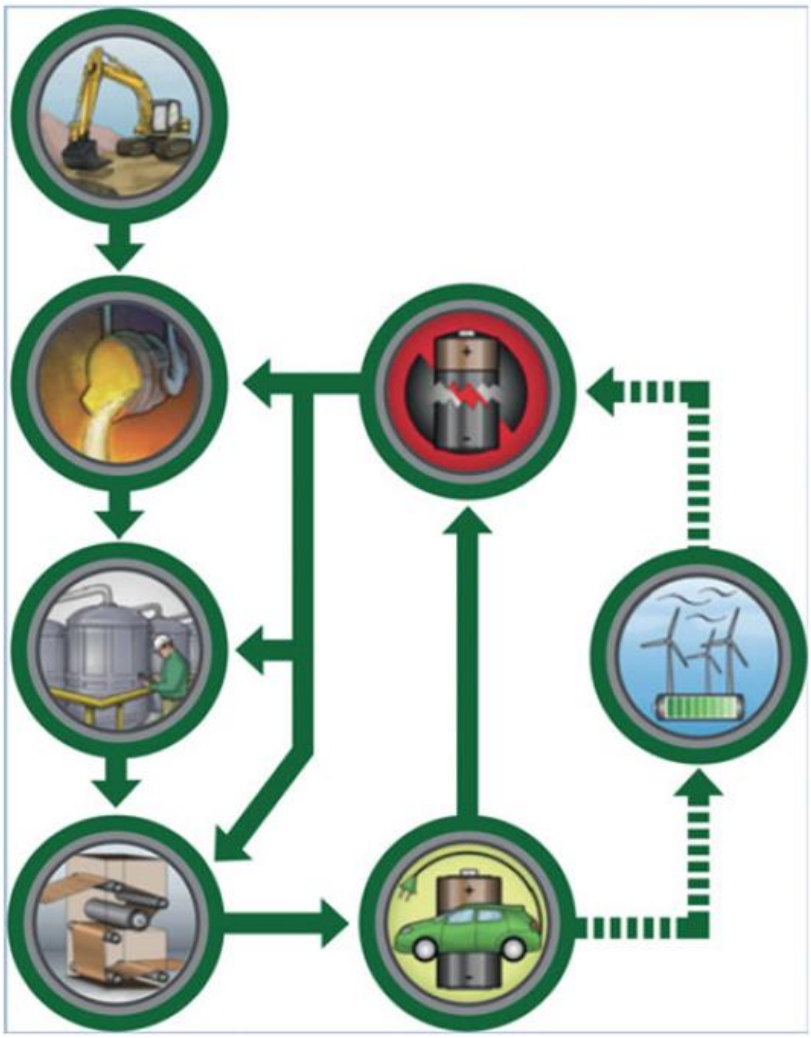

Figure 12 : Batteries recycled materials entering in the manufacturing process at different stages[27]

Recycling can be considered as a source of raw constituents of batteries. From an economic point of view, it is important to take into account the interval of time that exists between the moment when the battery will be available to be recycled and its entrance in the market. In the case of an electric vehicle battery, its lifetime is around 10 years[3]. This means waiting at least ten years before recycling can provide a part of the raw material supply. As a consequence, electrical vehicle batteries recycling will not be an immediate source of raw materials. Nevertheless, the electric vehicles batteries constitute one of the most important sources due to the high quantities of valuable materials in them, given by their sizes.

Electronic devices market uses nowadays a huge portion of the batteries production. Generally, these kinds of devices contain batteries whose lifetime is of around 3 years[3]. Recycling this kind of batteries will lead to a raw material supply in a relative short period of time. Another source of raw material, which is available even in a better delay, is the one found in the battery production scraps. In fact, this material will be directly accessible to be recycled and its impact on the raw material supply will be seen immediately[3].

Furthermore, the choice of the materials to be recycled is of great importance. It is crucial to recover initially materials whose extraction from low-concentration ores is very energy-guzzling[3]. Extraction also implies several environmental issues such as toxic gas emissions. Recycling appears as an alternative to reduce this impact. An example of this can be observed in Figure 13 for the sulfur oxide emissions in LCO production process[3]. As it is shown in Figure 13, the quantity of sulfur oxides emitted by extraction process is at least twice the one emitted by the recycling methods.

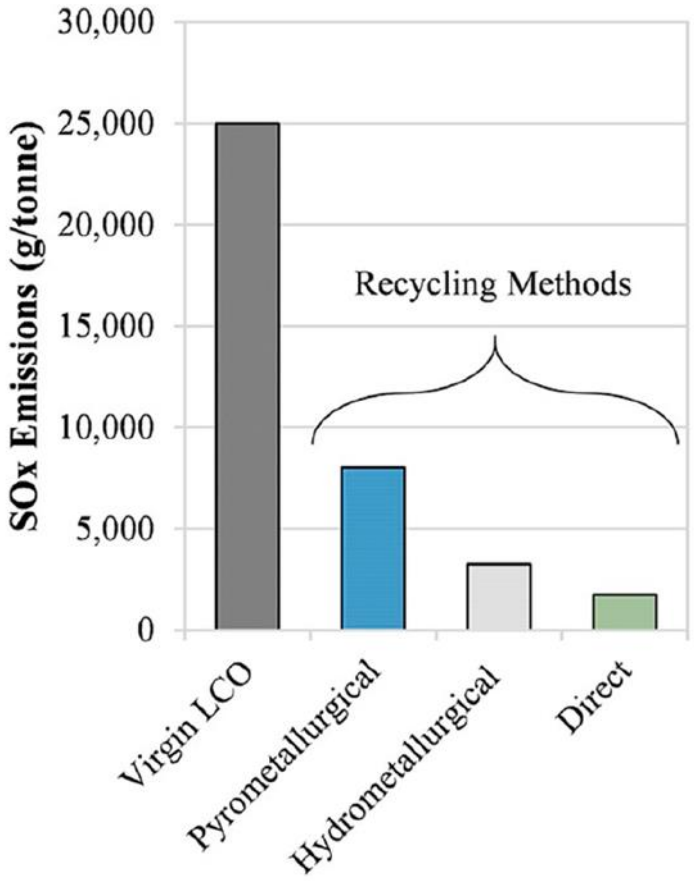

Figure 13 : Sulfur oxides emissions comparison between extraction and recycling methods for producing LCO

3.3. Existing Li-ion batteries recycling methods

There are several methods that have been developed for Li-ion batteries recycling. According to their feasibility, maturation state, cost-effectiveness, and environmental impacts some of them have been chosen to be applied at industrial scales. The existing methods can be classified in: pyrometallurgy, hydrometallurgy and direct recycling[3]. All the recycling methods include a preliminary pretreatment step which is performed before metals recovery[2].

3.3.1. Pretreatment

Pretreatment comprehends several steps that prepares the Li-ion battery and its materials for recycling. The first stage consists in the sorting of batteries according to their type. Then, batteries are deeply discharged, due to the residual power that remains in them at the end of life[2]. This stage prevents the possible short-circuiting and self-ignition which can take place because of a compressive shock or overheating respectively [28]. Li-ion batteries are then dismantled manually or mechanically to identify the battery composition and take off battery plastic and metallic shells[29]. After dismantling, in some cases, the electrode materials from current collector are separated by chemical or mechanical processes[2,11].

3.3.2. Pyrometallurgy

The pyrometallurgy process consists in heating the elements of the battery, at a temperature over 1000°C, in order to recover metal alloys[11]. The metal alloys contain basically elements such as Co, Fe, Ni and Cu. Each one of these metals is then separated by leaching or hydrometallurgy.

Aluminum and lithium are not achieved to be recovered and remain on the slag portion. In order to provide heat to the process and reduce the transition metals, aluminum and all the remaining organic compounds are oxidized[3]. The remaining slag containing lithium is sold to the construction industries as a road base[11]. Even if this process enables a good recovery of a good portion of metals, there are a big portion of the batteries constituents that is volatilized or lost in the slag. This portion constitutes around 60-70% of the battery[11].The volatilized products are usually harmful gases and fluorine compounds. A big budget must be always planned to the gas treatment[3]. The main advantage of this method is that it can treat batteries with different cathode compositions.

3.3.3. Hydrometallurgy

This process consists in the dissolution of active materials in an aqueous solution and then a selective recovery of its components by precipitation. For doing this, several acids, bases or salts are used. The first stage, known as leaching, consists of dissolving the cathode active material into an acidic solution at a temperature range between 30 to 90°C. To do this, strong acids in a high concentration are used. HCl, HNO_3 and H_2SO_4 are used in most of the cases[30]. A reducing agent can be added to the acidic solution to facilitate the metal reduction in the medium. The efficiency of this first step will depend on several parameters: the acid strength, the acid concentration, the temperature and the concentration of the reducing agent[30]. For example, some studies show the possibility of recovering several metals by using a mixture of H_2SO_4 and H_2O_2 (as reducing agent) by the following reaction (Eq. 4)[31]:

$$2LiCoO_2 + H_2O_2 + 3\,H_2SO_4 \rightarrow 2Li^+ + 2Co^{2+} + 3SO_4^{2-} + 4H_2O + O_2 \qquad \text{(Eq. 4)}$$

Once dissolution of the active materials has been achieved, an extraction step follows for recovering the constituents of the active material. Usually, precipitation using a basic solution is added to extract one by one the different constituents. Most of the time, NaOH is used as base. The characteristics of the solution used (such as pH) will allow the selective separation of metals[32,30]. Other approaches use the leaching solution as electrolyte for deposing the dissolved active material[33]. Nowadays, numerous groups have focused their efforts in optimizing hydrometallurgy approach.

As a consequence, innumerable researches, focused on reducing the environmental impacts of the leaching step or improving the extraction step in the last few years. Concerning the leaching step, many attempts have been done to substitute the strong and high concentrated acids used at this stage by less hazardous agents. In this way, several alternatives have been developed such as: ionic liquids mixed with acid solutions[34,35], mild phosphoric acid[36] , oxalic acid[37], citric acid[38]. Even biological approaches using bacteria such as: Acidithiobacillus ferrooxidans[39], Acidithiobacillus thiooxidans[40] or Leptospirillum ferriphilum[40] have been developed for leaching. Other studies focus on improving the extraction stage. For example precipitation method has been optimized by adding salts, in order to control the ratio of the different metals in the solution[41]. This initiative leads to the recovery of hydroxides with the

form $Ni_xMn_yCo_z(OH)_2$ (x+y+z=1) that are directly used to synthesize active materials $LiNi_xMn_yCo_zO_2$[41,42].

Hydrometallurgy shows the advantage of being not an energy-intensive method. Due to the absence of high temperature heating, there are no direct carbon emissions from it[41]. Nevertheless, it uses big volumes of effluents (acids or bases) during the process. The effluent treatment is a delicate aspect that must be considered when using this process because it can pollute environment.

3.3.4. Direct recovery

Some studies have been done in the recent years in order to develop a new alternative approach for Li-ion batteries recycling: direct recovery. It consists in the relithiation of the spent cathode materials by two kinds of processes: a liquid regeneration process and a solid-state synthesis[43]. In the liquid process, spent cathode material regeneration is achieved in a basic solution, generally constituted of LiOH, by hydrothermal treatment or by high-voltage power applied to the solution[43,44,45].The treated cathode powder is then washed to eliminate the lithium excess, dried and annealed. The solid-state synthesis consists in mixing the spent cathode with Li_2CO_3 for relithiating the material, followed by sintering of the obtained powder[43,46]. Before mixing both materials together the mass contents of carbon, lithium and cobalt are measured by Inductively coupled plasma (ICP) in order to calculate the exact quantity of Li_2CO_3 to have a Li/Co ratio of 1.05[46].

3.3.5. Principal recycling companies

There are several conditions to fulfill if we want to consider a process in an industrial context. Firstly, the process should be eco-friendly by having a low environmental impact. It should also be scalable to be used at an industrial scale. Finally, it should be cost-efficient and be able to close the loop so that industrials find a profit to do it[11]. Moreover, recycling has to be able to cope with the treatment of a variety of chemical compositions present in Li-ion batteries.

Nowadays several companies are implied in the Li-ion batteries recycling to extract the valuable metals in most of the cases. Many recycling companies are presented in Asia, North America and Europe as shown in Table 3[42, 47]. As observed on Table 3, pyrometallurgy and

hydrometallurgy methods are the only ones used in industrial processes[42,47]. Furthermore, they can be sometimes combined.

Table 3 : Companies that recycle Li-ion batteries[42,47]

Company	Process classification	Annual capacity (t)	Country
GEM	Hydrometallurgical	30 000	China
Guandong Brunp Recycling Technology Co Ltd	Hydrometallurgical	10 000	China
Fangyuan New Energy Materials	Hydrometallurgical	36 000	China
Tianqi Lithium Corp	Hydrometallurgical	-	China
SungEel Hi	Hydrometallurgical	-	South Korea
LG Chem	Hydrometallurgical	-	South Korea
Retriev Technologies	Hydrometallurgical	3500	United States
Umicore	Pyrometallurgical + Hydrometallurgical	7000	Belgium
Recupyl Insolvent since 2018	Hydrometallurgical	110	France
Euro Dieuze Industrie	Hydrometallurgical	6000	France
Xstrata	Pyrometallurgical	3000	Switzerland
Batrec Industrie	Mechanical treatment +Hydrometallurgical	1000	Switzerland
Accurec Recycling GmbH	Pyrometallurgical	1000	Germany
Duesenfeld	Hydrometallurgical	-	Germany
Neometals	Hydrometallurgical	-	Australia

There are other companies that dedicate some of their research and development activities to Li-ion batteries recycling. This is the case of Eramet that is interested in lithium recycling.

3.4. Legislative initiatives for facing the difficulties of recycling

Recycling is facing a big concern regarding one of the initial steps of the treatment: batteries sorting. To optimize the recycling process, it is essential to separate Li-ion batteries into different flows according to their chemical composition[3]. The real problem behind this aspect is that batteries are not clearly identifiable according to their composition nowadays. To try to solve this problem the Battery Recycling Committee of the Society of Automotive

Engineers (SAE) develop a label recommended to stuck on the battery's pack by manufacturers[30]. The label contains precious information about the battery system (Li-Ion, Pb-Acid, NiMH, NiCd), the cathode elements (ex: Fe, Co, Mn, S, Ni, Al), the anode elements (ex: C, Si, Ti, Sn, Li), the miscellaneous properties, the manufacturer ID (optional) and the manufacture date[48]. Moreover, it could be read by humans and machines. This label is completed by a color attribution to the label's background according to the battery system. The same color attribution has been adopted for the labels developed by the Battery Association of Japan[49]. Figure 14 shows an example of label developed by SAE[48]. The essential information which facilitates the recycling process and enables to consider the precautions needed, are present in this label. If each battery manufacturer applies this recommendation, incidents could also be prevented. For example, when a Li-ion battery gets into a Pb-acid batteries smelter, fire and explosions can occur. It will also contribute to avoid the ignorance of dealing with dangerous materials such as lead[3]. Other big difficulty for recycling Li-ion batteries comes from the complexity of their cell's composition and geometry. These cells contain many different materials which are disposed in various geometries and sizes.

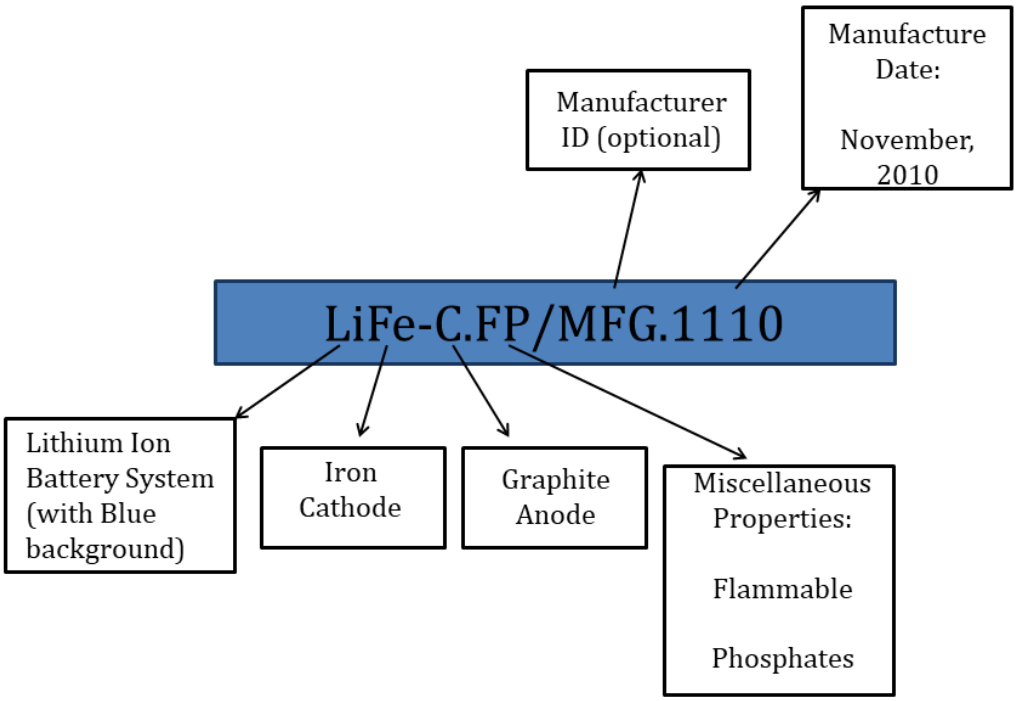

Figure 14 : Label for batteries identification developed by SAE, based on SAE J2984[48]

4. Molten salts generalities

4.1. Definition, classification and properties

Molten salts or fused salts are non-aqueous solvents. In fact, they involve the ionic compounds which are used at their molten state[50]. These liquid systems are well organized over quite long distances, from the first shell of neighbors up to the nanometer length scale[51].This structure, which is less organized than the crystallized one, confers molten salts a higher chemical mobility[50].

Many organic and inorganic compounds can be dissolved in molten salts systems, some of them in high concentrations. Furthermore, using molten salts enables to work in total absence of water as solvent[52]. Moreover, thanks to the high temperatures used for this kind of systems, chemical reactions occur fast and ions can adopt oxidation states which are unusual in other media[52]. Other important characteristics of molten salts include: high thermal conductivity and capacity, wide range of thermochemical stability, a good electrochemical stability, high electrical conductivity[5354]. They show also very interesting transport properties such as: a moderate viscosity and density which can enable an easy separation of the obtained products from the medium[52].

There are two kinds of molten salts: the neutralized and the oxidizing salts[55]. The neutralized salts include alkali carbonates and halides[55]. The oxidizing salts include metal salts of different types : nitrate, nitrite, sulfate, hydroxyl, metal oxides and chlorates[55].

4.2. Examples of molten salts applications

The real origin of molten salts used is not clearly defined in history. From a popular point of view, it is assumed that these media were firstly used when the glass industry appeared, in ancient Phoenicia[56]. However, it is only in the nineteenth century that the molten salt technology appeared concretely[56]. During this period of time, several remarkable discoveries in this field took place. In 1807, Humphrey Davy discovered the possibility of separating alkali metals from their hydroxides by electrolysis [57,58].Several years later in 1854, Deville developed a process to obtain aluminum from the electrolysis of the molten mixture $AlCl_3$-NaCl[58]. Later in 1886, Paul Héroult, and Charles Hall discovered independently at the same time a cost-efficient electrolytic process to produce aluminum. This process is still used nowadays and

consists in the reduction of molten aluminum oxide in molten cryolite[59]. This invention led to the creation of several large-scale extraction plants. Later in 1921, Gerard Herman Jelke Broers gave birth to a new discovery in fused salts field: molten carbonates fuel cells. Then, in the mid-1940 army decide to support the molten salt research and development with the aim of separating big amounts of uranium for the Manahattan project[56]. After the Second World War, Alvin Weinberg achieved the creation of a molten salts reactor and adapted them to the civilian power ones[60]. During the next decades, molten salts were developed in a broad horizon of applications and technologies. In the next section, the major applications of these systems will be discussed.

In order to give a general idea of the broad horizon of molten salts applications, the applications have been classified according to the following areas: materials, energy and recycling.

4.2.1. Materials synthesis and treatment

A variety of materials production has been developed in molten salt including: Non-metallic materials and metals. Concerning non-metallic materials, carbonaceous materials are obtained in molten salts for example. Nanopowders of carbons and amorphous carbon have been synthesized in molten carbonates and molten fluorides respectively [61,62,63]. These materials can find applications in several fields such as fluorine production by electrolysis[64] and as anodes in rechargeable lithium-ion batteries[65] .

Several metals manufacturing has been achieved in such media by electrolysis. This is the case of aluminum, sodium and magnesium for example. Aluminum is produced in a molten cryolite bath[59] while magnesium and sodium are produced in different kind of melts such as: chlorides, oxides and fluorides[66,67,68,69]. Refractory metals are also obtained by this mean. Molten chlorides, fluorides or molten borates are frequently used for the manufacturing of refractory metals like: molybdenum, tungsten, niobium and tantalum[68,70]. Metallic alloys as well can be produced in molten medium. Nickel–tantalum alloys for example can be manufactured by electrolysis in molten fluorides[71].

Metal treatment processes can also be realized in molten salts. The possibility of dissolving many organic and inorganic compounds in these media, make molten salts systems really useful for metal treatment. Metals surface modification, protection, cleaning, finishing,

cementation and brazing can be done by this mean[72,73]. For example aluminum alloys' surfaces are treated in molten medium such as chlorides to prevent corrosion in sea water[74]. Other examples are steel bluing and finishing which are done in molten nitrate-nitrite and molten-cyanide-carbonate mixtures respectively[72]. Several other examples exist in the industrial world but for a matter of time, they will not be detailed in this section.

4.2.2. Energy

Concerning energy production and storage, a great interest has been devoted to the molten salts field. Molten salts reactors, molten carbonates fuel cells and molten salts technologies for energy storage have appeared as a consequence. Concerning molten salts reactors, they provide an alternative way to produce hydrogen or electricity compare to nuclear steam suppliers[75]. Moreover they remain safe, sustainable, practical and stable systems [76,77]. Many advantages result from these types of reactors such as: the capability of producing fissile fuel, burning actinides[77].

Molten carbonates fuel cells have allowed generating 60 MW of stationary energy in Korea[50,53]. This technology is able to produce both electricity and heat[78]. Concerning energy storage applications there are two main molten salts technologies that have been developed: inorganic molten salt electrolyte batteries and sensible heat storage systems. Molten salt batteries contain molten chloroaluminate as electrolyte[79]. This kind of battery is generally used in electric vehicles.

Molten salts have also played a crucial role in the retreatment of wastes and recycling. Different kinds of wastes have been studied in this medium in order to develop a decomposition or a recovery process. For example, oxidizing of wastes in molten salts systems such as alkali carbonates appear as an alternative to wastes incineration. In this way, hazardous organic compounds such as cyanides can be trapped in the molten system[80].

4.2.3. Recycling

Recycling of inorganic wastes in molten salts (Molten Salts Oxidation or MSO) such as black liquor, coming from kraft pulping process, lead to the production of sodium oxide and sodium sulfide, which can then be used in other applications[81]. Other studies have focused on the recovery of different metals, some of them critical for the European Union. In this context, copper-rich compounds have been retrieved from electronic wastes[82], after being separated

from non-metallic components such as fiberglass, epoxy resin and plastics in molten hydroxides[82] or alkali carbonates[55]. By this way, other precious metals such as nickel, gold and silver can also be recovered[82]. Furthermore, most of the organic compounds were trapped in the bath and the rest decomposed in essentially hydrogen [82].

Irradiated nuclear fuel wastes processing has been developed in several countries, using different systems of molten salts such as fluorides and chlorides [83,84]. These kinds of retreatment sometimes include a electrorefining step which enables the production of high purity uranium, used for power generation [84,85]. Uranium is in this way separated from a mixture of: plutonium, americium, curium, neptunium, cadmium and some rare-earth fission products[84]. Other studies show the possibility of applying oxidizing salts like alkali carbonates, which allow the separation of uranium and plutonium from the spent fuel in the form of salts[86,87]. Other studies focused on the retrieving of rare-earth elements from the remaining portion of fission products. For example, some rare earth elements (La, Ce, Pr, Eu, Tb, Dy, Nd, Pm, Sm) have been reported to be recovered as phosphates in a molten chlorides-phosphates mixture[86,87]. Other lanthanides elements such as gadolinium can be extracted in molten fluorides mixtures[88].

As described, molten salts show plenty of applications in different industrial fields. The aim of this section is to give an idea as exhaustive as possible of the vast world of applications. According to the application, one or several molten salts families will fulfill the properties required to achieve the desire objective.

4.3. Choice of molten salts systems

The objective of this project is to study the possibility of recycling Li-ion battery organic and inorganic compounds in one molten salt system. Concerning the inorganic compounds, in the context of this study, the attention will be specially attached to the cobalt recovery. As observed in this chapter, cobalt shows the most critical situation (social, economic and environmental issues). Two types of molten salts systems seem to be adapted for this study: molten carbonates and molten chlorides.

To start with, molten carbonates are well known for their capacity to decompose organic compounds (as seen in section 3.3), which can be very useful for treating Li-ion battery organic ones. Secondly, molten chlorides show very attractive characteristics for dissolving metal oxides (as seen in section 3.3). Furthermore, they constitute reaction medium in which a vast

diversity of metals is produced by electrolysis (as seen in section 3.3). These reasons make molten chlorides a very interesting medium for studying the possibility of recovering Li-ion batteries cobalt from cathode materials.

4.3.1. Physico-chemical properties of alkali carbonates

The most important alkali carbonates are: Li_2CO_3, Na_2CO_3 and K_2CO_3. These compounds are interesting reaction medium due to their physico-chemical properties. They are stables in the range between 400 and 1000 °C [89]. Furthermore, they are characterized by a low vapor pressure[89]. Alkaline carbonates melt at high temperatures, when they are used in a single salt system. Nevertheless, when they are used in eutectic mixtures, alkaline carbonates melt at lower temperatures. Table 4 shows some other properties: composition, molar weight, and melting point[54,90].

Table 4 : Properties of the principal molten alkaline carbonates and their eutectic mixtures[54,90]

Carbonates mixtures	**Composition (molar %)**			**Molar weight (g. mol^{-1})**	**Melting point (°C)**
	Li_2CO_3	**Na_2CO_3**	**K_2CO_3**		
K_2CO_3	0	0	100	138.2	899
Na_2CO_3	0	100	0	106	858
Li_2CO_3	100	0	0	73.9	726
Na_2CO_3-K_2CO_3	0	56	44	120.2	710
Li_2CO_3-K_2CO_3	42.7	0	57.3	110.7	498
Li_2CO_3-Na_2CO_3	62	0	38	98.3	488
Li_2CO_3-Na_2CO_3-K_2CO_3	43.5	31.5	25	100.1	397

4.3.1.1. Oxoacidity of carbonates

As for the aqueous systems, acido-basicity concept also applies to molten salts. In an aqueous medium, this notion is defined by the theory of Lowry-Brönsted, where a proton is given by an acid (or proton donor) and received by a base (or proton acceptor). In the molten salts systems, the acidity is defined by the Lux-Flood theory. By contrast, the oxobase is defined as the donor of an oxide anion (O^{2-}) and the oxoacid as the acceptor[91]. The reaction between the oxoacid and the oxobase is given by the following equation (Eq. 5):

$$oxobase = oxoacid + O^{2-} \quad \text{(Eq. 5)}$$

By this way, in the case of molten carbonates, the oxobase is the carbonate ion and its reaction with the oxoacid is given by (Eq. 6):

$$CO_3^{2-} \leftrightarrow CO_2 + O^{2-} \quad \text{(Eq. 6)}$$

From this reaction the level of oxoacidity in a molten carbonate medium is defined by the equation (Eq. 7):

$$pO^{2-} = -\log\left[a(O^{2-})\right] \quad \text{(Eq. 7)}$$

Where $a(O^{2-})$ is the activity of O^{2-}. Therefore, the increase of pO^{2-} rise the oxoacidity level.

The reaction of self-ionization or decomposition of a molten carbonate can be then expressed by (Eq. 8):

$$M_2CO_{3(l)} \rightarrow CO_{2(g)} + M_2O_{(s)} \quad \text{(Eq. 8)}$$

Where M is the alkaline ion (Li, Na, K), (l), (s) and (g) represent the liquid, solid and gas phases respectively. This equilibrium is characterized by the following equilibrium constant (Eq. 9):

$$K^* = \frac{a(M_2O)P(CO_2)}{a(M_2CO_3)} \quad \text{(Eq. 9)}$$

Where $a(M_2O)$ is the activity of the oxide, $a(M_2CO_3)$ the activity of the carbonate, and $P(CO_2)$ the CO_2 vapor pressure.

4.3.1.1.1. Case of a single carbonate

In the case of a single carbonate, the activity of the molten carbonate in the self-ionization equilibrium is equal to 1. Some studies in molten carbonates show that in the case of

alkali carbonates, at the same fixed temperature, the dissociation constants show the following relation (Eq. 10)[92,93]:

$$pK^*(Li_2CO_3) < pK^*(Na_2CO_3) < pK^*(K_2CO_3) \quad \text{(Eq. 10)}$$

Molten carbonates are used in the form of eutectic mixtures composed of at least two constituents because of their lower melting point compared to a single salt system.

4.3.1.1.2. Case of a mixture of several molten carbonates

In a mixture of several carbonates, the self-ionization equilibrium is given by the formation of the less soluble oxide, which sets the basic limit in the oxoacidity range of the system. The acid limit is given by highest pressure of CO_2 that is of 1 atmosphere. For alkali carbonates the self-ionization reactions are given by the following reactions (Eq. 11), (Eq. 12) and (Eq. 13):

$$Li_2CO_{3(l)} \rightarrow Li_2O_{(s)} + CO_{2(g)} \quad \text{(Eq. 11)}$$

$$Na_2CO_{3(l)} \rightarrow Na_2O_{(s)} + CO_{2(g)} \quad \text{(Eq. 12)}$$

$$K_2CO_{3(l)} \rightarrow K_2O_{(s)} + CO_{2(g)} \quad \text{(Eq. 13)}$$

In the case of a mixture of molten carbonates, the activity of the molten carbonate is not equal to 1. In this case the self-ionization constant K^* becomes K_d^* and is defined by the following relation (Eq. 14):

$$K_d^* = a(M_2O)P(CO_2) = K^* a(M_2CO_3) \quad \text{(Eq. 14)}$$

The stability order for alkali oxides is the following: $Li_2O > Na_2O > K_2O$. Consequently, for the mixtures Li_2CO_3-K_2CO_3, Li_2CO_3-Na_2CO_3 and the ternary mixture made of Li_2CO_3-Na_2CO_3-K_2CO_3, lithium oxide will be the first to precipitate while in the case of the mixtures constituted of Na_2CO_3-K_2CO_3, sodium oxide will be the first one.

4.3.2. Physico-chemical properties of molten alkali chlorides

As for alkali molten carbonates, the most important molten alkali chlorides are: LiCl, KCl and NaCl. Table 5 shows the principal melts used with some of their properties: composition, molar weight and melting point, organized from the highest melting point to the lowest one[54,94,95].

Table 5 : Properties of the principal molten alkaline chlorides and their eutectic mixtures[54,94,95]

Carbonates mixtures	**Composition (molar %)**			**Molar weight (g. mol^{-1})**	**Melting point (°C)**
	LiCl	**KCl**	**NaCl**		
NaCl	0	0	100	58.44	808
KCl	0	100	0	74.56	770
NaCl-KCl	0	50	50	66.5	658
LiCl	100	0	0	42.39	610
LiCl-NaCl	65.58	34.42	0	47.91	554
LiCl-KCl-NaCl	43	24	33	55.40	357
LiCl-KCl	55.7	44.3	0	56.64	355

4.3.2.1. Chloroacidity of chlorides

The analogue concept of oxoacidity exists for molten chlorides: chloroacidity. Chloroacid is defined as the acceptor of a chloride anion (Cl^-) and a chlorobase as the donor[96]. The reaction given by the chlorobase and the chloroacid is given by the following equation (Eq. 15):

$$chlorobase = chloroacid + Cl^- \quad \text{(Eq. 15)}$$

For example LiCl is a chlorobase and its reaction is given by (Eq. 16):

$$LiCl \leftrightarrow Li^+ + Cl^- \quad \text{(Eq. 16)}$$

The chloroacidity of the molten chloride medium is defined by the equation (Eq. 17):

$$pCl^- = -\log\left[a(Cl^-)\right] \quad \text{(Eq. 17)}$$

Where $a(Cl^-)$ is the activity of Cl^-. Therefore, the increase of pCl^- rises the chloroacidity level.

4.3.2.2. Metal oxides dissolution in molten chlorides

Molten chlorides are known for having a good capacity to solubilize metallic cations of oxides. This property has led to the possibility of producing several metals by electrolysis from their oxides such as: Ti[97], Ta[98], Nb[98], Ce[99]. To do it, two different kinds of processes have been developed around the year 2000: Fray, Farthing and Chen (FFC) process (or direct reduction)[97] ; and Ono and Suzuki (OS) process (or indirect reduction)[100] of the oxide. Both processes were initially developed for titanium production and then applied to other metal manufacturing in molten chlorides. The case of titanium manufacturing in molten $CaCl_2$ is used as an example for explaining the reaction mechanisms taking place at the cathode for each case:

FFC process or direct reduction process (Eq. 18)[97]:

$$TiO_x + 2xe^- \leftrightarrow Ti + xO^{2-} \quad \text{(Eq. 18)}$$

OS process or indirect reduction process (Eq. 19) and (Eq. 20) [100]:

$$Ca^{2+} + 2e^- \rightarrow Ca \quad \text{(Eq. 19)}$$

$$xCa + TiO_x \rightarrow Ti + xCa^{2+} + xO^{2-} \quad \text{(Eq. 20)}$$

5. Strategy

In the first place, some battery organic compounds decomposition will be studied in molten carbonates. Then Li-ion cathodes behavior in eutectic molten Li_2CO_3-K_2CO_3-Na_2CO_3 carbonates will be studied by electrochemical techniques, in order to explore the possibility of recovering cobalt by electrodeposition. The success of this method depends on the cobalt solubility in the molten carbonates medium and the electrode material choice.

In the second place, Li-ion cathode material behavior in eutectic molten LiCl-KCl chlorides will be studied by electrochemical techniques, in order to recover it by electrodeposition. As for carbonates, cobalt solubility in the molten medium and the electrode material choice will be discussed in order to facilitate cobalt electrodeposition.

Chapter II: Study of Li-ion battery compounds in molten salts by X-ray absorption spectroscopy

"Premier principe : ne jamais se laisser abattre par des personnes ou par des événements."

Marie Curie

1. Introduction

In the context of exploring the possibility of recycling cobalt by electrolysis from eutectic Li_2CO_3-Na_2CO_3-K_2CO_3 several questions show up: what happens to cobalt from cathode materials once it is in the melt? Which is its speciation? Does its oxidation state change in the medium? How does it interact with the electrode during the electrolysis? Which is the reaction taking place at the electrode? Answering these questions is essential to determine if the choice of the molten solvent and electrode are appropriate or not. Furthermore, with the knowledge of the oxidation state of cobalt in the molten system, it is possible to quantify its solubility in medium by electrochemical techniques.

The objective of this chapter is the study of cobalt in molten carbonates (liquids) during the electrolysis by X-ray absorption spectroscopy (XAS). XAS has been chosen for this study face to other techniques because it is a powerful analytical tool, that enables to characterize the local atomic order in any material (crystal, amorphous, liquids, polymers,..) contrary to XRD which can be done only on crystalline solids. This technique gives information on interatomic distances, nature and coordination of the neighbors surrounding the absorbing atom and oxidation state of the studied element. X-ray spectroscopy shows numerous advantages. In fact, it can characterize material at particular experimental conditions of : vacuum, controlled atmosphere, pressure, high temperatures (around 1200 °C), diluted samples, in situ reactions with a time resolution < 1s[101]. In addition, the selectivity of this technique allows us to study each element in the sample separately. In the context of our study, XAS is the only available technique that enable us to determine cobalt speciation and oxidation state in a liquid at high temperature (> 500°C).

This project implies a major challenge: creating an entire device (molten salt container heating system and electrochemical set-up) adapted to synchrotron facilities. This involves several difficulties. In fact, the device materials must ensure the sample's sealing, heating temperature stability and good contact between the sample and the electrodes. Furthermore, the chosen materials must ensure the good transmission of the beam, and cope with high temperatures of about 600 °C for long periods of time (several days) to be used for the several experiments. During this project we deal with a supplementary difficulty which concerns the cobalt XAS measurements, because its binding energy is close to potassium one, which is one

of the constituents of the molten solvent. One by one these technical constraints have been overcome in our team and the results are presented in this chapter.

1.1. X-ray absorption spectroscopy (XAS) technique

The principle of interaction of X-rays with matter

X-rays are electromagnetic radiations that show different interactions with the matter: inelastic and elastic scattering, and photoelectric effect. XAS relies on this last one, where the absorption of a photon causes the ejection of an electron from a core shell level of the absorbing atom and is followed by a photoelectron emission. The electron is promoted to a final state that can be a bounded or unbounded. The final state depends on the energy of the absorbed photon and the binding energy as given in the following relation[102]:

$$E_f = \hbar\omega - E_0 \quad \text{(Eq. 21)}$$

Where:

E_f: the final level energy

E_0: the binding energy

$\hbar\omega$: the absorbed photon energy

The absorption is measured by scanning a range of X-ray energies which includes the binding energy of core shell electrons of the studied element. The absorption of X-ray is defined by Beer-Lambert's law according to the following relation[102]:

$$I = I_0 e^{-\mu x} \quad \text{(Eq. 22)}$$

Where:

I: the intensity transmitted through the sample

I_0: the X-ray intensity incident on a sample

x: the sample thickness

μ: the absorption coefficient which gives the probability that X-rays will be absorbed

The absorption spectrum is divided into two main regions, as shown on Figure 15: EXAFS (Extended X-ray Absorption Fine Structure) and XANES (X-ray Absorption Near Edge Structure). This distinction between both regions is arbitrary as there is not a clear definition that distinguishes the near-edge and extended structure.

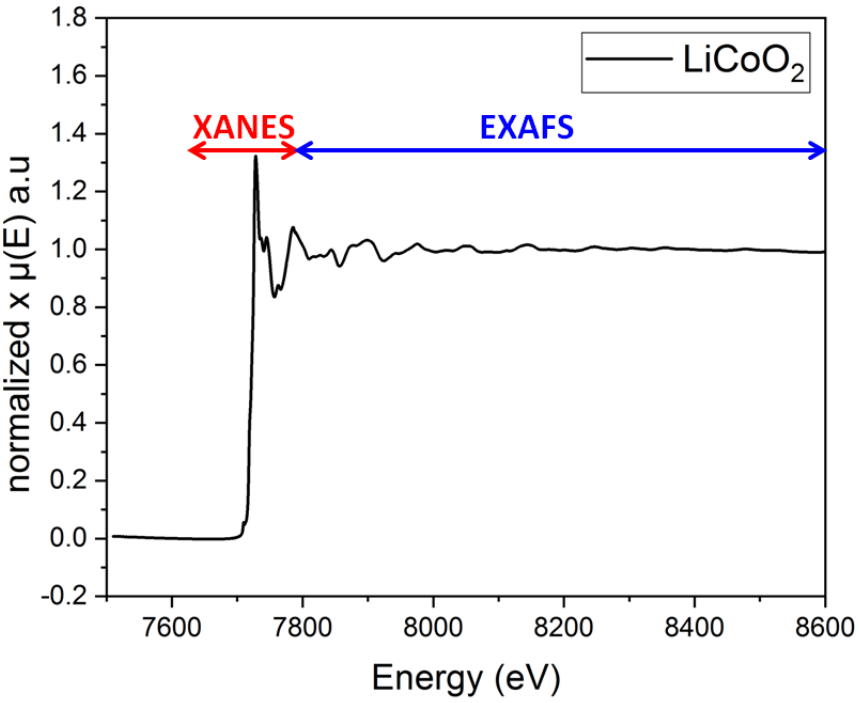

Figure 15: Co K-edge absorption spectrum of $LiCoO_2$

At the edge (where $E_f = E_0$) the contributions observed correspond still to bounded resonances[103]. But above this value of energy, the final state belongs to the continuum spectrum. In this case, a photoelectron escapes from the absorbing atom and its energy is defined by the following equation:

$$E_f = \hbar\omega - E_0 = \frac{\hbar^2 k^2}{2m} \qquad \text{(Eq. 23)}$$

Where:

k: the photoelectron wavevector

m: the electron mass

The emitted photoelectron probes its local environment. Its wave is scattered from the photoabsorbing atom to another atom at a distance photoabsorber-scatterer (R_{as} in Figure 16) and then returns to the absorbing atom (Figure 16). The photon electron wave travels a total distance of $2R_{as}$ to complete a round trip. The final-state wavefunction at the absorber is modified by the back-scattered wave and results in a quantum interference effect; that is visible as an oscillation of the absorption as function of the photon energy. This phenomenon is known as extended X-ray absorption fine structure (EXAFS)[103]. This region generally includes the oscillations above the edge with a range generally of 40-1000 eV. The frequency of these

oscillations is correlated to interatomic distances between the photoabsorber and the neighboring atoms. Their amplitude depends on the nature and number of surrounding atoms, the thermal and structural disorder of the system.

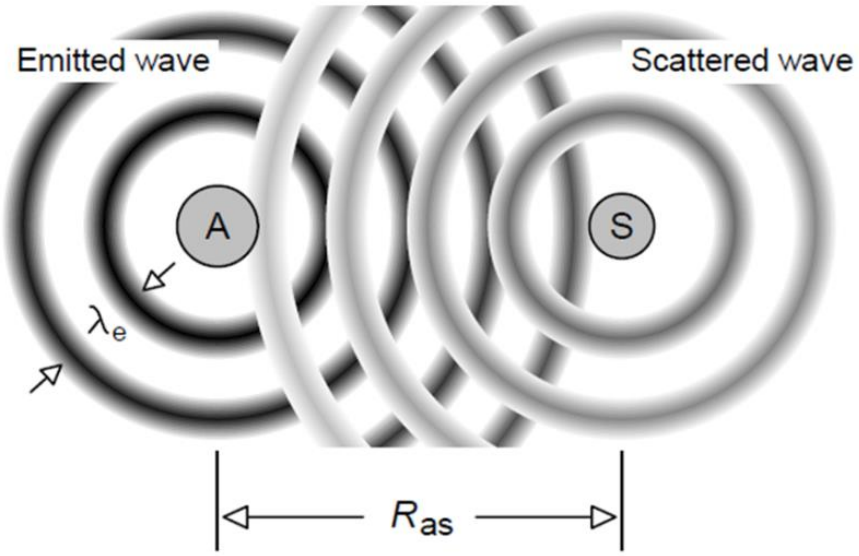

Figure 16 : Atom A emitted a photoelectron which is back-scattered by the scattering atom S[104]

The EXAFS signal is defined by the following equation:

$$\chi(k) = \sum_j \frac{N_j}{kR_j^2} e^{-2R_j/\lambda_j(k)} \left|f_j(k,\pi)\right| \sin\left(2kR_j + 2\delta_l'(k) + \emptyset_j(k)\right) e^{-2\sigma j^2 k^2} \quad \text{(Eq. 24)}$$

Where:

$\left|f_j(k,\pi)\right|$: the backscattering amplitude of neighbors j

$\emptyset_j(k)$: the phase function of neighbors j

$\delta_l'(k)$: l = 1 phaseshift for the photoabsorber atom

$\lambda_j(k)$: the phenomenological mean-free-path accounting for inelastic losses

R_j: distance photoabsorber-neighbor j

$e^{-2\sigma j^2 k^2}$: EXAFS Debye-Waller factor

EXAFS can also be defined as function of the absorption coefficient μ(E) by equation 25:

$$\chi(E) = \frac{\mu(E) - \mu_0(E)}{\mu_0(E)} \quad \text{(Eq. 25)}$$

Where:

E: the photon energy

μ(E): the measured absorption coefficient

μ_0(E): the smooth background function representing the absorption of an isolated atom

Concerning XANES, it corresponds to the part of the spectrum in the vicinity of the edge. This region is of great interest in our case as it gives the information about the oxidation state of the absorbing atom. The energy of the edge is not well defined as it is usually considered as the energy corresponding to the inflexion point (half height), also known as the maximum of the first derivative with respect to the energy. This energy is essential to determine the oxidation state of the absorbing element. Edge energy increases when the oxidation state increases. This is explained by the fact that more energetic X-rays are needed to eject an electron of atoms with a higher oxidation state as they have a higher charge.

Transmission XAS measurements

There are different types of XAS measurements: fluorescence, polarized and transmission. This last mode was used for our study. Figure 17 shows the typical apparatus for transmission XAS measurements[102].

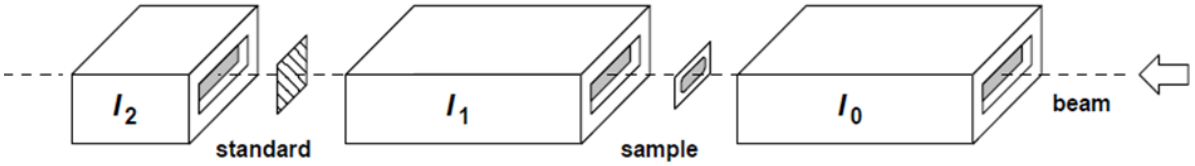

Figure 17 : Schema of the typical equipment for transmission XAS measurement[104]

In this case, X-ray beam's intensity is measured before and after the sample. The absorption coefficient μ is calculated by (Eq. 22). Ionization detectors, which consist in a chamber filled with a gas or a gas mixture, is used to measure X-ray intensity. Two detectors are positioned along the beam axis, in front of and behind the sample. A third one is usually added on the same axis for XAS measurement of a standard after the sample. The spectrum obtained from the standard is used to calibrate the energy scale with a known one.

2. Results and discussion

2.1. Developing a new device for in situ XAS measurements in molten salts

As mentioned before the objective of our study is to monitor cobalt behavior in molten carbonates during the electrolysis by XAS. Several challenges and requirements appear in the conception of the device for the measurements. Firstly, a cell constituted of a material with the minimum X-ray absorption between 7 keV and 8 keV (Co-K edge) was needed. The same condition was unavoidable for the heating system. Both set-up parts must show a thermal resistance up to 600°C. Kapton which is usually used as sample container cannot be used as it does not resist temperature over 400°C.

The cell material must not react with the molten mixture (molten carbonates + cobalt precursor). Furthermore, a perfect contact must be ensured between the electrodes and the sample. Once the salts melt, there is supplementary difficulty that appears: ensuring the homogenous distribution and filling of the molten mixture in the cell for the XAS and electrochemical measurements. Finally, studying cobalt in the eutectic Li_2CO_3-Na_2CO_3-K_2CO_3 implies a supplementary challenge as the absorption energies of potassium and cobalt are close. In this way potassium absorb part of the photons dedicated for cobalt characterization.

Only few studies reported the use of XAS for molten salts characterization at high temperature due to the peculiar technical difficulties that it involves. Some devices for in situ XAS measurements of molten salts have already been reported in the literature as shown on Figure 18. We analyzed one by one the proposed devices and inspire ourselves from them to create our set-up.

According to the type of molten salt and the experimental conditions, the designs of them have been adapted. In this way Mikkelsen, J. C. *et al*, have developed a boron nitride or graphite cell that can be used for the molten materials such as molten chlorides and solids up to 1000 °C[105]. The idea of using graphite for the salt container for our set-up seems a suitable alternative as it shows a good stability to temperature (in the absence of oxygen), low absorption compared to cobalt and it is a relatively cheap material. Two parts composed the Mikkelsen J. C *et al* set-up: the screw-together holder and the sample containing insert (Figure 18 (a)). Ensuring the sealing of the sample seems to be delicate as the set-up is closed only by two points as seen on Figure 18 (a), and no proof of the set-up reliability has been shown.

Filipponi A. *et al*. proposed another set-up for studying molten bromides or metals up to 3000 K under vacuum, which is also constituted of graphite[106,107]. The set-up is constituted by the sample container (graphite crucible) and a glass vessel as shown in Figure 18 (b). The sample container is tight to two stainless-steel cylindrical bars which work as electric conductors, providing the heating to the graphite crucible. As our final objective is to carry out electrochemical measurements, a direct contact between the sample container and the electric conductors must be avoided. For this reason, this set-up design is not suitable for our project.

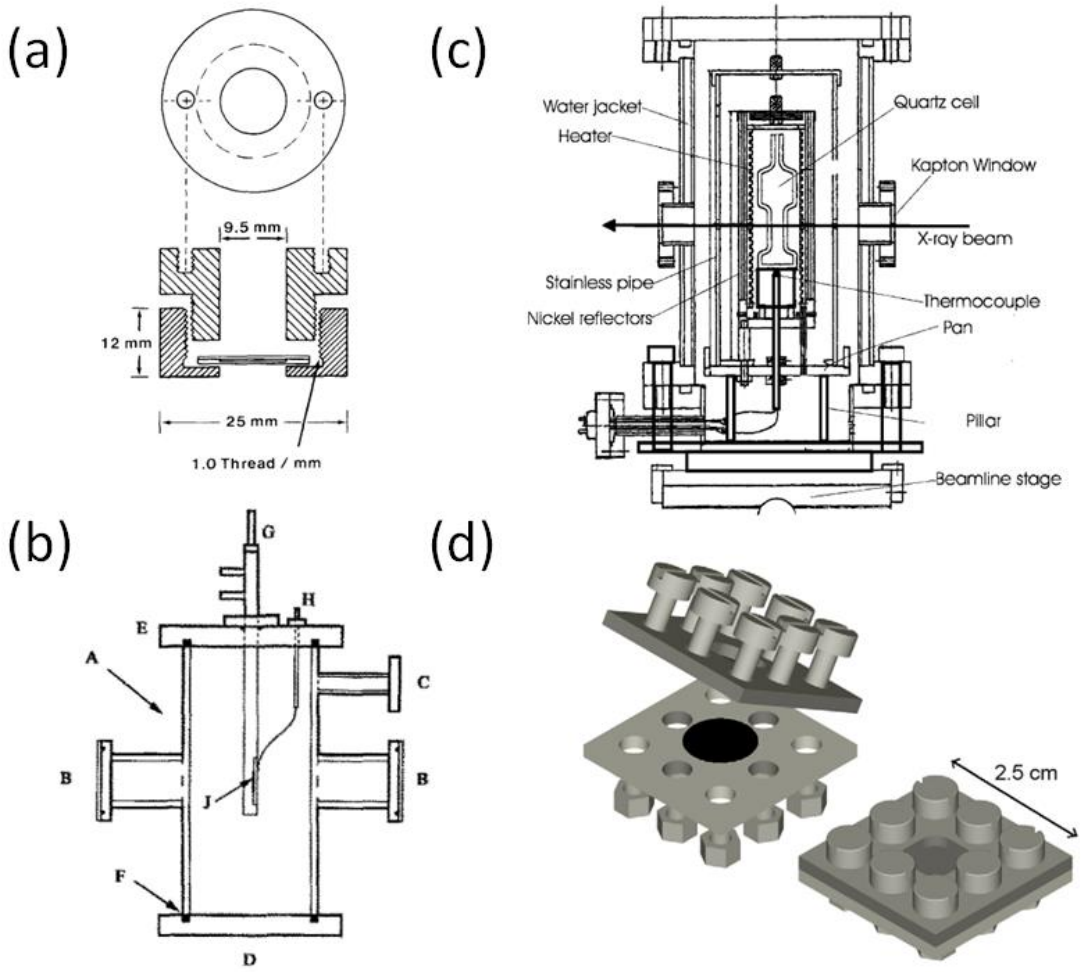

Figure 18 : Mikkelsen J.C. *et al.* sample cell showing the screw- together two-part holder and the sample-containing insert made of boron nitride or graphite (a). (b) shows Filipponi A. *et al* set-up, where A is the glass external container, B are Kapton windows, C the glass inlet for gases, D and E are Teflon covers, F Vyton O-ring, G are the electric conductors, H feedthrough for thermocouple, J is the planar graphite crucible. (c) shows Okamoto Y. *et al* set-up. Rollet A-L. *et al*. two-plate cell in pyrolytic boron nitride which is closed by stainless steel screws (d).

Lauday *et al*, proposed a contactless device for the measuring molten alumina up to 2500 °C[108]. This is possible thanks to an aerodynamic boron nitride levitator. This set-up is not adapted to our experiments as we need a cell container to prevent vaporization and composition evolution during measurement and also to install all the electrochemical elements.

Okamoto, Y. *et al*, proposed a quartz cell for measuring molten chlorides solvents containing lanthanum[109] (set-up device on Figure 18 (c)). The quartz cell has a sandglass form. This cell form can be used for our experiment, as it guarantees the complete filling of the cell section where the beam goes through, once the sample is melted. Quartz shows a good stability to high temperatures (about 1000 °C) but it has a higher absorption than graphite. For this reason, we did not consider the possibility of using this material for our set-up. Furthermore, the pasting of the electrodes on this material can be complicate. Finally, Rollet *et al*, developed a pyrolytic boron nitride cell to study lanthanide in molten fluorides (Figure 18 (d)) [110]. As there might exist an interaction between boron nitride and the melt (carbonates + cobalt), we decide not to consider this material as an option. Furthermore, this set-up design was not suitable for our study as electrodes could not be added on it for a matter of space.

Among all the cell materials used for salt container manufacturing in literature, we chose graphite, already used for the sample container by Mikkelsen *et al*[105]; Filipponi *et al* [106]. Graphite was selected for its good stability to the high temperatures (in the absence of oxygen) and because it is cheap. Furthermore, we opt for using Okamoto *et al*'s[109] cell form (sandglass) as it enables to ensure the total filling of the cell for the measurement, once that the salt melts. As a first step, we developed the set-up and tested it for cobalt study in molten carbonates without electrochemical measurements. The development of this device is shown in the next section.

2.1.1. Sample container and sample thickness

To meet the sample container or cell requirements mentioned before, quartz used by Okamoto *et al*[109] for mixtures of molten chlorides and lanthanides shows a too high absorbance with respect to cobalt absorption. Besides, using pyrolytic boron nitride material is not either a suitable candidate as there might be an interaction between the molten carbonate and it. As a consequence, both reported set-ups materials cannot be used.

Graphite and glassy carbon appear to be good alternatives as both have been already been used in reported studies of molten carbonates without problems[61]. Moreover, graphite shows the

qualities of absorbing X-ray in low level and being easily machining. Nevertheless, a thin grain quality is indispensable to manufacture thin cell's walls. Furthermore, graphite possesses an optimal resistance to very high temperatures and under thermal stress it does not deform, burst or shrink. Lastly, it is stable in corrosive environments. For all these reasons, the graphite R6710 from Final Materials has been chosen as sample container material.

Sample and container thicknesses are important in order to optimize the X-ray transmitted through the sample. The probability of X-ray to be absorbed by the sample and the cell can be checked through Beer-Lambert's Law (Eq. 22).

The maximal absorption was found when the cell was 200 µm thick. Inspiring from Okamoto setting approach, we achieve to the design shown on Figure 19. A cavity of 300 or 400 µm thick was done. Above it, a reservoir was built to ensure the complete filling of the cavity when the salt was melted. Both of them were filled with the solid sample. Machining graphite with a low thickness with the available laboratory tools was one the greatest challenges in the manufacturing of the cell. For these reasons, we make thicker (300 µm) the wall for part A and a complete hole for part C on Figure 19. This counterpart of the cell (C) was combined with a very thin glassy carbon sheet, with thicknesses of 60 or 100 µm.

To ensure the total and optimal filling of the cell, we decide to put the maximum amount of salt in by the pellet method. Pellets were composed of salt grinded for at least 10 minutes and then pressed with 5 tons pressure at room atmosphere. Pellets have the exact cavity's thickness and were set into the cell's cavity and reservoir in the same atmosphere conditions. Then the empty space was filled with salt powder. Finally, the three parts A, B and C were fixed together with graphite glue form Final Materials.

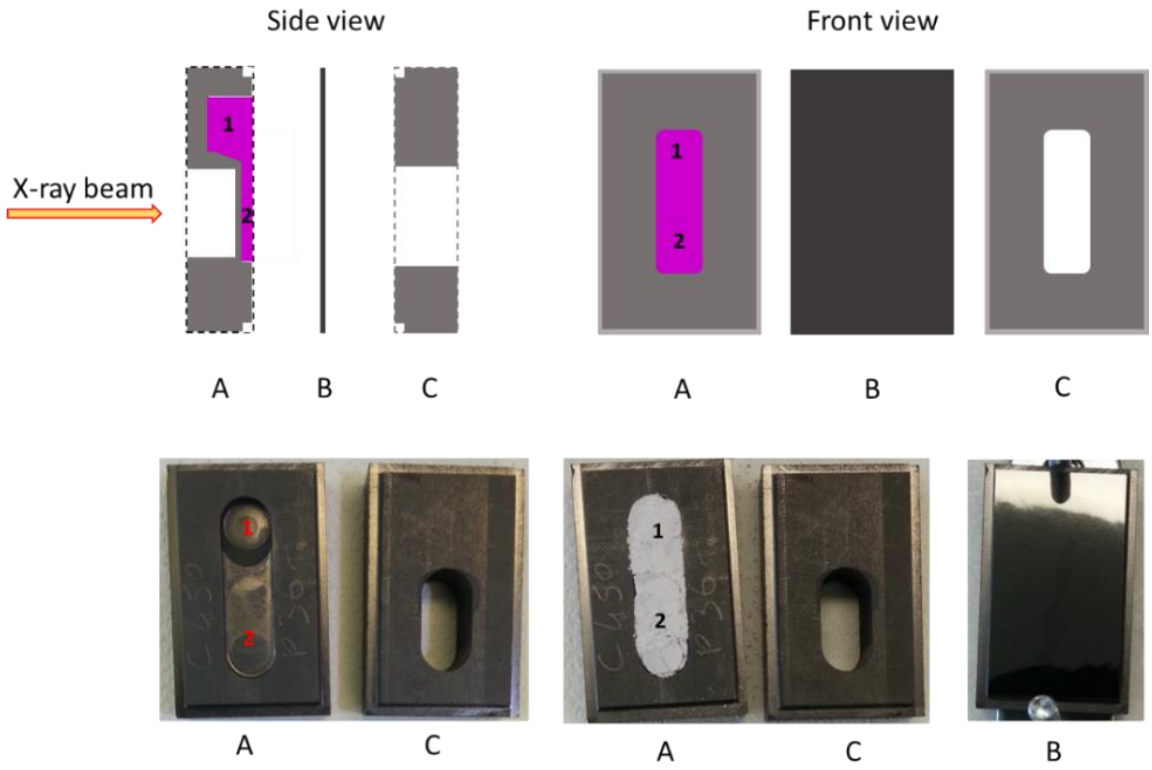

Figure 19 : On the top left, schema of the side view of the cell with the part (A) in which the cavity (2) and the salt reservoir (1), the part (B) is glassy carbon sheet and the part (C) that is the counterpart of the cell. On the top right, schema of the front view of the same elements A, B and C. Below, pictures of the different part of the cell (empty and filled).

2.1.2. Heating elements

New heating equipment was developed due to the small space available on synchrotron beamline instead of using a traditional furnace. A 0.5 mm thick and 1.2 mm wide kanthal wire was chosen for this purpose. Its resistance corresponds to 1.93 Ω/m, so 0.5 m of this wire was used to obtain a resistance of 0.965 Ω. The maximum number of turns with the wire was done to obtain the highest electrical resistance possible, see Figure 20 (a). As graphite is an electrical conductor material, the direct contact with the resistance must be avoided. For this reason, in the first test, the wire was embedded in ceramic Rescor 750 Base from Cotronics as shown on Figure 20 (b).

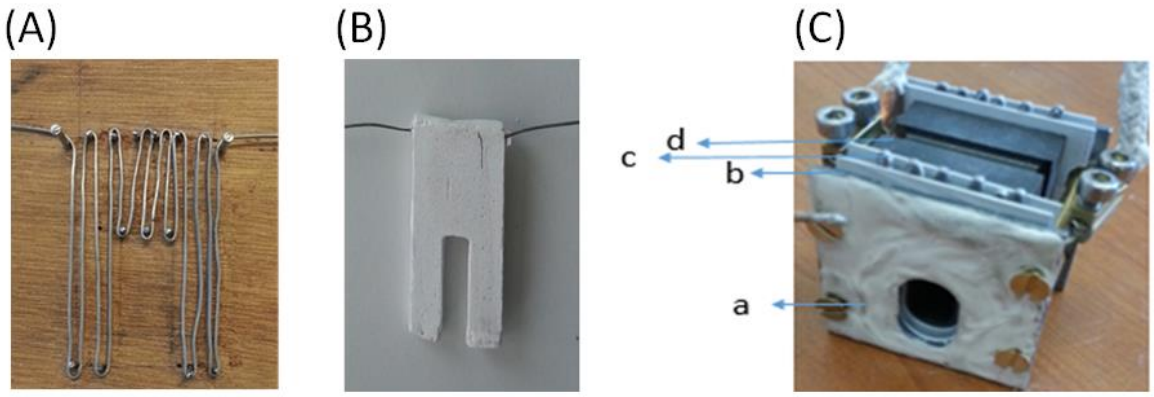

Figure 20 : Picture (A) shows the resistance, Picture (B) shows the resistance in ceramic, picture (C) shows the heating sandwich where (a) is the inox plate coated with ceramic, (b) and (d)are Boron Nitride plates, and (c) the resistance

With this initial idea, the heating of cell up to 400 °C was achieved, but with no stability. In fact, a temperature oscillation higher than ± 20°C was present due to a bad contact between the heating system and the cell. In a second attempt, the cell was coated with high purity alumina ceramic (Resbond 989F from Final Materials). The coated cell was in contact with the resistance through an inox plate coated with the same ceramic. With this heating material, 600 °C could be reached with a stability of ± 2°C and a maximum ramp of 20 °C/min. However, this heating system cannot be used to perform several experiments as the coating was very fragile after the first heating. In the third test and final one, the resistance (c on Figure 20(c)) was sandwiched between 2 Boron Nitride plates (b and d) as shown on Figure 20 (c). This material was chosen for its properties of good electrical isolation, thermal conductivity and easy machining. This last heating set-up fulfilled all the requirements of temperature stability and robustness to being used for several experiments. A hole was drilled on each plate to allow the beam pass through.

2.1.3. The chamber

A ceramic chamber has been built around the heating system in order to ensure the thermal insulation during the heat (a on Figure 21). Three types of ceramic were tested for the chamber: Durapot 804 powder, Rescore 750 base precision castable ceramic and Resbond 989F high-purity alumina ceramic. The first two were very fragile and do not resist even the low thermal test as they can handle up to a temperature of 400 °C only. The last one possesses the

thermal stability required to be used. The chamber was constituted by several pieces fabricated separately and then assembled with ceramic glue (Final Materials).

To protect and isolate the whole system, we enclosed it in an aluminum chamber (c on Figure 21). This chamber has a height of 127 mm and a hole on two parallel sides to allow the beam to pass through (b on Figure 21). Both holes were covered by Kapton to ensure the total closing of the system. To monitor the temperature of the molten system with a thermocouple, a hole on the graphite cell and on both chambers was made.

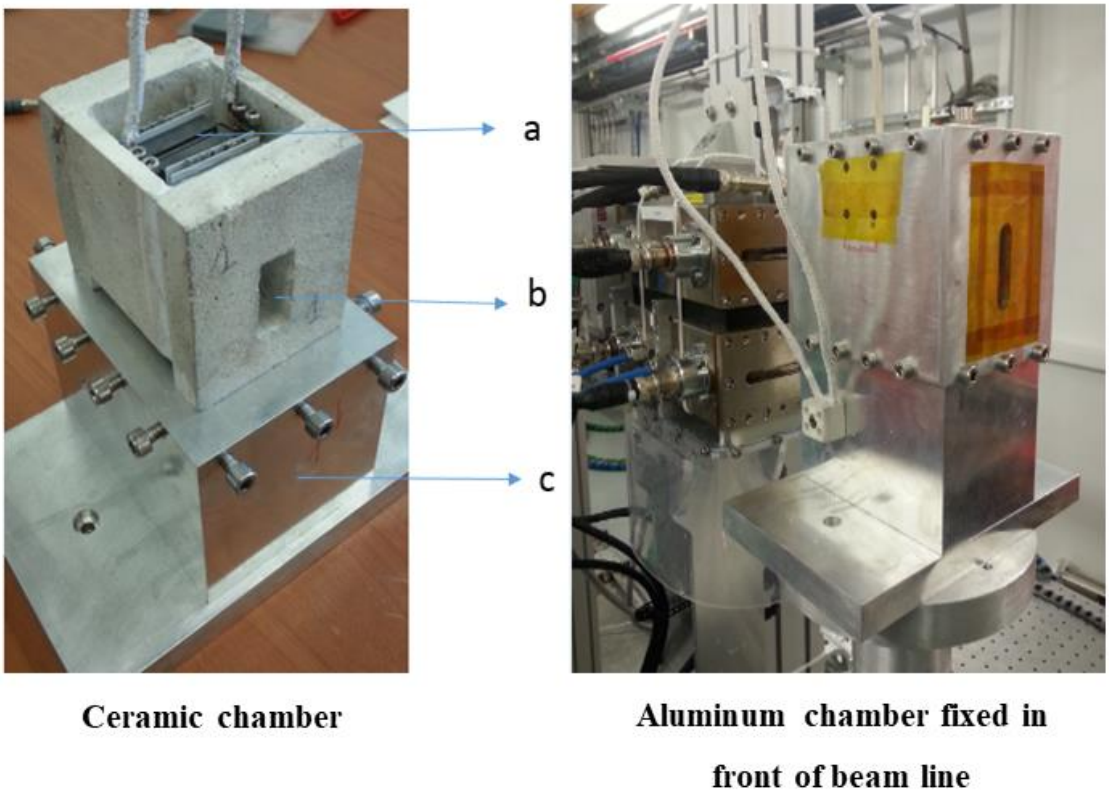

Figure 21 : (a): graphite cell, (b): the window for beam passage, (c): aluminum stand

2.1.4. Experimental conditions for in situ measurements

Atmosphere

To avoid the entrance of oxygen from the atmosphere into the chamber, an inert vector gas was used. The first reason involves the possible reaction between cobalt from the sample and oxygen. The second one implies graphite burning in presence of oxygen at high temperatures. The vector gas chosen must have a high thermal conductivity and no oxygen.

Helium and nitrogen appear to fulfill these requirements. For simplicity we chose nitrogen. A hole was added to both chambers (ceramic and aluminum) to allow the entrance of gas.

Synchrotron experimental conditions

X-ray absorption spectroscopy measurements at Co K-edge (7709 eV) were performed in transmission mode at ROCK (Rocking Optics for Chemical Kinetics) beamline of SOLEIL Synchrotron facilities[111]. This beam line is dedicated to material science and high temperature studies combining X-ray diffraction and absorption in a tunable energy range (4-40 keV).

ROCK beam line enables to carry out quick experiments and by the way monitoring fast kinetic processes. For this reason, we chose this line for our experiments. The monochromated X-ray beam focused on the sample, has the dimensions: 80 µm x 350 µm. The requested energy range was of 7300-8500 eV. Cobalt metallic foil was used as reference of energy for each measurement.

Heating conditions

The samples were heated up with a ramp of 10°C/min. We increased the temperature stepwise (350 °C, 450 °C and 550 °C). The temperature stability at each plateau was achieved at about 2-3 minutes. This was detected by the observation of a stability of the transmitted intensity. In this condition, the absorption spectrum was recorded. After the last plateau at 550 °C, the system's temperature decreased in a steady way.

Samples

The samples used for all the experiments in this chapter come from molten baths already used for electrochemical studies (all of them are presented in chapter III). For each case, we heated in the cell at synchrotron facilities only a portion of the homogenous purple zone. For all of them Li_2CO_3-Na_2CO_3-K_2CO_3 eutectic mixture was used as solvent. For the experimental details about the preparation of these molten systems see experimental section in chapter III.

Reference compounds

The following list of compounds has been used as references as they have a known oxidation cobalt state as shown on Table 6. Each reference compound powder was mixed with Boron Nitride, then grinded and pressed with 5 tons for about 3 minutes to make a pellet. The

pellets obtained had a thickness of about 500 µm. Then, Kapton tape was used to seal the pellet from both sides. The measurements took place at room temperature and atmosphere.

Table 6 : List of reference compounds for XAS measurements

Compound	Cobalt oxidation state
Co foil	Co (0)
CoO	Co (II)
$Co(NO_3)_2$. $6H_2O$	Co (II)
$CoSO_4$	Co (II)
$CoCO_3$	Co (II)
Co_3O_4	Mixture of 1x Co (II) and 2 x Co (III)
$LiCoO_2$	Co (III)

2.2. Reliability of the high temperature device for in situ XAS measurements

With the developed device, described in section 2.1 of this chapter, we achieved to measure XAS spectra of cobalt K-edge for cobalt carbonate and oxides dissolved in molten carbonates up to 550 °C. We fixed this maximum of temperature due to scientific interest and not for technical limits of our device. An example of the achieved experiment is shown in Figure 22. As observed on this figure, there is a stability of the recorded successive spectra (200 ms recording time per spectrum), at 550°C which proves the reliability of the developed device.

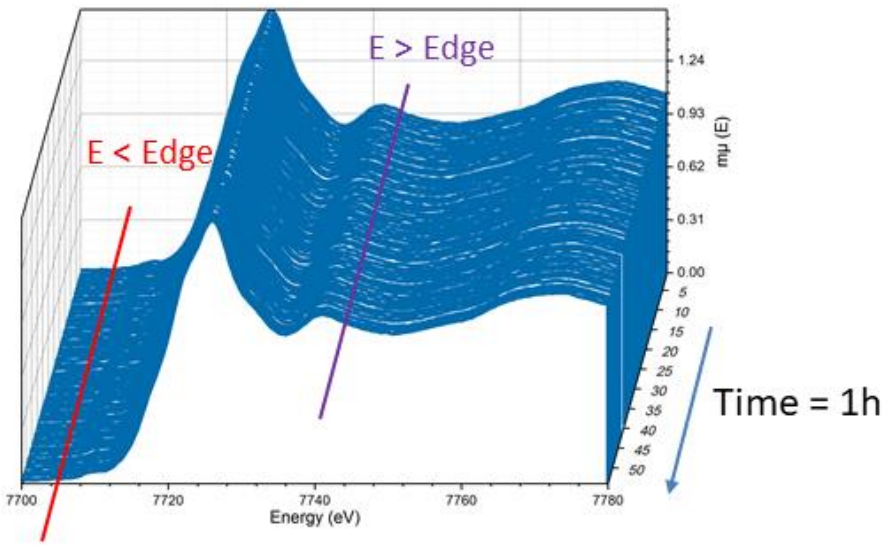

Figure 22 : Evolution over the time of Co K-edge XANES spectrum for $LiCoO_2$ in molten carbonates at 550 °C

To verify the total sealing and melting of the sample we monitor the position of it before and during the heating. Figure 23. shows the cartography of the sample position before and during the heating. For the cartographies acquisition, we tuned the X-ray energy to a value just below cobalt's edge energy and we measured the transmitted intensity as function of the position (x,z). Then, we repeated this operation at an energy value just above cobalt's edge energy. We collected by this way a cartography "before cobalt edge" and "after cobalt edge". The resulting cartography comes from the ratio of the cartographies "before and after cobalt edge". As observed on Figure 23, the salt has moved during the heating, which confirms that the melting of the mixture was achieved.

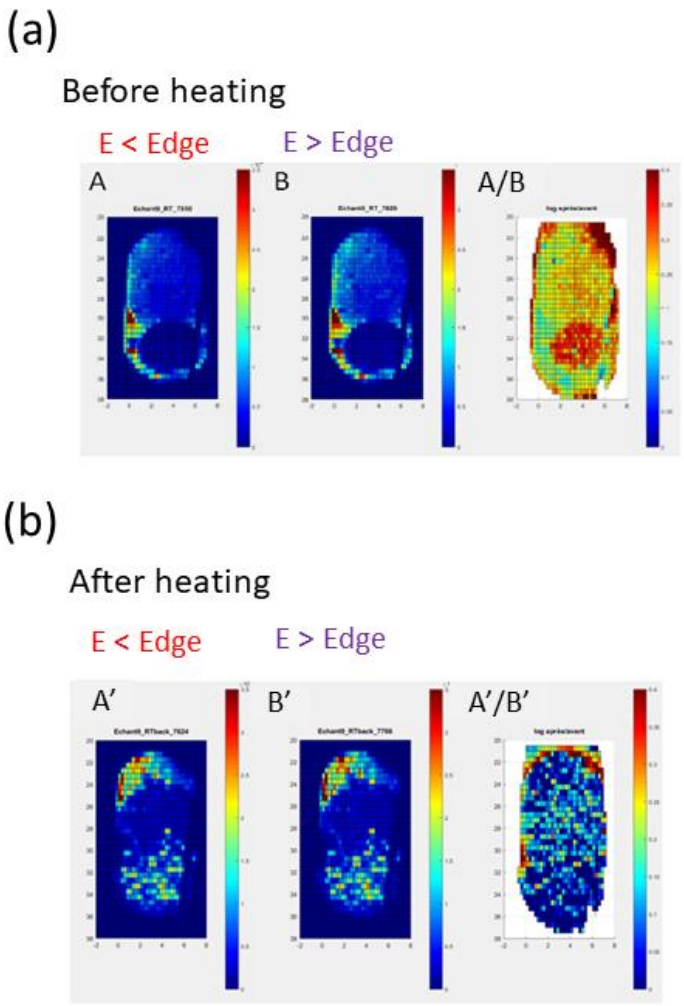

Figure 23 : Cartography of $LiCoO_2$ bath before the heating (a), where A and B are the cartographies before and after cobalt edge respectively, A/B is the resulting cartography from the ratio before and after. Cartography of $LiCoO_2$ bath after the heating (b), where A' and B' are the cartographies before and after cobalt edge respectively, A'/B' is the resulting cartography from the ratio before and after

2.3. In-situ measurement of $LiCoO_2$ (LCO) in molten Li_2CO_3-Na_2CO_3-K_2CO_3 eutectic

Determining cobalt average oxidation state

In situ measurements of the molten baths containing cathode materials LCO, NCA, NMC and different reference compounds $CoCO_3$ and Co_3O_4 studied in chapter III, have been carried out on April 2019. For a matter a time, only LCO study will be presented in this section. Figure 24 shows (a and b) in situ Co K-edge XANES before, during and after the heating for $LiCoO_2$, and after for NCA and NMC. At the bottom of Figure 24 (c) the Co K-edge XANES of the references compounds is shown.

To determine the oxidation state, we follow the method proposed by Capehart and al[112]. In a first step, the integral of the normalized absorption spectra A_{ref} is measured for an arbitrary range in the absorption edge zone as depicted in the Figure 25 for a reference compound. In our case the reference was Co foil and the energy range was from 7690 to 7715 eV. In a second step, the upper energy limit (E_C) is determined, to calculate the integral for a series of well-defined compounds, i.e. with known oxidation state, in a way that the value of the integral is the same as for the reference. In a third step, the values of the edge energy shift are calculated and plotted as a function of the oxidation state.

$$\delta E = E_C - E_R \qquad \text{(Eq. 26)}$$

Where E_C is the edge energy of the compound in eV and E_R is the edge energy of the reference point in eV.

A linear regression is performed in order to obtain a calibration line. In a final step, the E_C is similarly determined for the compound with unknown oxidation state and reported on the calibration line to obtain the oxidation state.

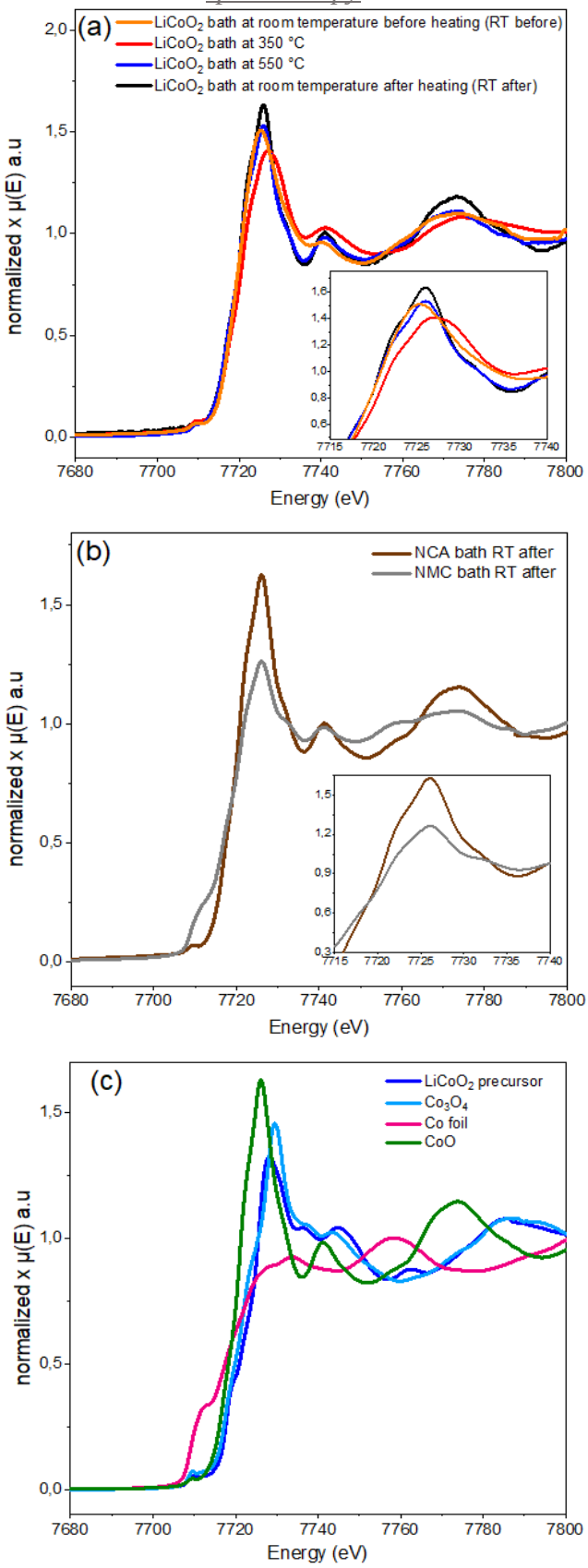

Figure 24 : In situ Co K-edge XANES of $LiCoO_2$ bath at different temperature plateaus (a), NCA and NMC bath at room temperature after the heating (b) and 4 reference compounds (c)

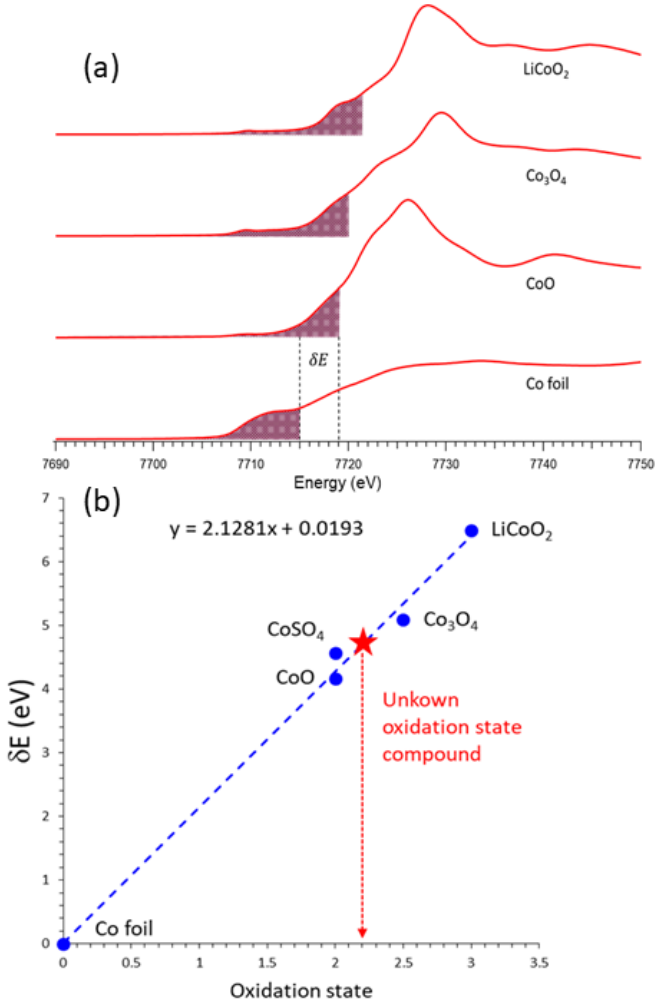

Figure 25 : XANES Co K-edge of different reference compounds used. The purple-filled part of the spectrum corresponds to a constant area arbitrary area (a). Calibration curve employing different reference compounds (b).

This approach has been tested and proved to be accurate by Capehart T.W. *et al*. Furthermore, it has been used by Krylova, G. *et al*, Huck-Iriat C. *et al*, in studies implying XAS cobalt studies at K-edge [113, 114]. As edge energy shift can be influenced by the oxidation state but also by several effects concerning the beam line equipment such as calibration, this method considers an internal reference point as unavoidable[112,114]. For cobalt this reference point is set at 7709 eV[114].

The determination of the average oxidation state from XANES is usually obtained by the maximum of XANES region derivate. We used Capehart T.W. *et al*. approach instead of the derivate one for several reasons. First of all, Capehart T.W. method is more robust when

several compound phases are present in the studied system. Furthermore, Huck-Iriat C. *et al*, Krylova, G. *et al*, applied this approach to compounds which are similar to the ones used in this project. They used cobalt oxides reference compounds such as: CoO, Co_3O_4, $LiCoO_2$, with the aim of analyzing Co-based catalysts for steam reforming of ethanol[114] or the synthesis of multicomponent nanocrystals[113].

With this procedure the edge shift is determined for $LiCoO_2$ in molten carbonates sample at different temperatures, and the respective average oxidation state is determined Figure 26. It is important to notice that before the heating in the EXAFS setup, cobalt shows an average oxidation state of +II and not +III as expected for native $LiCoO_2$ because the sample are taken from bath of electrochemical experiments. This means that the reduction of Co (III) from cathode materials into Co (II) takes place in carbonates medium. But does cobalt from $LiCoO_2$ bath shows the same oxidation state in solid and molten carbonates? The Figure 26 shows the evolution of the oxidation state of cobalt in the bath during the heating.

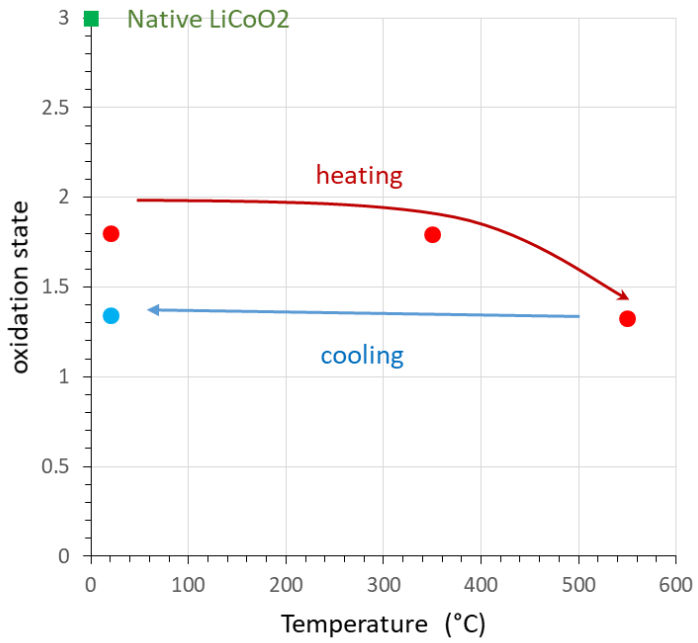

Figure 26 : Average oxidation state for $LiCoO_2$ bath as function of temperature

$LiCoO_2$ bath shows a slight decrease of the average oxidation state as the sample is heated. This trend is also observed when the temperature is decreased to room temperature after the heating. As a consequence, the oxidation state determined afterwards on the sample coming the bath of the electrochemical experiments can be considered as a good approximation of the

cobalt oxidation state during these experiments. Hence, cobalt is mainly in the Co (II) form in the molten Li_2CO_3-Na_2CO_3-K_2CO_3 eutectic. Table 7 shows a summary of the edge shift obtained for calibration curve references and the studied samples.

Table 7 : Edge shift results for samples and reference compounds

Compound	δE (eV)	Oxidation state
Co foil	0	0
$LiCoO_2$	6.49	3
CoO	4.17	2
$CoSO_4$	4.57	2
Co_3O_4	5.09	2.5
$LiCoO_2$ bath RT before	3.85	1.8
$LiCoO_2$ bath RT after	2.88	1.4
$LiCoO_2$ bath at 350 °C	3.84	1.8
$LiCoO_2$ bath at 550 °C	2.87	1.3
NCA bath RT before	3.71	1.8
NMC bath RT before	3.86	1.9
Co_3O_4 bath RT before	4.62	2.2

It is observed in all the cases, that cobalt presents an average oxidation state of +II. This confirms the reduction of cobalt Co (III) into Co (II) in molten carbonates. A slight decrease in the oxidation state is observed for NCA, Co_3O_4 and NMC baths. $CoCO_3$ bath is analyzed at room temperature before the heating as the transmitted signal was too low to carry out the measurement at high temperatures. This explains the absence of decrease of the oxidation state.

The surprising point is to find oxidation state lower than 2 possibly indicating the reduction of a portion of Co (II) into metallic cobalt. We suppose that graphite from the cell, which is in a big quantity compared to the sample, leads to a reduction process. This phenomenon is known for iron oxides in the presence of carbon, but at much higher temperature >1000 °C[115]. To verify this hypothesis supplementary studies must be carried out.

In-situ EXAFS

In a second step, we are interested in determining cobalt phases or environments at different temperatures studied using the EXAFS part of the absorption spectra. In liquid, it is laborious to obtain the different contributions of the absorber atom neighbors as they are constantly moving. Simulation is generally used to face this problem[109, 116]. In our case, we have surprisingly achieved to model the XAFS spectra in solid and liquid states using a linear combination of solid reference compounds XAFS spectra at room temperature (Figure 27).

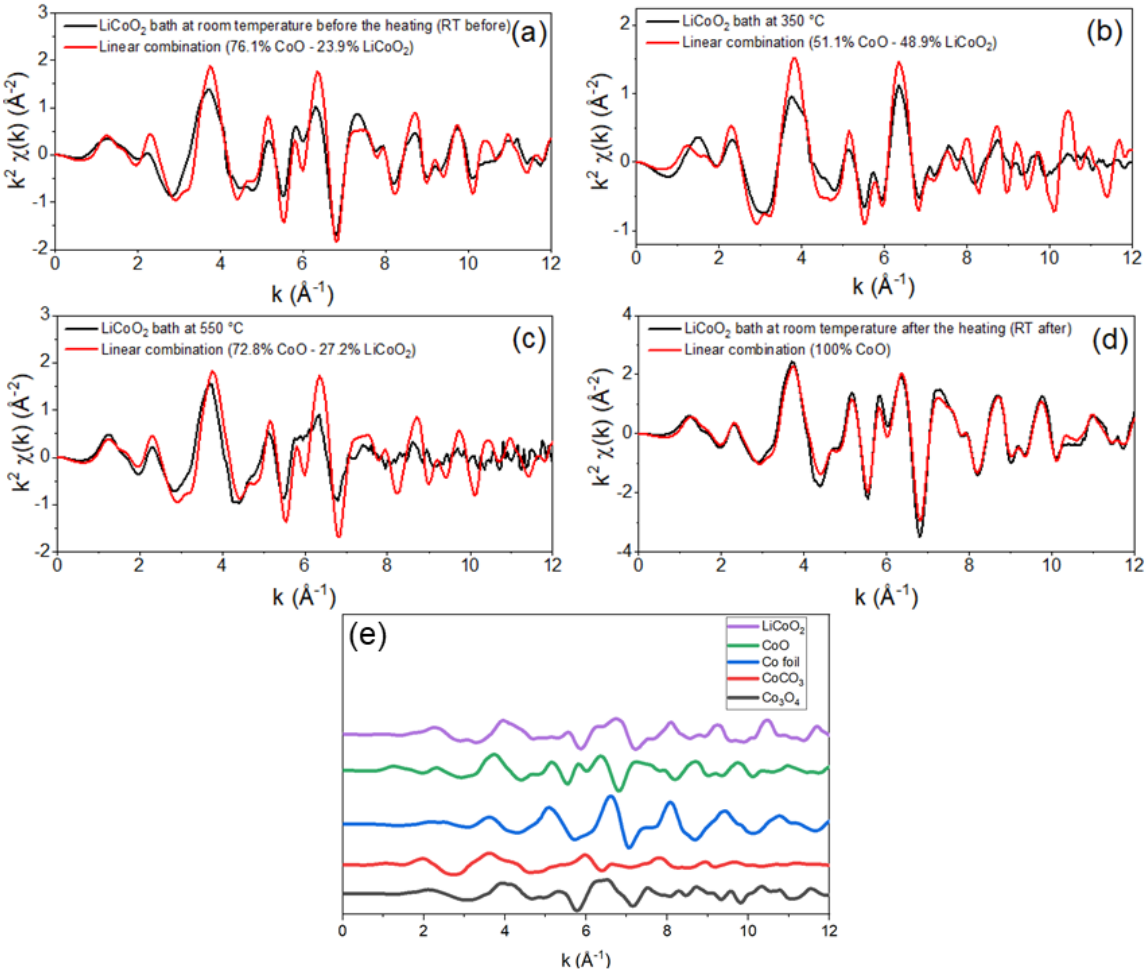

Figure 27 : Experimental and linear combinations of EXAFS contributions for $LiCoO_2$ bath at different temperature conditions: room temperature before heating (a), 350 °C (b), 550 °C (c), room temperature after heating (d). EXAFS experimental data for reference compounds

In the case of $LiCoO_2$ in molten carbonates, these reference compounds are the crystalline solids previously used for the calibration curve: $LiCoO_2$, CoO, $CoCO_3$ and Co metallic.Figure 27 (a), (b), (c) and (d) show the comparisons between the linear combinations and the experimental EXAFS contributions, for LCO in Li_2CO_3-Na_2CO_3-K_2CO_3 eutectic at different temperatures. Figure 27 (e) exhibits the EXAFS experimental data of references compounds. Only two components, CoO and $LiCoO_2$, were sufficient to model the spectra. The fits are rather good for the RT before heating and at 350°C and it is excellent at RT after heating. In the melt (550°C), the fit misses a part of the experimental data. The residue does not correspond to any individual component of Co-O or Co-Co (first coordination sphere) that can be extracted from any of the solid reference spectra. The missing component may come from cobalt ions dissolved in the melt, which was the main expected component. The fact that it is possible to model the XAFS spectra with solid seems to indicate that the cobalt is mostly in the

form of small aggregates in the bath and not dissolved ions. A slight decrease in the oxidation state is observed for NCA, Co_3O_4 and NMC baths. $CoCO_3$ bath is analyzed at room temperature before the heating as the transmitted signal was too low to carry out the measurement at high temperatures. This explains the absence of decrease of the oxidation state.

This result needs to be confirmed by running X-ray absorption experiment over a longer duration, about several days that correspond to the standard duration of electrochemical experiments described in the following chapter.

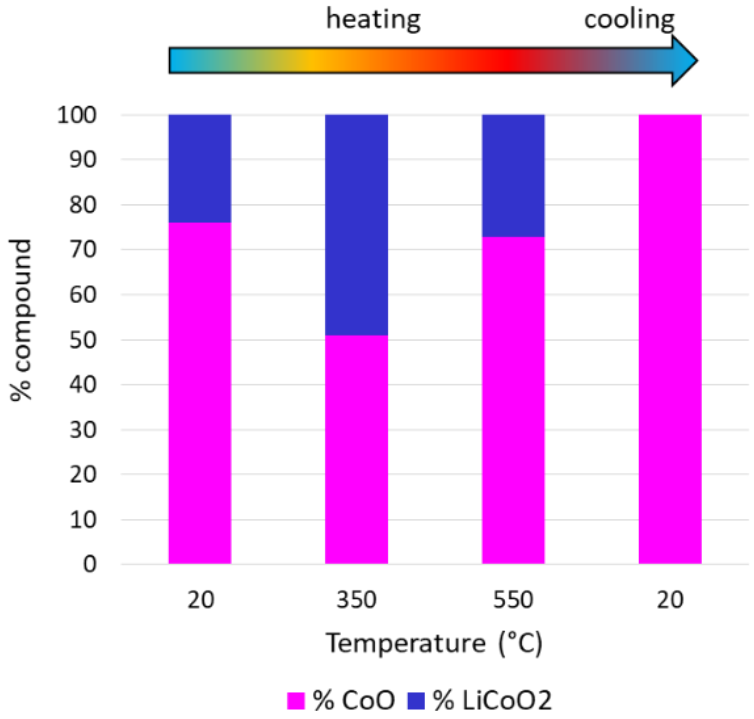

Figure 28 : Evolution of CoO and $LiCoO_2$ proportion in $LiCoO_2$ bath as function of heating temperature

The evolution of the CoO and $LiCoO_2$ proportion during the experiment is depicted in Figure 28. The most dominant component is CoO, which decreases in a first step and then increases until it becomes the only component left. The transformation of the $LiCoO_2$ to CoO raises the question of the role played by the graphite in the mechanism. After the experiment, the cell has been opened and black deposit were observed within the salt. To check that no reaction occurred between the salt (Li_2CO_3-Na_2CO_3-K_2CO_3 eutectic) and the graphite cell, X-rays diffractograms of the sample before and after the EXAFS experiments have been recorded. Both diffractograms superimpose indicating that no parasite reaction occurred. It must be noted

that the graphite cell has been prepared and closed in air atmosphere, leading to the presence of oxygen within the cell that could induce the slight oxidation observed at 350°C; the procedure could hence be improved by preparing the samples and the cells inside a gloves box.

The EXAFS spectrum of the sample at room temperature after experiment shows that only CoO compound is present. This result is in quite disagreement with the XANES analysis that indicates an average oxidation state of Co of 1.4 instead of 2 for CoO. Though the method chosen here for the determination of oxidation state in the XANES part is sensitive to the choice of the integral value, it is interesting in the case of mixtures of compounds like in our samples.

To sum up, in-situ EXAFS analysis shows divergences compared to the precedent one (in-situ XANES). In-situ XANES analysis illustrates a supplementary reduction than expected for the total system (mixture of Co (II) and metallic cobalt presence). On the other hand, EXAFS analysis shows a mixture of Co (III) and Co(II) in the system. Nevertheless, the general trend is similar for both results: a reduction of Co(III) of cathode material into Co(II). Further experiments need to be done in the future to verify these results.

3. Conclusions

The development of a whole setup to measure the absorption spectrum of cobalt at the K-edge in molten carbonate has been carried out to investigate the oxidation state and the speciation of cobalt dissolved in these media. The setup has been proven to provide reliable conditions to perform measurements at 550°C for several hours.

It has been possible to determine the cobalt oxidation state and the solid compound formed in the cooled bathes of the electrochemical experiments in one hand and in another hand to follow the cobalt behavior *in situ* when these bathes are put into the molten state again. The results clearly show that the oxidation state of cobalt is reduced from +III to +II in molten Li_2CO_3-Na_2CO_3-K_2CO_3 eutectic for all standard cathode materials LCO, NMC and NCA. For LCO cathode material, it is transformed into CoO. Furthermore, in the running conditions of synchrotron experiments, i.e. experiments that last 3-4 hours, cobalt stays mainly in CoO aggregates at 550°C and is not dissolved in isolated ions as expected.

Chapter III: Study of Li-ion battery compounds in molten carbonates medium

"J'ai appris que la voie du progrès n'était ni rapide ni facile."
Marie Curie

1. Introduction

As mentioned in chapter one the main objective of this project is to determine the feasibility of recycling Li-ion battery organic and inorganic compounds in molten salts. Alkali carbonates show the capacity of decomposing organic compounds[55] due to their oxoacidity properties. This characteristic makes alkali carbonates good molten solvent candidates for this project. This chapter is dedicated to the study the behavior of some particular Li-ion batteries cathode materials, containing cobalt (in form Co^{III}): LCO, NCA, NMC in molten carbonates. The challenge of recovering cobalt from these materials requires a deep comprehension of its behavior in this medium as oxide and lithiated oxide. The scientific community has made efforts in studying cobalt oxides in these systems with the aim of using it as cathode compounds in molten carbonates fuel cells (MCFC).

Concerning cobalt oxide, a vast study has been carried out on the behavior of cobalt oxide Co_3O_4 behavior in binary systems. Mendoza *et al*. have investigated deposited thin films of this oxide on nickel substrates in (52 mol % Li_2CO_3-48 mol % Na_2CO_3),in a mixture of air/CO_2 70/30 (mol%) at 650 °C[117,118]. Their X-ray diffraction (XRD) and X-ray photoelectron spectroscopy (XPS) results show that Co_3O_4 is transformed spontaneously within some minutes in $LiCoO_2$ which seems to diffuse in nickel substrates within some hours (less than 50h). Co_3O_4 dissolution in the same melt and atmosphere was later reported by Escudero *et al*.[119], by using Induced Couple Plasma- Atomic Emission Spectroscopy (ICP-AES) technique. This study reported a value of 3.5 wt.ppm or 1.2 10^{-7} mol.cm^{-3} after 50h in the melt.

Several studies of lithiated cobalt oxide $LiCoO_2$ behavior in molten carbonates have been reported. Veldhuis *et al* studied this compound in molten (62 mol % Li_2CO_3-38 mol % K_2CO_3) at 650°C with 66% CO_2-33% O_2 [120]. They proved by square wave voltammetry that Co(II) is the single electroactive specie in the melt and $LiCoO_2$ transformation into CoO in the medium is presumed to be possible. Furthermore, their dissolution measurements obtained by ICP-AES showed that cobalt dissolution in the medium ranges between 2-13 wt ppm or (6.6 10^{-8} to 4.3 10^{-7} mol.cm^{-3}).

Ota *et al*. deepened the study of $LiCoO_2$ solubility dependency on the atmosphere and its saturation in 62 mol % Li_2CO_3-38 mol % K_2CO_3. They used an Ar-CO_2-O_2 mixture where they varied the CO_2 pressure with a fixed O_2 one and vice versa [121]. It has been proved by flame atomic absorption spectroscopy (F-AAS) that $LiCoO_2$ shows the best dissolution in the highest

oxoacidic (1 atm CO_2) and oxobasic (5.10^{-5} atm CO_2) atmospheres. Between both conditions, the fully oxoacidic atmosphere shows the highest dissolution (exceeding 60 mol ppm or $1.2\ 10^{-6}$ mol.cm^{-3} at 200 h, with no dissolution saturation detected) compared to a saturated value of 0.6 mol ppm or $1.2\ 10^{-8}$ mol.cm^{-3} at 200 h in oxobasic atmosphere. They proposed a reaction for both conditions which implies cobalt reduction into Co(II) in oxoacidic atmosphere and its oxidation into Co(IV) in oxobasic one. Furthermore, they studied the influence of temperature, between 600 and 800 °C, on $LiCoO_2$ dissolution by the same technique. Results show that in both conditions the dissolution increases with temperature. Table 8 summarizes the dissolution values seen in the literature and their experimental conditions.

Table 8 : Summary of cobalt compounds dissolution reported in the literature

Melt composition	**Cobalt compound studied**	**Atmosphere conditions**	**Cobalt dissolution value in mol. cm^{-3}**	**Authors**
52 mol % Li_2CO_3-48 mol % Na_2CO_3	Co_3O_4	air/CO_2 70/30 (mol%)	$1.2\ 10^{-7}$ mol.cm^{-3} at 50 hours	Escudero *et al.*[119]
62 mol % Li_2CO_3-38 mol % K_2CO_3	$LiCoO_2$	66% CO_2-33% O_2	$6.6\ 10^{-8}$ - $4.3\ 10^{-7}$ mol.cm^{-3}	Veldhuis *et al.*[120]
62 mol % Li_2CO_3-38 mol % K_2CO_3	$LiCoO_2$	1 atm CO_2	About $1.2\ 10^{-6}$ mol.cm^{-3} at 200 h	Ota *et al.*[121]
62 mol % Li_2CO_3-38 mol % K_2CO_3	$LiCoO_2$	5.10^{-5} atm CO_2	$1.2\ 10^{-8}$ mol.cm^{-3} at 200 h	Ota *et al.*[121]

Regarding one of the aims of this project, recovering cobalt from Li-ion batteries, several important aspects are to be considered from the literature. The choice of a working oxoacidic atmosphere seems to be the most suitable as $LiCoO_2$ dissolution appears to be the highest (about $1.2\ 10^{-6}$ mol.cm^{-3} with not saturation detected over 200h) in this condition (1 atm CO_2)[121].

Lithium-containing molten salts systems seem to appear as a good option as $LiCoO_2$ shows almost a double dissolution in this kind of mixture compared to a lithium-free mixture in the same experimental conditions. Nevertheless, low solubility of $LiCoO_2$ in molten carbonates (maximal value reported around $1.2\ 10^{-6}$ mol.cm^{-3} seems to represented an important potential difficulty for recovering cobalt from this cathode material in molten carbonates.

Eutectic 43.5 mol % Li_2CO_3- 31.5 mol % Na_2CO_3- 25% K_2CO_3 lithium containing mixture is the chosen mixture for the aim of this project for several reasons: its low melting point at 397°C compared to binary systems (less energy intensive heating) and no cobalt behavior been reported in this molten medium. Inspiring Veldhius *et al.*, Ota *et al.* previous

works, we will report the kinetics and quantify cobalt dissolution for LCO, NCA and NMC in this ternary system. Furthermore, we will explore the possibility of recovering cobalt from this medium by electrolysis. Finally, preliminary studies of Li-ion battery organic compounds (binders and separator) decomposition in molten carbonates will be discussed. The attention will be concentrated on three Li-ion battery compounds currently used: polypropylene (PP), carboxymethyl cellulose (CMC) and polyvinylidene fluoride (PVDF).

2. Experimental part

The first part of this section presents the set-up used for the different experiments done in molten carbonates: furnace, heating cells, precursors used and molten salts mixing protocol. In a second place the experimental conditions used for the electrochemical characterizations are presented. Finally, we describe experimental conditions used for the other characterizations. Figure 29 shows the schema of the different stages used for studying cobalt in the molten ternary eutectic Li_2CO_3-Na_2CO_3-K_2CO_3.

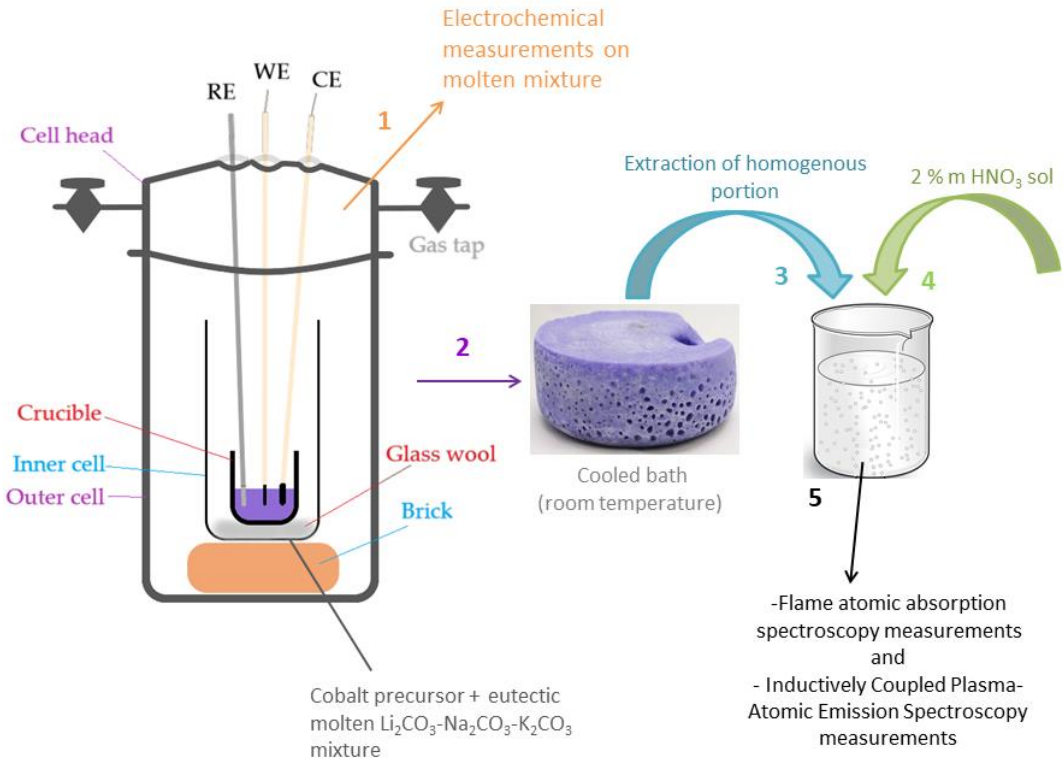

Figure 29 : Process schema used for cobalt study in molten ternary eutectic Li_2CO_3-Na_2CO_3-K_2CO_3

2.1. Experimental set-up

The furnace

For all the experiences a vertical furnace was used. It heats up to the maximum temperature of 900°C. It consists of an alumina vertical tubular center and most likely a type of Kanthal wire wrapped around it for heating. The heating is thus achieved by the Joule effect. The whole is contained in a steel casing. Temperature control is managed by a Eurotherm control system which enables the melt to be kept at 450 ±1°C consistently throughout all experiments.

Heating cell

For experiments in the eutectic binary system 56 % mol Na_2CO_3- 44 % K_2CO_3

The heating cells were composed of an inner and outer steel cell. Inside the inner one an alumina crucible containing the salts mixture was placed. The inner steel cell was placed in an outer and larger steel cell, which was closed at the top with a steel head. Both pieces were sealed by a lid seal and the locking ensured by screws.

For experiments in the eutectic ternary system 43.5 % Li_2CO_3-31.5 % mol Na_2CO_3-25% K_2CO_3

The heating cells were constituted of an internal Pyrex cell containing a thin layer of glass-wool at the bottom to ensure homogenous heating. Inside of it, a glassy carbon crucible containing the salts mixture was placed. The inner Pyrex cell was placed in an outer and larger Pyrex cell, which was closed at the top with a Pyrex cell head. Both pieces were sealed using silicone-free high vacuum Apiezon H grease, suitable for high temperatures. Two metallic closing pieces joined by screws were used in order to isolate both Pyrex pieces from the room atmosphere.

Molten salt container (crucible)

The molten salts were melted in glassy carbon crucibles from HTW SIGRADUR, in the case of experiments carried on Li_2CO_3-Na_2CO_3-K_2CO_3. For the experiments done in the eutectic system Na_2CO_3-K_2CO_3 alumina crucibles from SCERAM with a purity of 99.7% were used.

Precursor compounds and molten salts used

Table 9 shows the different chemical compounds used for the experiments in molten carbonates: cobalt precursors and alkali carbonates

Table 9 : List of chemical compounds used

Compound	Form	Purity	Supplier
Li_2CO_3	Powder	>99.8 %	AnalaR NORMAPUR for analysis
Na_2CO_3	Powder	>99.8 %	AnalaR NORMAPUR for analysis
K_2CO_3	Powder	>99.8 %	AnalaR NORMAPUR for analysis
$CoCO_3$	Powder	-	Synthethised at the laboratory
Co_3O_4	Powder	≥99.99%	Merck
$LiCoO_2$	Powder	99.8%	Merck
$LiNi_{0.82}Co_{0.15}Al_{0.03}O_2$	Powder	-	SAFT
$LiNi_{1/3}Co_{1/3}Mn_{1/3}O_2$	Powder	-	SAFT

All the salts and cobalt precursors were dried under vacuum at 200 °C for 72h. The cobalt precursors were then stored in a glove box and carbonates salts in the oven at 200 °C.

Eutectic Li_2CO_3-Na_2CO_3-K_2CO_3 and cobalt precursor mixture preparation

The eutectic mixture is composed of 31, 5% mol Na_2CO_3, 43,5 % Li_2CO_3 and 25% mol K_2CO_3. The quantity of cobalt precursor used was weighted in glove box to avoid the compound to take moisture. Weighting carbonates was done very quickly under air and then manually grinded with the cobalt precursor for 30 minutes. The grinded mixture was then put into a glassy carbon crucible.

All the experiments were performed under CO_2 atmosphere, a flow of 38 mL min^{-1}. Furthermore, 50 mL of molten salts were used and a cobalt concentration 2.5×10^{-5} mol. cm^{-3} for each bath. The temperature of the bath ramps up to 450°C by step of 3°C per minute. The density of the eutectic molten Li_2CO_3- Na_2CO_3-K_2CO_3 system is 2.11 g cm^{-3} at 450°C [122]. The Figure 30 (a) shows the phase diagram of the ternary system Li_2CO_3- Na_2CO_3-K_2CO_3[123]. The heating period was around 168h for each experiment.

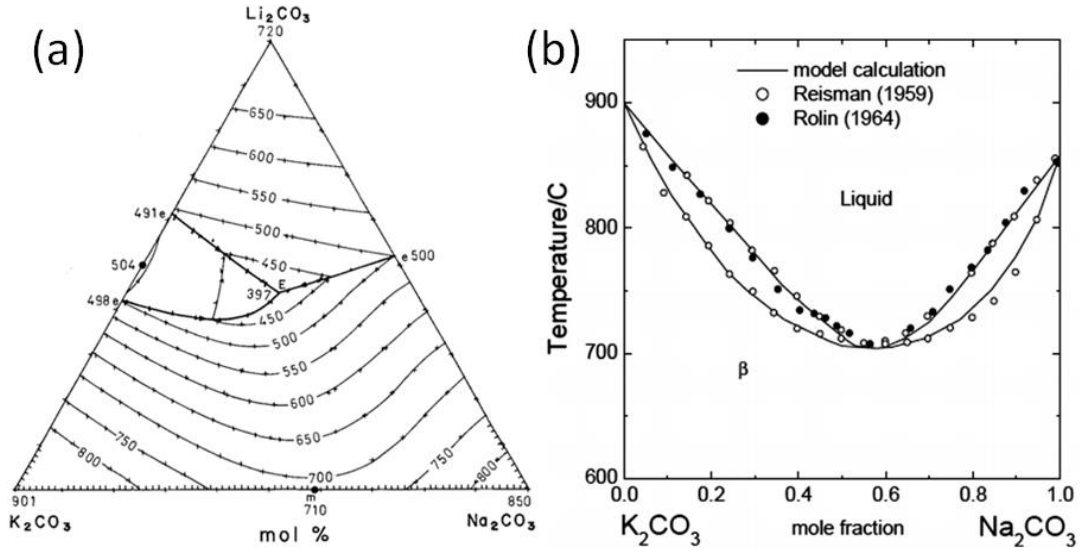

Figure 30 : Diagram of the ternary system Li_2CO_3- Na_2CO_3-K_2CO_3 with T (°C) [123] on (a). Phase diagram of the binary system Na_2CO_3-K_2CO_3 with T (°C) on (b)[124]

Eutectic Na_2CO_3-K_2CO_3 preparation

The eutectic mixture is composed of 56% mol Na_2CO_3 and 44% mol K_2CO_3. Weighting carbonates was done very quickly under air and then manually grinded for 30 minutes. The grinded mixture was then put into an alumina crucible. The temperature of the bath ramps up to 800°C by step of 3 °C per minute. Figure 30 (b) shows the phase diagram of the binary system Na_2CO_3-K_2CO_3.

Preliminary studies of metallic cobalt dissolution in eutectic (56% Na_2CO_3-44% K_2CO_3) at 800°C were carried out. A mixture of 0.1 atm CO_2- 0.9 atm Ar was the initial atmosphere conditions of all the experiments done in this molten medium with a total flow of 25 mL min^{-1}. Then, the atmosphere was gradually changed into a more basic one by the cutoff of CO_2 followed by the addition of Na_2O oxide. A 0.5 mm thick massive plate of cobalt was immersed in the molten mixture at the beginning of the experiment. Cobalt dissolution was measured by Inductively Coupled Plasma - Atomic Emission Spectroscopy (ICP-AES) with portions of the melt taken over time.

2.2. Electrochemical measurements

Cyclic voltammetry

Cyclic voltammetry allows a deep characterization of an electrochemical system. With the aim of recovering cobalt by electrolysis, the comprehension of its electrochemical behavior was explored by this technique.

For cobalt dissolution investigations in molten carbonates, cyclic voltammograms were recorded with EG&G Princeton Applied Research potentiostat/galvanostat Model 273A. For all the measurements, the potential was swept from the open circuit potential (OCP) towards the cathodic one and vice versa to complete the cycle. The potential range sweep was adapted for each precursor in order to observe the totality of cobalt electrochemical potential range.

Chronoamperometry

For exploring cobalt recovery by electrodeposition in molten carbonates, chronoamperometry technique was used. All the measurements were carried out with EG&G Princeton Applied Research potentiostat/ galvanostat Model 273A. The potential steps, for each measurement, were applied from the open circuit potential (OCP) to the cathodic potential corresponding to cobalt reduction on the working electrode.

Electrodes

A three-electrode system has been used for all the electrochemical measurements.

-The reference electrode: a pseudo-reference electrode composed of pure cobalt 4.2 mm diameter rod welded to a steel tube. This electrode was chosen as it enables to avoid the liquid junction potential that is present in Ag^{I}/Ag^{0} references. The cobalt (purity : 99.99%) was provided by Goodfellow.

-The counter electrode: An 8 mm diameter graphite rod (Carbon Lorraine) was connected to a 1 mm diameter copper wire. Both materials have been chosen as they show good electrical properties and they are cheap. Moreover, graphite does not pollute the melt as it does not oxidize when current is applied.

-The working electrodes:

- A 1 mm diameter silver wire 99.99 % pure from Goodfellow

- A glassy carbon plate with the dimensions: 10mm * 25.4mm, and thickness of 3mm, from HTW SIGRADUR, which is connected to a 1 mm diameter copper wire.

The plunged length of the working electrodes was measured with a caliper at the end of the measurements. All the electrodes were cleaned in a 1 mol HCl solution, then rinsed with distilled water and dried. The metallic wires and rods constituting the different electrodes were then polished with sandpaper (SiC paper # 1200, Struers), rinsed with ethanol and then dried. The working and counter electrode wires were maintained in the molten system by an alumina sheath with a 4mm diameter, from SCERAM.

2.3. Other characterizations

X-ray Diffraction (XRD)

This technique has been used for analyzing the deposit from electrolysis. We have used for our measurements D8 ADVANCE powder diffractometer from BRUKER. It has a Cu target and 1D detector Lyn Eye from BRUKER. For the measurements we used Bragg-Brentano scan type. All the measurements were done at room temperature and atmosphere.

Thermogravimetry analysis (TGA- DSC)

Thermogravimetry analysis was used to determine the compound thermal stability of $CoCO_3$ reference compound. The measurements were done on a thermogravimeter SETSYS Evolution from SETARAM. The initial mass used for the measurements was of 25,2 mg. Its mass loss evolution was monitored from 20 to 700 °C at 5 °C/min under CO_2 atmosphere.

Flame Atomic Absorption Spectroscopy (F-AAS)

Flame atomic absorption spectroscopy was used to determine the dissolved cobalt concentration in the molten media for cobalt reference compounds and the studied Li-ion battery cathode materials. For the F-AAS measurements a solution was prepared with: a grinded portion of the homogenous zone of the cooled bath (after electrochemical measurements) and a 2% mass HNO_3 solution. The measurements were done on Atomic Absorption Spectrometer PinAAcle 500 from PerkinElmer, which has a precision of 2-3%.

Inductively Coupled Plasma- Atomic Emission Spectroscopy (ICP-AES)

Inductively Coupled Plasma-Atomic Emission Spectroscopy was also used to determine the dissolved cobalt concentration in the molten media. For the ICP measurements, a solution was prepared in the same way as for (F-AAS). The measurements were done on ICP-AES iCAP6200 Thermofisher spectrometer, which has a precision of < 5%. The vector gas was argon 4.5 Linde (min 99.995%).

3. Results and Discussion

3.1. Metallic cobalt dissolution

Recovering cobalt from Li-ion battery cathode materials may imply the formation of massive layers of deposit at the electrode during the electrolysis. For this reason, studying massive metallic cobalt behavior in molten carbonates appears as important for this project. Preliminary studies of metallic cobalt dissolution in eutectic Na_2CO_3-K_2CO_3 were carried out. For the experimental details see section 2.1 of this chapter. The results obtained for cobalt dissolution over time can be seen on Figure 31.

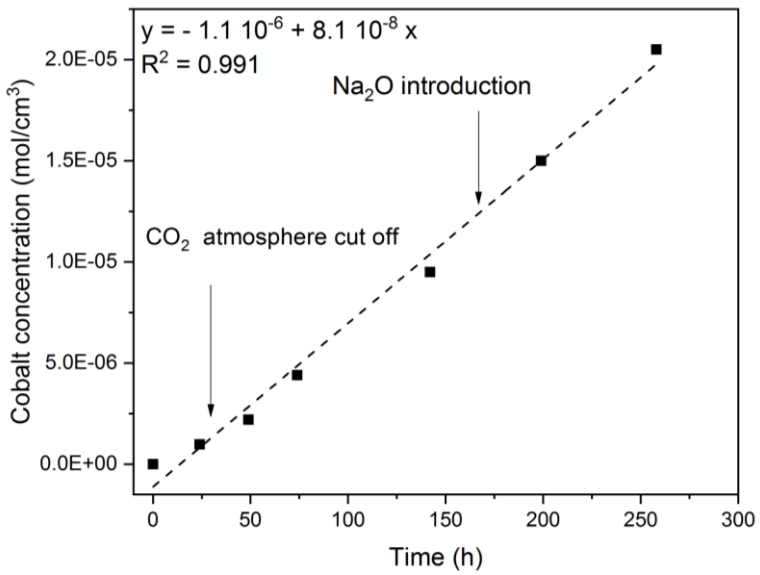

Figure 31 : Evolution of metallic cobalt (0.5 mm thick massive plate) dissolution over time when the oxobasicity is increased in eutectic Na_2CO_3- K_2CO_3, at 800 °C

Metallic cobalt solubility increases almost linearly with the time when the oxobasicity of the melt is increased (after 50 h of heating when the CO_2 flow is cut). The same trend is

observed even after the Na_2O introduction. This observation leads to the conclusion that Na_2O introduction does not play a major role in metallic cobalt dissolution increase.

In Figure 31, it can be observed that cobalt dissolution increase is slow and low over the time (after 225 h of heating in the absence of CO_2 atmosphere, a dissolution of 2.10^{-5} mol.cm^{-3} is detected) and not saturation is observed after the total heating time (225h). These results confirm previous studies carried out by P. Tomczyk *et al*[125] ,and Yang *et al* [126,127] , which show the existence of a non-zero dissolution of metallic cobalt (0.05-1 µm thick films) in molten carbonates. Massive metallic cobalt shows a higher dissolution compared to that of thin layers which is about 2 times higher than the one reported by Yang *et al* for thin layers ($1.8\ 10^{-5}$ molar fraction or $3.5\ 10^{-7}$ mol. cm^{-3} at 100 h of immersion)[126], after the same time of immersion in the melt. This may be explained by the difference of oxobasicity of the melt between these results and the literature[126] after 100 h of immersion. The existence of a non-negligible dissolution of metallic cobalt could be a significant difficulty for its recovery by electrolysis.

3.2. Electrochemical behavior of cobalt in molten carbonates

In this section, three different forms of cobalt precursors were studied in molten carbonates Na_2CO_3-Li_2CO_3-K_2CO_3 eutectic system. First, the study of molten carbonates mixture without cobalt was realized in order to define the electrochemical active window. Then $CoCO_3$ and Co_3O_4 were studied as reference compounds. Finally, the behavior of three cathode materials actually present in the Li-ion batteries market: $LiCoO_2$ (LCO), $LiNi_{0.82}Co_{0.15}Al_{0.03}O_2$ (NCA) and $LiNi_{1/3}Co_{1/3}Mn_{1/3}O_2$ (NMC) are presented. Table 10 summarizes the oxidation states of the cobalt precursors studied in this chapter.

Table 10 : List of cobalt precursors studied in molten carbonates

Compound type	Compound formula	Compound oxidation degree
Reference	$CoCO_3$	Co (II)
Reference	Co_3O_4	Mixture of 1x Co (II) and 2 x Co (III)
Cathode material	$LiCoO_2$	Co (III)
Cathode material	$Li\ Ni_{0.82}Co_{0.15}Al_{0.03}O_2$	Co (III)
Cathode material	$LiNi_{1/3}Mn_{1/3}Co_{1/3}O_2$	Co (III)

3.2.1. Determination of the diffusion coefficient

For electrochemical studies, it is necessary to acquire the values of different parameters: cobalt diffusion coefficient and the number of electrons exchanged at the electrode during the reduction and oxidation reactions, to determine dissolved cobalt concentration in the medium. In our case, we have approximated the diffusion coefficient value to the autodiffusion coefficient one, as no reference compound in this medium has been found to determine the diffusion coefficient by electrochemical means (see section 3.2.3). The cobalt autodiffusion coefficient in the medium can be calculated by the Stokes-Einstein relation, which links the autodiffusion coefficient of the active specie with the electrolyte viscosity by the following equation (Eq. 27):

$$D_{M^{x+}} = \frac{k_B T}{6\pi\eta R} \qquad \text{(Eq. 27)}$$

Where:

$D_{M^{x+}}$: the diffusion coefficient of the active specie in $m^2.s^{-1}$, in this case $D_{Co^{+II}}$

k_B: the Boltzmann contant $1.38\ 10^{-23}$ in $J.K^{-1}$

T: the temperature in K

η: the viscosity in Pa.s

R: the radius of the spherical particle in m

We applied (Eq. 27) to estimate diffusion coefficient $D_{Co^{+II}}$ in our system. From the literature, it is known that the viscosity of the eutectic ternary Li_2CO_3-Na_2CO_3-K_2CO_3 at 450°C is 36.8 mPa.s[128]. Furthermore, we know from XANES results in the first chapter, that cobalt oxidation in our carbonates mixture is +II. Two limit cases appear as we think of cobalt speciation. It might form complexes with a long lifetime or with a too short one. We consider as hypothesis the coordination of 6 because cobalt is frequently in this coordination in compounds containing oxygen. In the first case, the radius of the spherical particle might be equal to $R = R_{Co(II)} + 2\ R_{C(IV)} + 2\ R_O^{-II}$, where $R_{Co(II)}$ is the radius of ionic cobalt Co^{+II}, $R_{C(IV)}$ the radius of C^{+IV} and R_O^{-II} the radius of O^{-II} . The corresponding values of ionic radius considered are equal to $R_{Co(II)} = 0.65$Å[129], $R_{C(IV)} = 1.4$ Å[129] and $R_O^{-II} = 0.32$ Å[129]. This leads to a spherical particle radius equal to 4.09 Å. The diffusion coefficient $D_{Co^{+II}}$ calculated with this value corresponds to 3.5 10-7 $cm^2.s^{-1}$. In the second limit condition, cobalt complexes lifetime might be too short, so that ionic cobalt is assumed to be alone in the molten medium most of

the time. In this situation, the spherical particle radius corresponds to 0.65 Å [129]. With this hypothesis, cobalt diffusion coefficient $D_{Co^{+II}}$ is equal to 2.2 10^{-6} $cm^2.s^{-1}$. In a molten salt system, the lifetime of a complex formed between ions is of around 10^{-11} or 10^{-12} s[130]. For this reason, we assumed that cobalt diffusion coefficient in our system is estimated to be of 2.2 10^{-6} $cm^2.s^{-1}$.

3.2.2. Electrochemical stability window of eutectic molten carbonates Li_2CO_3-Na_2CO_3-K_2CO_3 mixture

The voltammogram in Figure 32 shows the electrochemical window of molten carbonates. The starting potential point was 0.6 V vs Co^{II}/Co^0. The potential sweeps from the open circuit potential (OCP) towards the cathodic potentials and vice versa as indicated in Figure 32. The electrochemical window is about 2.8 V and it is delimited by the oxidation and reduction of molten carbonates according to (Eq. 28) and (Eq. 28):

At the anode:

$$2CO_3^{2-} \rightarrow 2CO_2 + O_2 + 4e^- \quad \text{(Eq. 28)}$$

At the cathode:

$$CO_3^{2-} + 4e^- \rightarrow C + 3O^{2-} \quad \text{(Eq. 29)}$$

Nine other peaks are present on the voltammogram: 6 anodic peaks noted as A_1, A_2, A_3, A_4, A_5, A_6 and 3 cathodic peaks: C_1, C_2 and C_3. Towards negative potentials, we can assume that the reduction of C-based species is observed and their further oxidation appears in peaks A_1, A_2 and A_3. Regarding the most oxidative potentials, (A_4, A_5, A_6) may be the oxidation of O-based species and their reduction are observed in peaks C_2 and C_3.

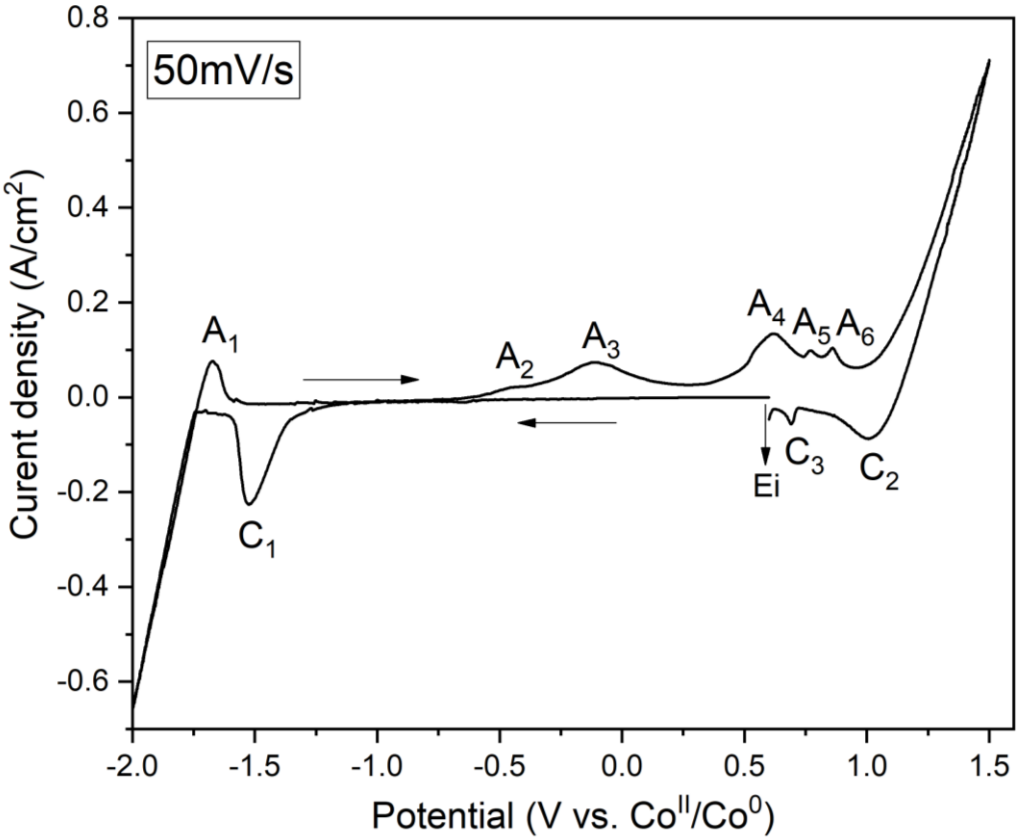

Figure 32 : Voltammogram of eutectic Li_2CO_3-Na_2CO_3-K_2CO_3 on silver wire working electrode at 450°C, 1 atm CO_2

No further experiments were carried out to study the carbon and oxygen systems as the interesting potentials for cobalt systems are in the range of [-0.5, +0.6V] vs. Co^{+II}/Co^0. In this range, only cobalt system is observed as shown in Figure 33 (a).

3.2.3. Cobalt references compounds $CoCO_3$ and Co_3O_4 in eutectic molten carbonates Li_2CO_3-Na_2CO_3-K_2CO_3 mixture system

Dissolution kinetics

To evaluate cobalt recovery feasibility in our studied melt, it is important to determine its dissolution kinetics and value. A recovery process to be considered as viable needs to fulfill two main conditions: an important dissolution of cobalt and in a short time. We show as example Co_3O_4 reference compound dissolution kinetics that has been studied by cyclic voltammetry, as shown in the Figure 33 (a).

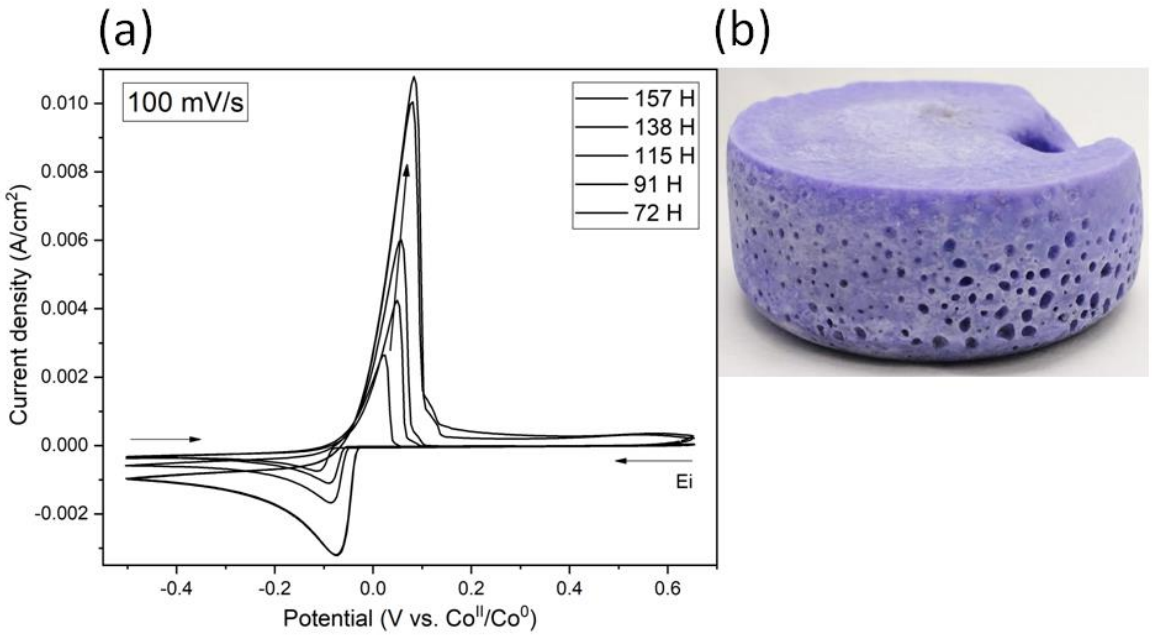

Figure 33 : (a) Voltammogram evolution in function of time of solution containing Co_3O_4 in molten eutectic ternary Li_2CO_3-Na_2CO_3-K_2CO_3, on silver wire working electrode at 450°C 1 atm CO_2. Appearance of the cooled bath after 157h of heating (b)

The potential sweeps from the open circuit potential at 0.6 V vs. Co^{II}/Co^0 to -0.5 V vs. Co^{II}/Co^0 and vice et versa (for details see experimental section 2.2 of this chapter). During all the heating process the presence of only one anodic and cathodic peak is detected. Both peaks are very close to 0 V, which confirms that cobalt redox system is observed. Figure 33 (a) shows that for the same scan rate (100mV/s) there is an increase in the both peaks current density over time until the saturation, which is achieved at about 157h. This result leads to the conclusion that cobalt dissolution kinetics is slow in this molten medium. We know from the literature that Co_3O_4 transforms into $LiCoO_2$ in lithium containing salts[118,117]. From this transformation, we did not expect dissolution saturation after this period of heating hours, as Ota *et al*. did not detect it over 225h in the same atmosphere conditions[121].

The dissolution of cobalt in the molten melt was confirmed by the physical aspect of the bath at the end of the heating period for both reference compounds, as seen in Figure 33 (b). The purple color of the solidified bath can be attributed to cobalt as molten carbonates mixture alone is white.

Looking for a reference compound

First, $CoCO_3$ has been chosen as reference compound for studying cobalt behavior in molten carbonates, as Co(II) is supposed to be more soluble than Co(III). To verify the possibility of considering $CoCO_3$ as a reference compound, the thermal stability of this compound has been studied by thermogravimetric analysis as shown on Figure 34.

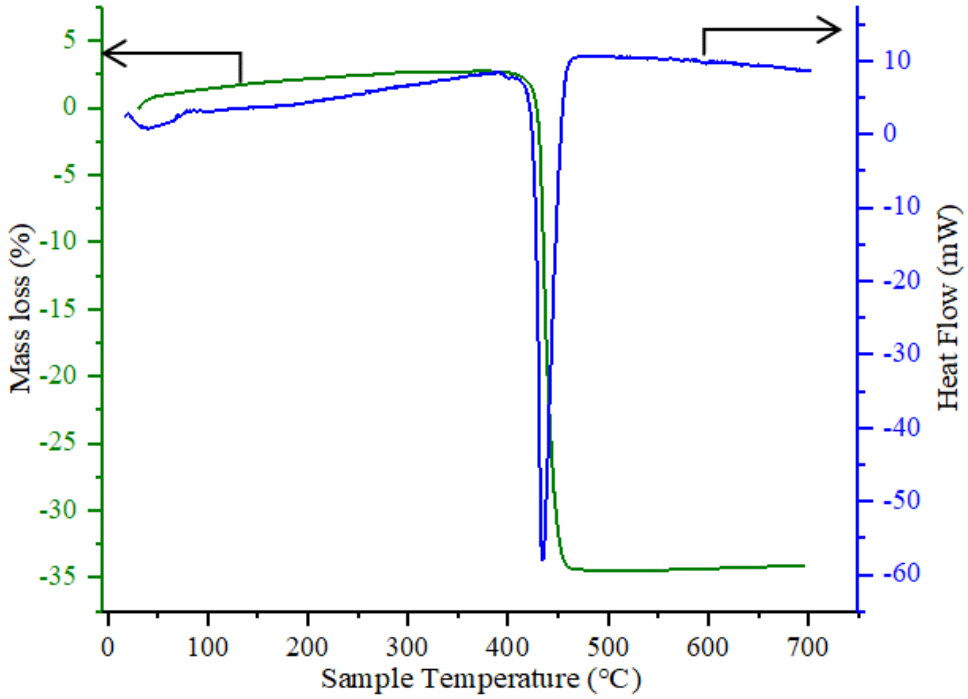

Figure 34 : Thermogravimetric analysis of $CoCO_3$ between 20 to 700 °C at 5 °C/min under CO_2 atmosphere

An important endothermic peak at around 400 °C is detected in Figure 34. In order to identify the reaction corresponding to the endothermic peak seen at 400 °C, the remaining product has been analyzed by X-ray diffraction (XRD), seen in Figure 35. As observed, there are two important peaks present on the XRD measurement which correspond to CoO structure.

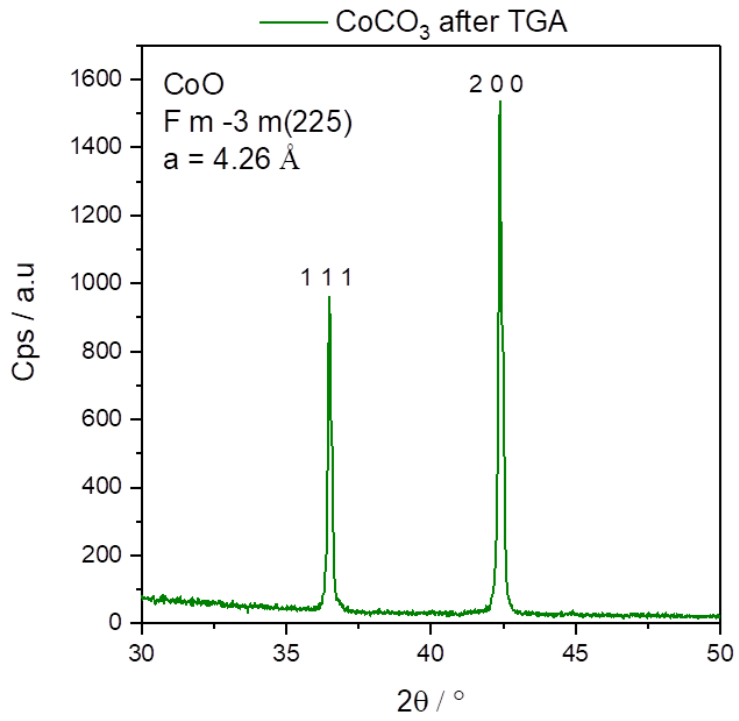

Figure 35 : X-ray diffraction measurement of $CoCO_3$ after thermogravimetric analysis (TGA-DSC)

The reaction that takes place is shown on (Eq. 30):

$$CoCO_3 \rightleftarrows CoO + CO_2 \qquad \text{(Eq. 30)}$$

The mass loss percentage observed by ATG-DSC is 35%. This mass percentage is consistent to CO_2 loss with respect to (Eq. 30).

From the thermal stability study of $CoCO_3$, it can be concluded that for all the following electrochemical studies that are shown for $CoCO_3$ as starting material, it is in reality CoO that is observed in the molten medium. As a consequence, $CoCO_3$ does not constitute a real reference compound in molten carbonates because it decomposes below the working temperature (450°C). Even if the $CoCO_3$ is not stable, it is still a Co(II) species that are present.

Electrochemical characterization

Three techniques have been used for quantifying cobalt dissolution in the molten medium: Cyclic Voltammetry (CV), Flame Atomic Absorption Spectroscopy (F-AAS) and Inductively Coupled Plasma- Atomic Emission Spectroscopy (ICP-AES). Figure 36 shows the

cyclic voltammograms of both reference compounds $CoCO_3$ and Co_3O_4. One anodic and one cathodic peak are observed in each case, whose position slightly varies depending on the measurement's scan rate. Table 11 shows the details concerning peaks potentials positions and the measurement starting potential for $CoCO_3$ and Co_3O_4. For the measurement details see experimental section 2.2 of this chapter. The proximity of the reduction peaks to zero (about 100 mV shift from zero) in Figure 36 confirms the presence of dissolved cobalt in the medium. Nevertheless, as a cobalt pseudo-reference has been used for the electrochemical measurements, it was expected that cathodic peak would appear at 0 V. This difference can be explained by the presence of an overpotential.

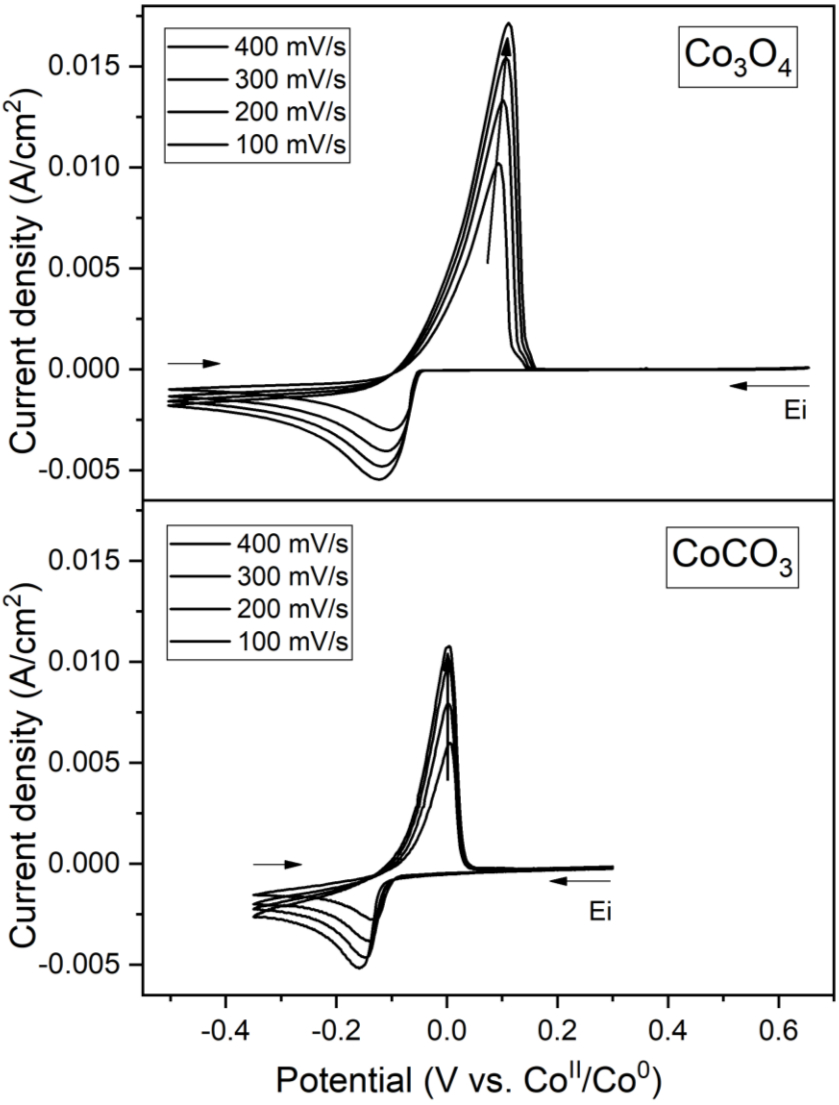

Figure 36 : Voltammograms of the solution containing Co_3O_4 and $CoCO_3$ in molten eutectic ternary Li_2CO_3-Na_2CO_3-K_2CO_3, on silver wire working electrode at 450°C (168h), 1 atm CO_2

Table 11 : Anodic peak, cathodic peak and starting measurement potentials of voltammograms containing Co_3O_4 and $CoCO_3$ in eutectic molten Li_2CO_3-Na_2CO_3-K_2CO_3

Compound	**Anodic peak position (V vs. Co^{II}/Co^0)**	**Cathodic peak position (V vs. Co^{II}/Co^0)**	**Measurement starting potential (V vs. Co^{II}/Co^0)**
$CoCO_3$	0.004±0.002	-0.138 ±0.015	0.300
Co_3O_4	0.102 ± 0.008	-0.109± 0.013	0.650

The presence of only one anodic and cathodic peak leads to the hypothesis that the dissolution of cobalt occurs only under the form of Co^{+II}. This statement was confirmed by XANES results, shown in chapter II, which proves that the dissolved cobalt in the molten medium has an oxidation state of +II. We know from the literature that Co_3O_4 transformed into $LiCoO_2$ in lithium-containing molten systems [117,118]. Furthermore, Veldhius *et al.* proved that Co^{+II} was the only electroactive species in $LiCoO_2$[120]. As a consequence, cobalt average oxidation state +II, determined by XAS measurements in the previous chapter, is in agreement with Veldhius *et al.* work. As conclusion, Co (III) is reduced into Co (II) in molten carbonates.

The voltammogram peaks morphology indicates the presence of a metal electrodeposition phenomenon. From these results, it can be concluded that the redox reactions taking place at the working electrode are given by the following equations (Eq. 31) and (Eq. 32):

The reduction reaction:

$$Co^{2+} + 2e^- \rightarrow Co \qquad \text{(Eq. 31)}$$

The oxidation reaction :

$$Co \rightarrow Co^{2+} + 2e^- \qquad \text{(Eq. 32)}$$

In the case of a metal electrodeposition phenomenon, cyclic voltammogram anodic and cathodic peaks are linked to the concentration of the active species in the medium by Berzins and Delahay equation (Eq. 33)[131, 132,133]:

$$I_{peak} = 0.61\, n^{\frac{3}{2}} SF\left(\frac{vDF}{RT}\right)^{\frac{1}{2}}[M^{x+}] \qquad \text{(Eq. 33)}$$

Where:

I_{peak}: the peak current detected by cyclic voltammetry in A

S: working electrode surface in cm^2

n: the number of exchanged electrons

v: the potential scan rate in $V.s^{-1}$

D: the diffusion coefficient of the active specie in $cm^2.s^{-1}$, in this case $D_{Co^{+II}}$

F: Faraday constant 96485 in $C.\ mol^{-1}$

T: the temperature in K

R: the ideal gas constant 8.314 in $J.mol^{-1}.K^{-1}$

$[M^{x+}]$: active specie M^{x+} concentration in the bulk, in $mol.cm^{-3}$, in this case $[Co^{+II}]$

This equation was used to determine the dissolved cobalt concentration $[Co^{+II}]$. Figure 37 shows the cathodic peak current density as function of the square root of the scan rate.

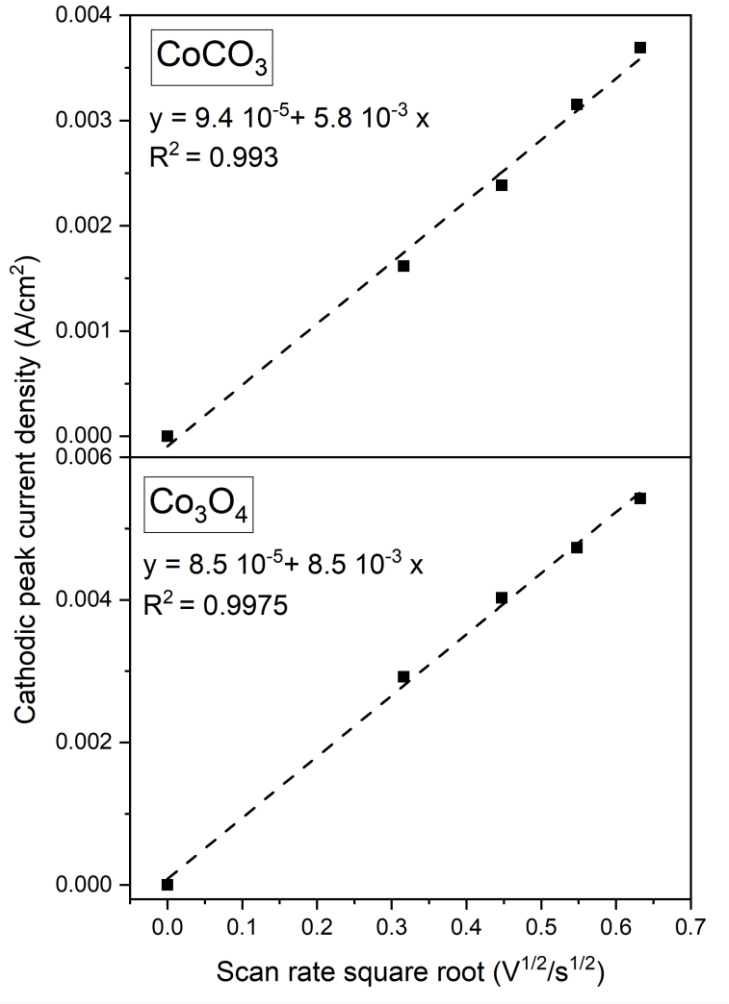

Figure 37 : Cathodic peak current density evolution in function of cyclic voltammetry scan rate square root for CoO and Co_3O_4 in eutectic ternary mixture Li_2CO_3-Na_2CO_3-K_2CO_3, at 450 °C, 1 atm CO_2

The slope value obtained from Figure 37 corresponds to $(0.61n^{\frac{3}{2}}F\left(\frac{D_{Co^{+II}}F}{RT}\right)^{\frac{1}{2}}[Co^{+II}])$. With this value, the respectively dissolved cobalt concentrations $[Co^{+II}]$ were calculated and compared with Flame atomic absorption spectroscopy (F-AAS) and Inductively Coupled Plasma- Atomic Emission Spectroscopy (ICP-AES) measurements, as shown in Table 12. For the details about the preparation of solutions and measurements for both techniques see experimental section 2.3 of this chapter.

Table 12 : Results of dissolved cobalt concentration $[Co^{+II}]$ for Co_3O_4 and $CoCO_3$ in eutectic molten Li_2CO_3-Na_2CO_3-K_2CO_3

Compound	$D_{Co^{+II}}$ **($cm^2.s^{-1}$)**	**Slope ($A.cm^{-2}.V^{-1/2}.s^{1/2}$)**	**Measured by CV $[Co^{+II}]$ ($mol.cm^{-3}$)**	**Measured by F-AAS $[Co^{+II}]$ ($mol.cm^{-3}$)**	**Measured by ICP-AES $[Co^{+II}]$ ($mol.cm^{-3}$)**
$CoCO_3$	$2.2\ 10^{-6}$	$5.8\ 10^{-3} \pm 0.2\ 10^{-3}$	$5.9\ 10^{-6}$	$0.98\ 10^{-6}$	$17.9\ 10^{-6}$
Co_3O_4	$2.2\ 10^{-6}$	$8.5\ 10^{-3} \pm 0.2\ 10^{-3}$	$8.6\ 10^{-6}$	$2.1\ 10^{-6}$	$25.8\ 10^{-6}$

Concentration values obtained by electrochemistry are well in between the values determined by flame spectroscopy and ICP-AES. It indicates that the estimated self-diffusion coefficient by Stokes-Einstein relation is correct. It must be underlined that the effect of matrix, in particular the presence of sodium, is a drawback for these analytical techniques. The values of dissolved cobalt concentration for Co_3O_4 are higher than the value reported in literature for Co_3O_4 ($1.2\ 10^{-7}$ $mol.cm^{-3}$ at 50h of cobalt exposure in the melt)[119]. This may be explained by the difference of oxoacidity between the experimental test (1 atm CO_2) and the literature (air/CO_2 70/30 (mol%) and the immersion time of cobalt in the molten melt (about 168h for the experiment and 50h in literature)[119].

3.2.4. Li-ion battery cathode materials in eutectic molten carbonates Li_2CO_3-Na_2CO_3-K_2CO_3 mixture system

Afterwards, we analyzed battery electrode materials. Three Li-ion battery cathode materials behavior were investigated in the molten medium: LCO, NCA and NMC. LCO behavior in this system was the first battery cathode material to be investigated as it contains only cobalt as transition metal. Secondly, NCA behavior was studied as it is constituted of two transition metals: nickel and cobalt. Finally, NMC behavior in molten carbonates was explored as it is composed of three transition metals: manganese, cobalt and nickel.

Dissolution kinetics

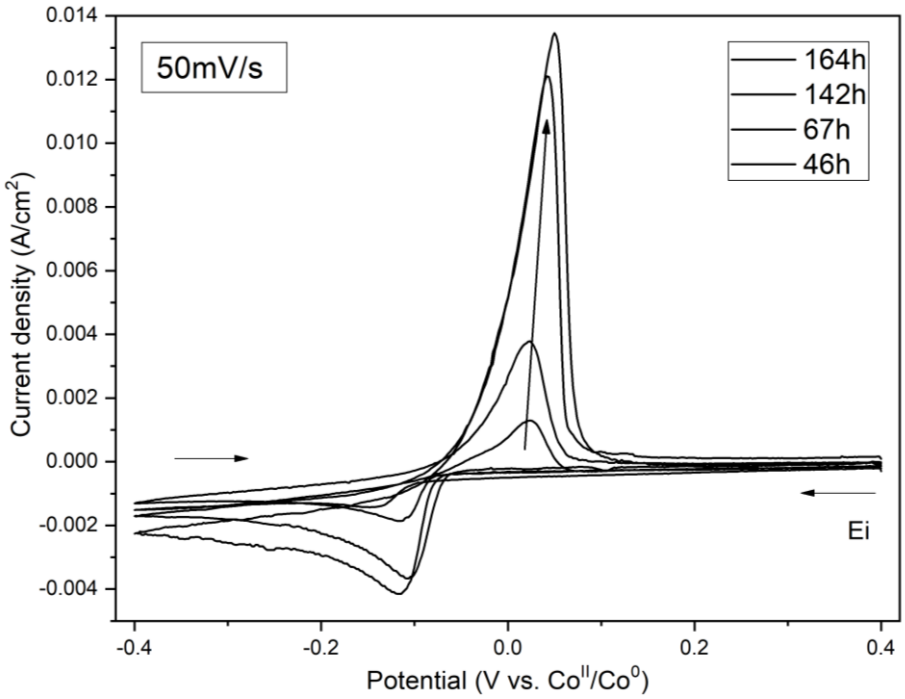

Figure 38 : Evolution of $LiCoO_2$ (LCO) voltammogram in function of time, in molten eutectic ternary Li_2CO_3-Na_2CO_3-K_2CO_3, on silver wire working electrode at 450°C (168h), 1 atm CO_2

Results from reference compounds dissolution over time (see section 3.2.3) show that the kinetics of the process is slow, about 160 h needed for maximal dissolution. To determine the feasibility of recycling valuable elements from Li-ion battery materials cathodes in a reasonable time the same study was carried out for LCO, NCA and NMC.

As an example, Figure 38 shows the cobalt dissolution evolution on time of LCO.A positive potential shift of the cathodic and anodic peaks is observed over time. For example, the cathodic peak potential varies from -0.14 (at 46h of heating) to -0.12 (at 164h of heating) V vs. Co^{II}/Co^0. The equilibrium of the reaction of each cathode material can be presumed to be reached at about 160 h because the voltammogram peaks intensity shows a low increase or almost no increase at all at this period of time. Concerning $LiCoO_2$ dissolution kinetics, it confirms Ota *et al.* results [121] as a slow process.

It can be concluded that cobalt dissolution from cathode materials was similar to reference compounds one. Furthermore, the same aspect of the solidified bath previously observed for reference compounds was obtained for each cathode material bath at the end of the heating.

The influence of the oxoacidity

As mention in chapter 1 in section 5.3.1.1, the level of oxoacidity in a molten carbonate medium is defined by (Eq. 7). Different oxoacidity levels have been tested to confirm the literature previous results which reported fully oxoacidic atmosphere (1 atm CO_2) as the optimal $LiCoO_2$ dissolution conditions[121,134]. Figure 39 (a) shows voltammograms obtained for $LiCoO_2$ in 3 oxoacidity levels: 100 % CO_2 (the highest acidity), 50% CO_2–50% Ar and 10% CO_2-90% Ar (the lowest oxoacidity).

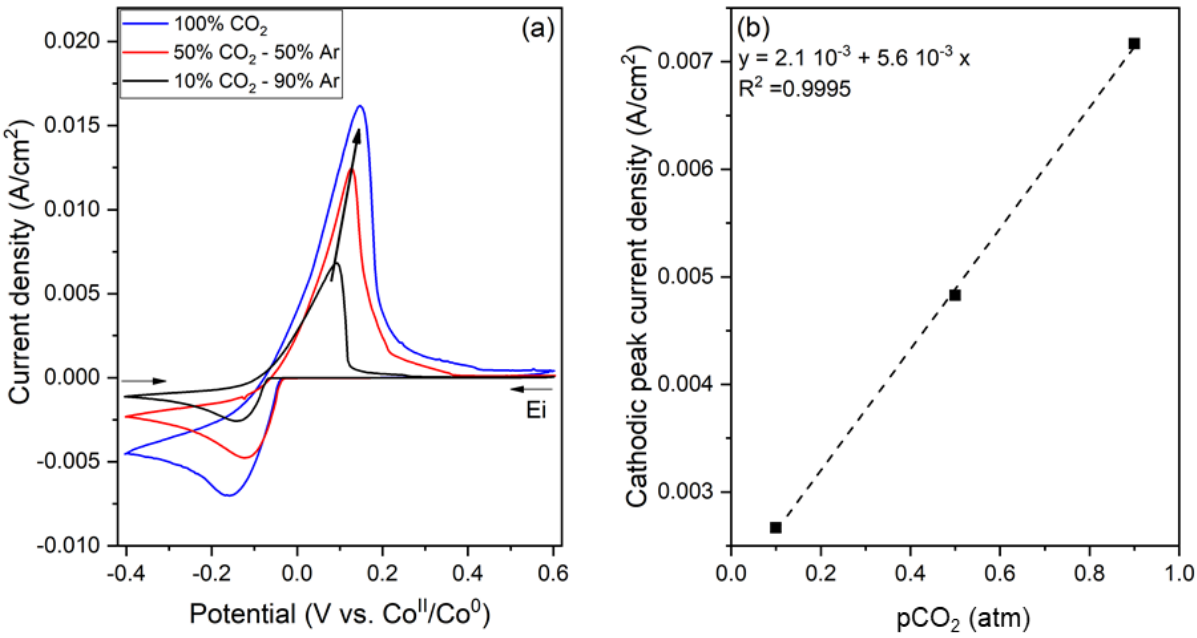

Figure 39 : Voltammogram evolution of the solution containing $LiCoO_2$ in molten eutectic mixture Li_2CO_3-Na_2CO_3-K_2CO_3 on silver wire working electrode at 450°C, as function of the oxoacidity level (a). Cathodic peak current density evolution as function of CO_2 partial pressure (b). Scan rate 100 mV/s

A shift in the cathodic peak and anodic peak toward the positive potential is observed with the increase of oxoacidity. From the voltammograms, the cathodic peaks current density has been analyzed as function of the medium oxoacidity (Figure 39 (b)). As observed, there is a proportional relation between the oxoacidity (increase in pCO_2 in the atmosphere) and the cathodic peak current density increase. These results are in agreement with those of Veldhuis *et al.*[120]l, Ota *et al.*[121] previous studies which reported the highest dissolution in fully oxoacidic conditions (1 atm CO_2).

Electrochemical characterization

Here we used the same methods used for quantifying the dissolution of the cobalt from reference compounds. Figure 40 shows the voltammograms of each cathode material: $LiCoO_2$ (LCO), $LiNi_{0.82}Co_{0.15}Al_{0.03}O_2$ (NCA) and $LiNi_{1/3}Co_{1/3}Mn_{1/3}O_2$ (NMC).

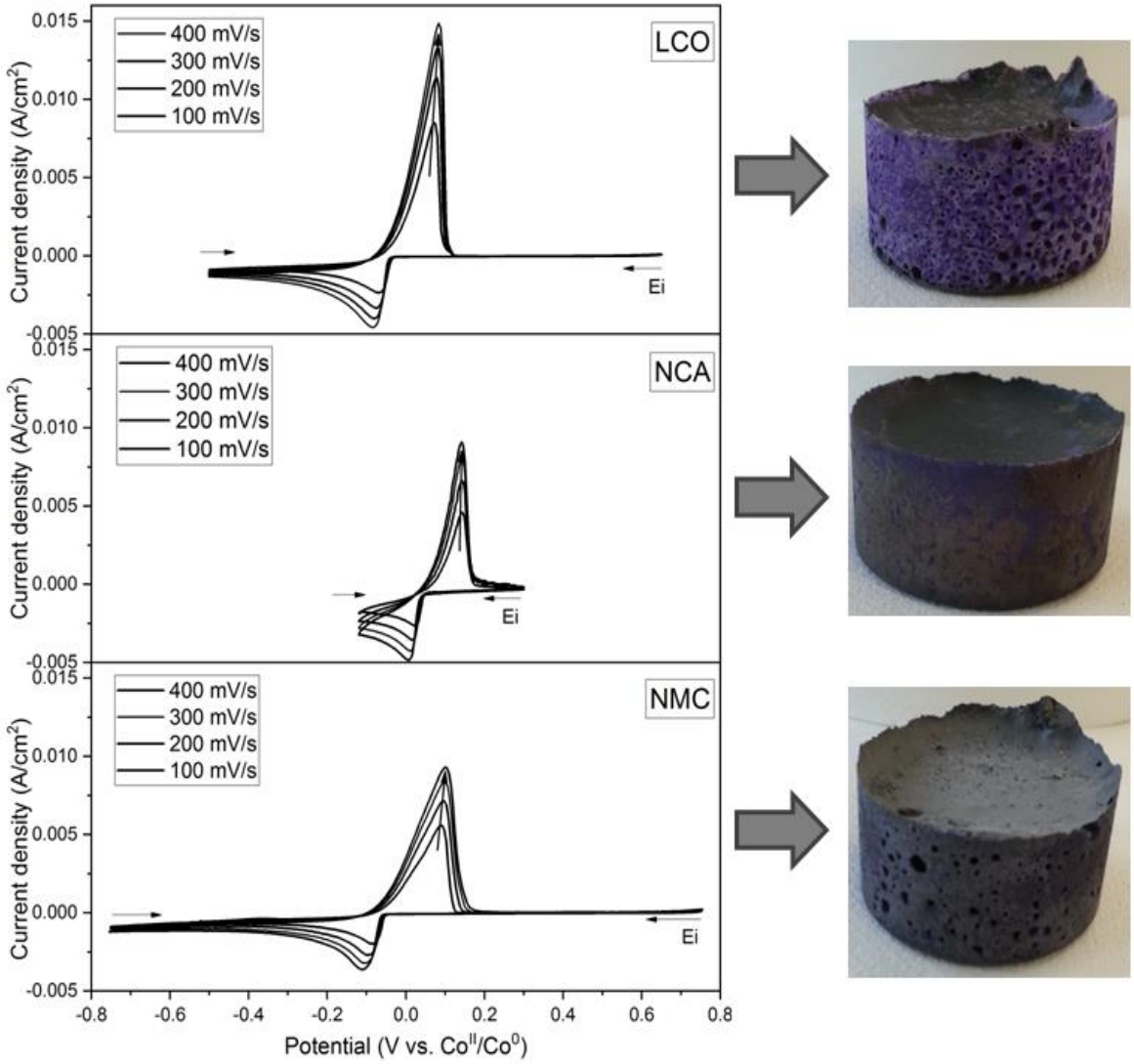

Figure 40 : Voltammograms of the solution containing LCO, NCA and NMC respectively in eutectic molten Li_2CO_3-Na_2CO_3-K_2CO_3, on silver wire working electrode at 450°C (168h), 1 atm CO_2. On the right the photos of each bath after 168h of heating

Only one anodic and one cathodic peak are observed in each case, which position slightly varies depending on the measurement's scan rate. We expected to observe the redox reactions of each transition metal present on the material. In this way, we expected 2 cathodic

and anodic peaks for NCA and at least 3 anodic and cathodic peaks for NMC. Table 13 shows the details concerning peaks' potentials positions and the measurement starting potential for each cathode material.

Table 13 : Anodic peak, cathodic peak and starting measurement potentials of voltammograms containing LCO, NCA and NMC in eutectic molten Li_2CO_3-Na_2CO_3-K_2CO_3

Compound	**Anodic peak position (V vs. Co^{II}/Co^0)**	**Cathodic peak position (V vs. Co^{II}/Co^0)**	**Measurement starting potential (V vs. Co^{II}/Co^0)**
LCO	0.079 ± 0.005	-0.077 ± 0.008	0.600
NCA	0.143 ± 0.002	0.019 ± 0.012	0.300
NMC	0.093 ± 0.008	-0.091 ± 0.019	0.650

In the case of LCO, the observation of only one electroactive specie is in agreement with Veldhius *et al* work[120]. This result is in coherence with XANES results in chapter II (dissolved cobalt in the molten medium has an oxidation state of +II). The same conclusions deduced from reference compounds voltammograms are obtained from LCO voltammogram analysis (metal electrodeposition phenomenon present, redox reactions given by equations (Eq. 31) and (Eq. 32).

It is known from the literature, that between the couple Co(II)/Co(0) and Ni(II)/Ni(0) there is a positive potential shift of 0.08V[135] in molten carbonates. LCO and NCA voltammograms cathodic peaks positions show a positive potential shift of about 0.07 V. This information leads to the conclusion that the active specie observed on NCA voltammogram is the redox reaction of nickel given by the following equations:

The reduction reaction:

$$Ni^{2+} + 2e^- \rightarrow Ni \qquad \text{(Eq. 34)}$$

The oxidation reaction:

$$Ni \rightarrow Ni^{2+} + 2e^- \qquad \text{(Eq. 35)}$$

To understand which active specie is observed (Co, Ni or Mn) in the case of NMC, the standard potentials of these elements in molten carbonates are required. The reaction potentials for manganese in molten carbonates have not been found in literature. Table 14 shows a

summary of the different reaction potentials for nickel, cobalt and manganese, found in literature, in several molten chlorides with a reference electrode Ag(I)/Ag(0)[135]. A negative shift potential of about 0.8V compared to cobalt and 1 V compared to nickel is observed for manganese in Table 14. Assuming that a similar relative potential shift is observed in molten carbonates, we can conclude that the voltammogram does not show a reaction involving manganese as active specie. The anodic peak of NMC is wider that LCO and NCA ones, and it englobes their potential range. For this reason, we suppose that both redox couples Co(II)/Co(0) and Ni(II)/Ni(0) the reaction are observed on NMC voltammogram. In this case, we cannot define the contribution of each element on the voltammogram. Simulations of this system could enable to determine these contributions in the future.

Table 14 : Different reaction potentials for nickel, cobalt and manganese found in literature for several molten salts with a reference electrode Ag(I)/Ag(0)

Melt	**Ni(II)/Ni(0) (V)**	**Co(II)/Co(0) (V)**	**Mn(II)/Mn(0) (V)**	**Mn(IV)/Mn(III) (V)**
LiCl-KCl	-0.068	-0.264	-1.122	Beyond the melt
$MgCl_2$-NaCl-KCl	-0.112	-0.290	-1.114	Not reported
$MgCl_2$-KCl	-0.167	-0.36	-1.208	Not reported

As for reference compounds, the morphology of voltammogram peaks corresponds to the presence of a metal electrodeposition phenomenon. Once again, Berzins and Delahay relation (Eq. 33) was used for calculating$[Co^{+II}]$ in the case of LCO, $[Ni^{+II}]$ in the case of NCA and both of them for NMC. Figure 41 shows the cathodic peak current density as function of the square root of the scan rate.

To calculate dissolved nickel concentration, the nickel diffusion coefficient value $D_{Ni^{+II}}$ was firstly calculated by using once again Stokes-Einstein relation (Eq. 27) and ternary eutectic viscosity value from literature[128] . Concerning the particle radius, we consider that, as for cobalt, the ionic radius nickel of Ni^{+II} is 0.69 °A[129]. From calculations a nickel diffusion coefficient value $D_{Ni^{+II}} = 2.1\ 10^{-6}\ cm^2.s^{-1}$ was obtained.

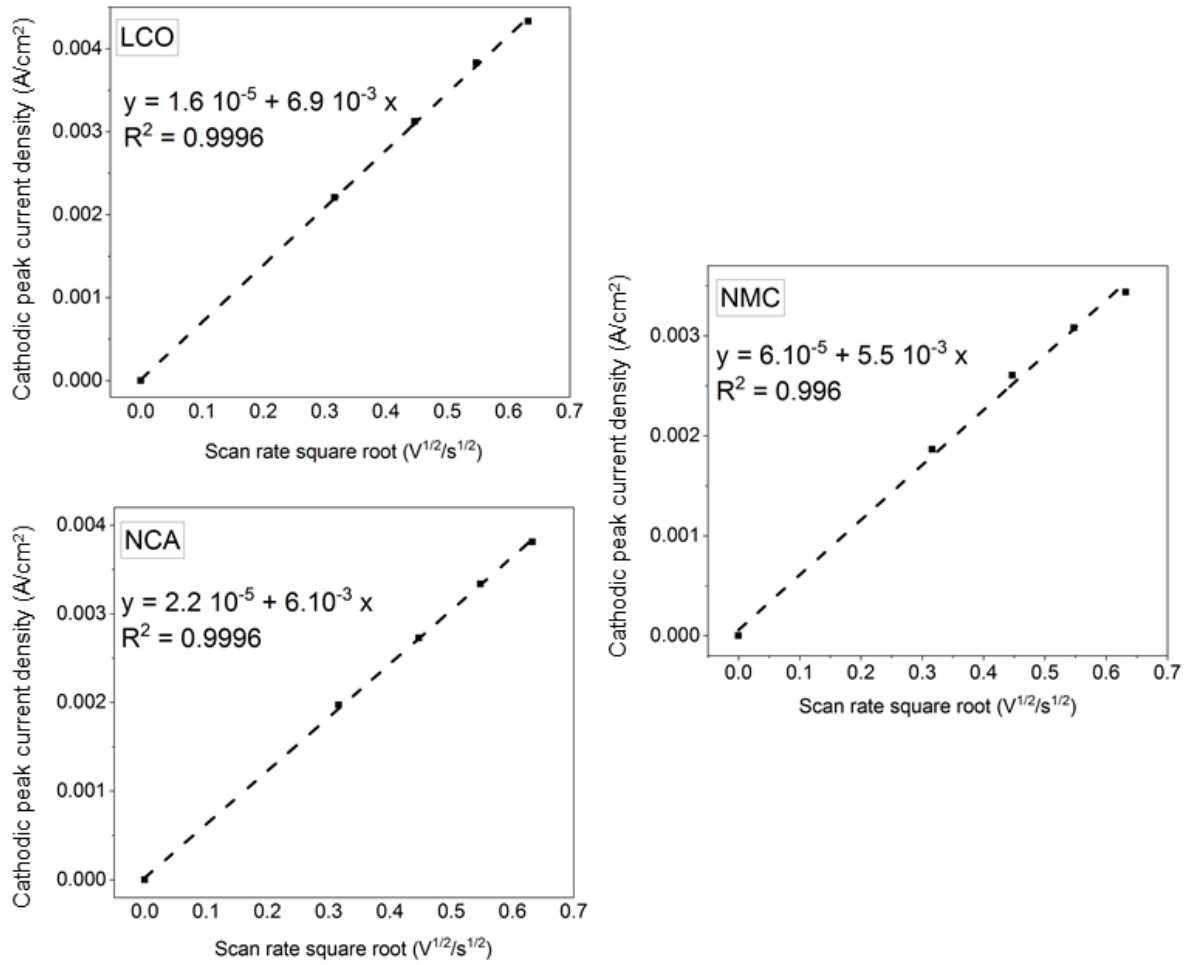

Figure 41 : Cathodic peak current density evolution in function of cyclic voltammetry scan rate square root for LCO, NCA and NMC in eutectic ternary mixture Li_2CO_3-Na_2CO_3-K_2CO_3, at 450°C (168h), 1 atm CO_2

Table 15 shows the results of dissolved cobalt $[Co^{+II}]$ and nickel $[Ni^{+II}]$ concentrations estimated by electrochemistry and compared with Flame atomic absorption spectroscopy (F-AAS) and Inductively Coupled Plasma- Atomic Emission Spectroscopy (ICP-AES) measurements.

The concentration values obtained by electrochemistry are in the case of LCO in between of the values determined by flame spectroscopy and ICP-AES, as observed for the reference compounds. In the case of NCA, the concentration values found by the three techniques are quite similar. For NMC, the concentration estimated by electrochemistry is not between the values determined by the other techniques. This can be explained as we do not determine the contribution of each element (nickel and cobalt) in the cyclic voltammogram.

Table 15 : Results of dissolved cobalt, nickel, aluminum and manganese concentrations for LCO, NCA and NMC in eutectic molten Li_2CO_3-Na_2CO_3-K_2CO_3

Cathode material	**LCO**	**NCA**	**NMC**
Slope ($A.cm^{-2}.V^{-1/2}.s^{1/2}$)	$6.9\ 10^{-3} \pm 0.2\ 10^{-3}$	$6.\ 10^{-3} \pm 0.1\ 10^{-3}$	$5.5\ 10^{-3} \pm 0.2\ 10^{-3}$
Measured by CV $[Co^{+II}]$ ($mol.cm^{-3}$)	7.10^{-6}	-	$5.6\ 10^{-6}$
Measured by F-AAS $[Co^{+II}]$ ($mol.cm^{-3}$)	$1.4\ 10^{-6}$	$1.3\ 10^{-6}$	$43.0\ 10^{-6}$
Measured by ICP-AES $[Co^{+II}]$ ($mol.cm^{-3}$)	$16.5\ 10^{-6}$	$2.7\ 10^{-6}$	$29.6\ 10^{-6}$
Measured by CV $[Ni^{+II}]$ ($mol.cm^{-3}$)	-	$6.2\ 10^{-6}$	$5.7\ 10^{-6}$
Measured by F-AAS $[Ni^{+II}]$ ($mol.cm^{-3}$)	-	$7.\ 10^{-6}$	$0.5\ 10^{-6}$
Measured by ICP-AES $[Ni^{+II}]$ ($mol.cm^{-3}$)	-	$7.9\ 10^{-6}$	$2\ 10^{-6}$
Measured by F-AAS $[Mn^{+x}]$ ($mol.cm^{-3}$)	-	-	$2.12\ 10^{-6}$
Measured by ICP-AES $[Mn^{+x}]$ ($mol.cm^{-3}$)	-	-	$5.7\ 10^{-6}$
Measured by F-AAS $[Al^{+III}]$ ($mol.cm^{-3}$)	-	$2.\ 10^{-6}$	
Measured by ICP-AES $[Al^{+III}]$ ($mol.cm^{-3}$)	-	$1.1\ 10^{-6}$	-

As before, we can conclude that the estimated self-diffusion coefficient by Stokes-Einstein relation is correct. The effect of matrix and in particular the presence of sodium is in this case a drawback for some flame spectroscopy and ICP-AES measurements.

Ota *et al.* reported the maximal cobalt dissolution of LCO in molten carbonates which exceeds $1.2\ 10^{-6}$ mol. cm^{-3} at 200 h which are quite similar to the values measured by flame spectroscopy for LCO.

Example of electrodeposition of cobalt from cathode material LCO in molten carbonates

Several tests have been done to recover cobalt from cathode materials LCO, NCA and NMC by electrodeposition in molten carbonates. Glassy carbon, graphite and silver have been used as working electrode during the experiments. The choice of cathodic potential to be applied during the electrolysis has been done, as in the example on Figure 42.

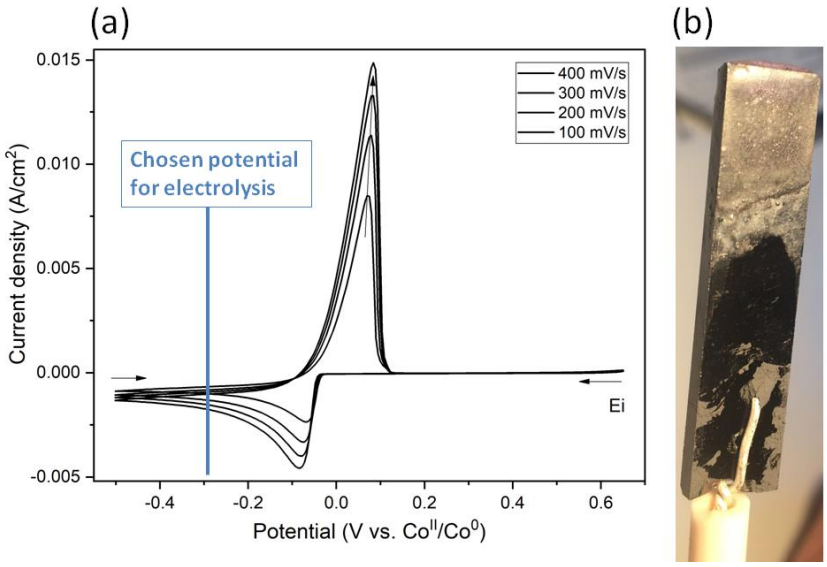

Figure 42 : Selected potential for electrolysis (-0.3 V vs. Co^{II}/Co^{0}) in (a), photo of the electrodeposited matter (b)

The recovered deposit was analyzed by X-Ray diffraction. Figure 43 shows as example the X-ray diffractogram of a deposit obtained by electrolysis, on glassy carbon working electrode. The deposit on the electrode was then analyzed by X-Ray diffraction showing only the presence of carbonates and graphite from the counter electrode in it.

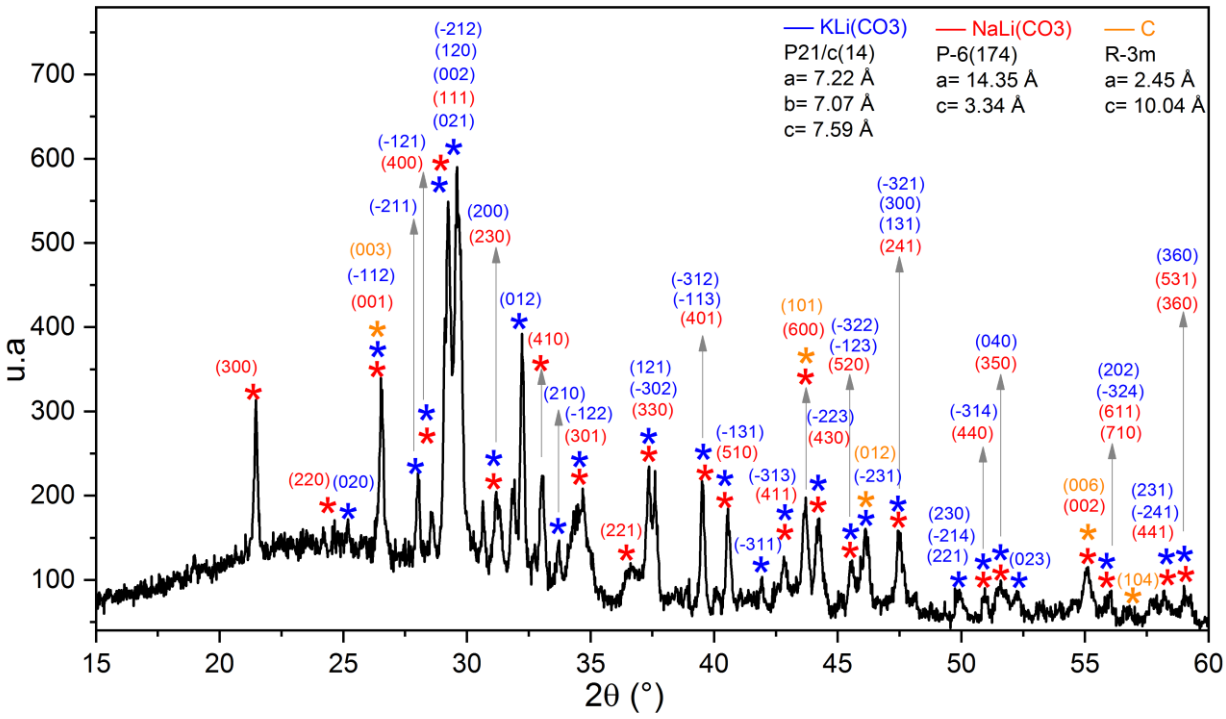

Figure 43 : XRD diagram of the electrodeposited matter

3.3. Battery organic compounds in molten carbonates

As Li-ion batteries cathode materials are composite materials containing organic matters, the study of cathode binders: polyvinylidene fluoride (PVDF) and carboxymethyl cellulose (CMC) were studied in our team. Furthermore, separator material polypropylene (PP) has also been investigated in molten carbonates. For more information about these Li-ion battery constituents, see details in section 2 of chapter I. This project was principally carried out by Arturo Melendez Ceballos (post-doc) and Gabriele Miranda (internship).

All these compounds were pyrolyzed in molten Li_2CO_3-Na_2CO_3-K_2CO_3. Two kinds of compounds were present in the materials studied: heavy (Tboil>20 °C) and light compounds (Tboil< 20°C). Figure 44 shows the set-up used for the pyrochemical reaction and the gas recovery. Several techniques were used to identify the structure of pyrochemical reaction products: Gas chromatography coupled to Mass Spectroscopy (GC-MS), Fourier Transform Infrared spectroscopy (FTIR), Nuclear Magnetic Resonance (NMR) and Diffusion Ordered Spectroscopy (DOSY). The solid products were analyzed by the following techniques: Scanning Electron Microscopy (SEM), Transmission Electron Microscopy (TEM), X-Ray Diffraction (XRD) and Brunauer-Emmett-Teller (BET).

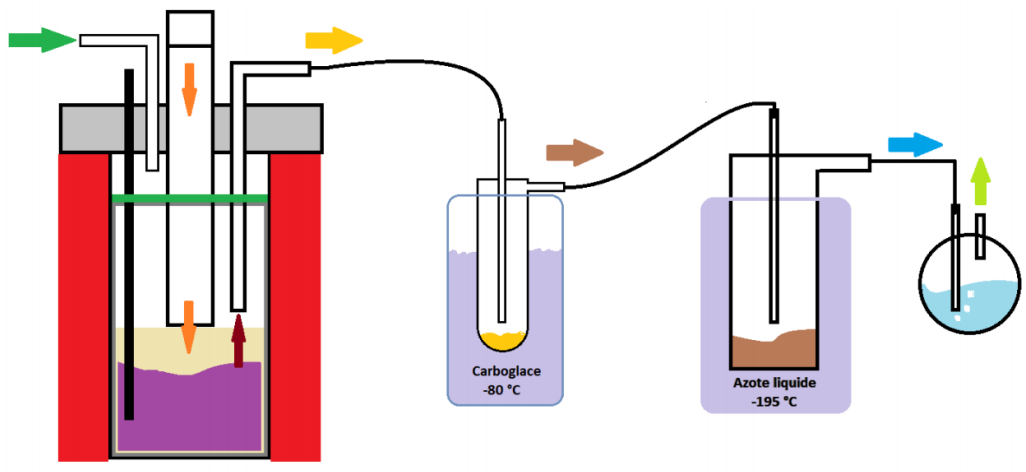

Figure 44 : Experimental set-up used for the pyrochemical reaction in eutectic molten Li_2CO_3-Na_2CO_3-K_2CO_3 carbonates at 450 ° C and gas recovery (from A. Meledez report)

The results show that for polypropylene (PP) pyrolysis leads to the formation of a great variety of products of different molecular weights. Most of the compounds were aliphatic

hydrocarbons (alkanes, alkenes and alkynes) ranging from 7 to 30 carbons. The other compounds present were oxygenated compounds.

Concerning the carboxymethylcellulose (CMC) pyrolysis products, they included acetic acid and two groups of hydrocarbon compounds: non oxygenated and oxygenated. The non-oxygenated hydrocarbons were constituted of aliphatic carbons (saturated and unsaturated) varying from 14 to 30 carbons. Their formula correspond to: C_xH_y $14 \leq x \leq 30$, $28 \leq y \leq 62$. The oxygenated hydrocarbons correspond to the following formula: $C_xH_yO_z$ $4 \leq x \leq 10$, $8 \leq y \leq 18$, $1 \leq z \leq 2$. Solid carbon has also been obtained from the pyrolysis. This carbon was tested as anodes in Li-ion batteries showing a poor performance.

Concerning polyvinylidene fluoride (PVDF) pyrolysis, three different kinds of products were obtained: liquid, solid and gaseous products. In fact, a yellowish liquid soluble in ethanol and acetone has been obtained. As for CMC, solid carbon was produced from pyrolysis. Concerning the gaseous products, mainly aromatic compounds were obtained, followed by small and medium length hydrocarbons. No HF vaporization was detected and the presence of LiF was detected in the molten salt.

From these preliminaries results, the global mass balance was established. It divides the pyrolysis products into three main fractions: solid residues, heavy organic compounds (olefins and paraffins) and volatile organic compounds. Figure 45 shows an example of the results obtained from this study.

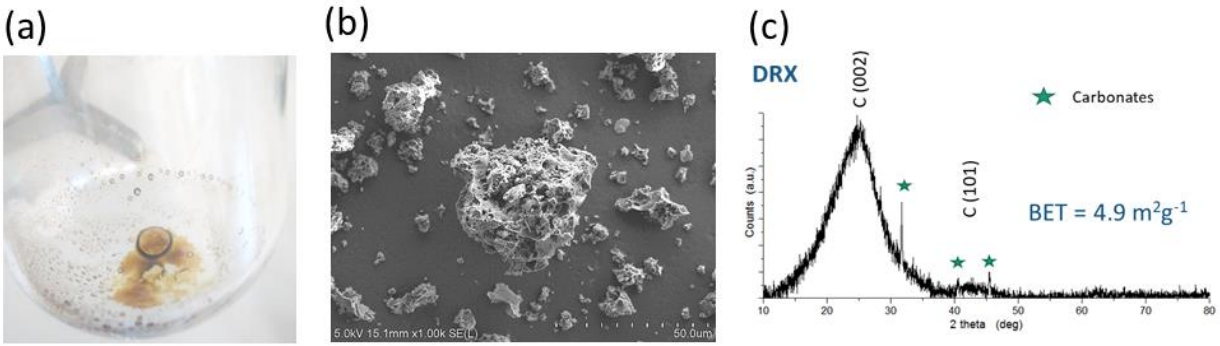

Figure 45 : Condensed product from CMC pyrolysis (a). MEB (b) and XRD (c) analysis of the solid product obtained after salt removal from CMC pyrolysis

The reuse of products proceeding from polymers pyrolysis can be a potential alternative to valorize them (which are burned at a large-scale process). Furthermore, giving Li-ion

batteries organic compounds a second life will contribute to the reduction of environmental impacts issues from Li-ion battery recycling (gas emissions) and may be the cost of some process steps (gas treatment before the emission).

Regarding Li-ion batteries recycling, the valuable elements of industrial interest to be recovered are essentially metals. For this reason, we studied the influence of this kind of organic compounds on cobalt dissolution. Figure 46 shows the comparison cobalt dissolution with and without the addition of polymer CMC. For both cases, the voltammogram shows the presence of an anodic and a cathodic peak. Their positions and current density can be seen in Table 16. For both measurements the starting point was corresponds to the OCP of each system.

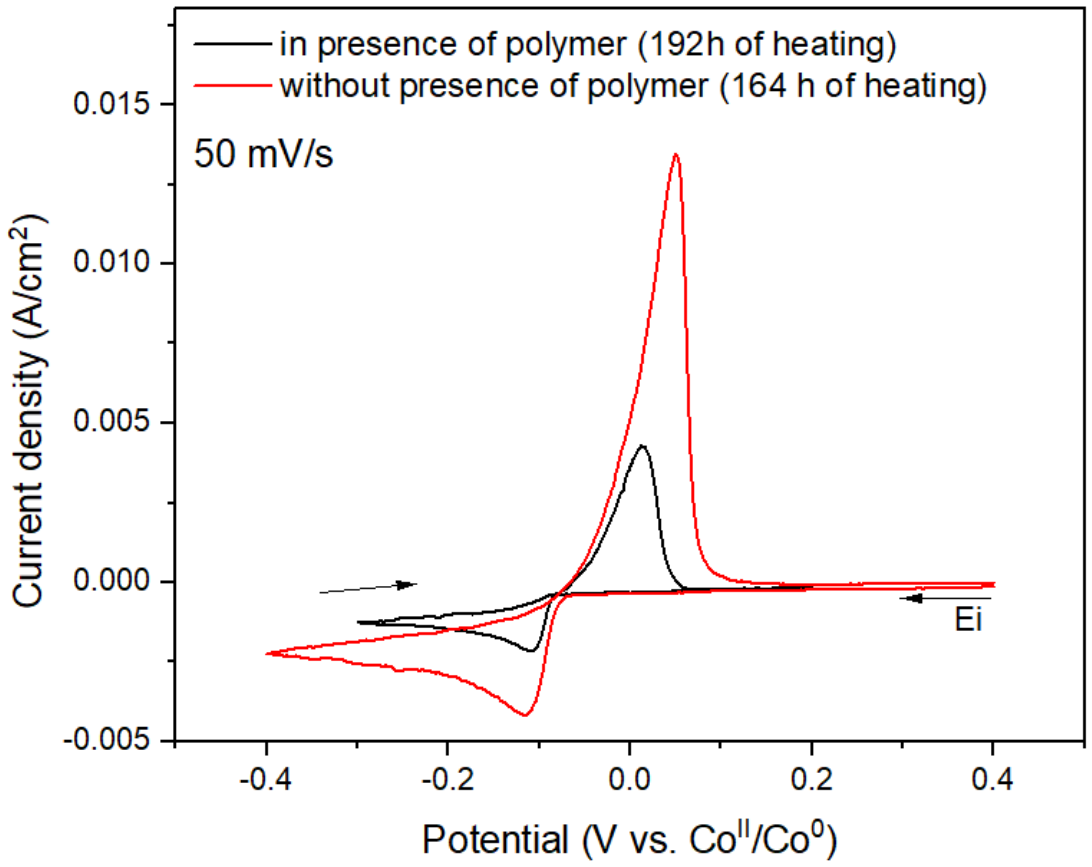

Figure 46 : Voltammograms of the solution containing LCO in eutectic molten Li_2CO_3-Na_2CO_3-K_2CO_3 in presence and without CMC polymer addition. Measurements on silver wire working electrode at 450°C (168h), 1 atm CO_2.

Table 16 : Anodic peak, cathodic peak and starting measurement potentials of voltammograms containing LCO in eutectic molten Li_2CO_3-Na_2CO_3-K_2CO_3 with and without CMC polymer addition

Compound	**Anodic peak position (V vs. Co^{II}/Co^0)**	**Cathodic peak position (V vs. Co^{II}/Co^0)**	**Cathodic peak current density ($A.cm^{-2}$)**	**Measurement starting potential (V vs. Co^{II}/Co^0)**
LCO with CMC addition	0.02	-0.11	$1.67\ 10^{-3}$	0.2
LCO without CMC addition	0.07	-0.12	$3.67\ 10^{-3}$	0.4

As the current density of both cathodic peaks is compared, LCO peak without CMC shows a current density about 2 times higher than when adding it. As peaks current density is linked to dissolved cobalt concentration (Eq. 33), it can be concluded CMC polymer presence decreases the solubility of cobalt from LCO in eutectic Li_2CO_3-Na_2CO_3-K_2CO_3.

4. Conclusions

Li-ion battery organic and cathode materials recycling feasibility was investigated in molten carbonates. Metallic cobalt dissolution was studied in molten carbonates. Electrochemical characterizations were carried out for different cathode materials in molten carbonates to quantify the dissolution process of the active species (cobalt or nickel) in the molten medium. Furthermore, electrochemical techniques allowed analyzing of the dissolution kinetics.

It was shown from cyclic voltammetry measurements that cobalt from $CoCO_3$, Co_3O_4, LCO, NCA and NMC cathode materials is dissolved in molten carbonates. Nevertheless, cobalt shows both a low and slow dissolution in that molten systems. The dissolved cobalt in the molten melt appears to be insufficient for recovering it by electrodeposition, as proved after analyzing the recovered matter after electrolysis. Regarding the conclusion withdrawn about the active species detected by cyclic voltammetry for NCA and NMC, test with metallic electrodes of nickel and manganese could be done to confirm the redox couple observed.

In what concerns Li-ion battery organic compounds, molten carbonates seem to be a good alternative to explore in the future. It was shown that the pyrolysis of all the studied

separators and binders leads to the production of hydrocarbons. The volatile compounds produced during the reaction were not recovered and are still to be characterized. Furthermore, in the case of PVDF binder, no HF vaporization was detected but the presence of LiF was detected in the molten salt.

Chapter IV: Study of Li-ion battery compounds in molten chlorides medium

“ Nous devons croire que nous sommes doués pour quelque chose, et que cette chose, à n'importe quel prix, doit être atteinte. ”

Marie Curie

1. Introduction

It has been shown in the precedent chapter that exploring Li-ion battery organic compounds in molten carbonates seems to be an interesting approach. Nevertheless, cobalt from cathode materials shows a low and slow dissolution in this medium. Molten chlorides medium may be an alternative for recovering this valuable metal from cathode materials. This chapter is dedicated to the behavior of cobalt from Li-ion battery cathode materials and its recovery in molten chlorides medium. It has been shown that molten chlorides are able to solubilize metallic cations of oxides such as Ti[97], Ta[98], Nb[98], Ce[99] and recovering them by electrolysis. Could this capacity of chlorides be applied for lithiated cobalt oxides?

In the previous chapter, it has been suggested that a "good" molten medium for cobalt recycling should exhibit two key features. On the one hand, it has to solubilize the oxides and cations found in Li-ion batteries; on the other hand, it should keep unchanged metallic cobalt that could be deposited onto the electrode. The literature provides information concerning the two key features needed for an efficient cobalt recovery. Indeed, few studies have been devoted to quantify cobalt dissolution and electrodeposition in alkali-containing chlorides, especially in eutectic LiCl-KCl and NaCl-KCl.

Few studies have been carried out on metallic cobalt and its oxides in alkali chlorides. Metallic cobalt has been reported as not reacting with the eutectic LiCl-KCl and NaCl-KCl melts[135] (melting points 355 °C and 657°C respectively[54,94,95]). This is an advantage face to metallic cobalt behavior in molten carbonates, where it does not remain totally stable. However, no value of its dissolution has been reported. Concerning cobalt oxides dissolution, it has not been widely studied in molten chlorides. Delarue started by studying the stability of a mixture of Co_3O_4 and Co_2O_3 in eutectic LiCl-KCl[136]. From this investigation, it was suggested that Co_3O_4 is transformed into Co_2O_3 in the melt and that both oxides are only partially soluble. Nevertheless, this study is essentially empiric. Concerning cobalt oxides dissolution, only one value has been reported in alkali chlorides mixtures. A solubility value of Co_3O_4 solubility has only been reported in 50% mol NaCl-50%KCl by Ishitsuka *et al.* This work was carried out at 727 °C in three different acidity conditions: 100%O_2 coupled with 10^{-2} molar fraction of Na_2O_2 introduction, 10% O_2-N_2, and 1% HCl-N_2 atmosphere. Ishitsuka *et al.* showed that Co_3O_4 highest solubility correspond to the most acidic condition, with a corresponding value of 750 ppm.

Cobalt electrodeposition has been carried out in LiCl-KCl confirming not only the recovery of metallic cobalt by electrolysis in molten chlorides, but also providing valuable pieces of information about the mechanism taking place during electrolysis. Cobalt electrodeposition was accomplished by Behl through linear sweep voltammetry technique. It was proven that cobalt ions Co(II) reduction is reversible and results in the deposition of solid metal at the electrode surface (glassy carbon working electrode)[137]. Later studies of the electroreduction of cations Co^{+II} carried on by Lantelme *et al.* by chronopotentiometry, provide similar results[138]. Delarue G. also investigated Co^{+II} cations by electrochemical means (curves potential-intensity). This technique proved that in this molten medium, Co^{+II} cation is reduced into Co (0) and Co^{+III} is too oxidant to exist (instead, chlorides reduction takes place). Co^{+II} reduction mechanism has been notably studied by Lantelme *et al.*, by cyclic voltammetry and chronopotentiometry[139]. The corresponding results show that cobalt ions reduction occurs in a single two-electron step, confirming Delarue previous qualitative result regarding the number of electrons exchanged during reduction[136].

In general, alkali molten chlorides seem to be a more promising alternative than molten carbonates as metallic cobalt is not soluble in them. Eutectic LiCl-KCl appears to be a more suitable choice than 50% NaCl- 50%KCl for several reasons. First of all, it has a lower melting point (355°C compared to 657°C). Furthermore, a low solubility of cobalt oxide has been quantified in NaCl-KCl while in LiCl-KCl there is only an empiric study. As a consequence, the experiments shown in this chapter are all done in LiCl-KCl eutectic. Concerning the atmosphere, we have chosen to work in an inert atmosphere for two reasons. The solubility studies carried out in NaCl-KCl, mentioned before, showed that the lowest solubility is obtained in basic atmosphere (oxygen atmosphere). We do not choose an acidic atmosphere (ex: HCl) even if it was reported to lead to best solubility for security issues.

2. Experimental part

2.1. Molten salt preparation

The same experimental set-up described in the chapter III for eutectic Li_2CO_3-Na_2CO_3-K_2CO_3 was used (furnace, heating cell and molten salt container). For details see section 2.1 of chapter III.

Precursor compounds and molten salts used

Table 17 shows the different chemical compounds used for the experiments in molten chlorides.

Table 17 : List of chemical compounds used

Compound	Form	Purity	Supplier
LiCl	Powder	≥99.0%	Merck
KCl	Powder	≥99.0%	Merck
$NaHSO_4$. H_2O	Powder	>99.5 %	Sigma Aldrich
$KHSO_4$	Powder	99.9%	Merck
$CoCl_2$	Powder	99.999%	Sigma Aldrich
$LiCoO_2$	Powder	99.8%	Merck
$LiNi_{0.82}Co_{0.15}Al_{0.03}O_2$	Powder	-	SAFT
$LiNi_{1/3}Co_{1/3}Mn_{1/3}O_2$	Powder	-	SAFT

Eutectic LiCl - KCl preparation

The eutectic mixture has a molar composition of 44,3% KCl and 55,7 % LiCl[94]. Before each experience, the salts and cobalt precursors were dried at 200°C under vacuum for 72 h to remove all the water traces. After drying them, all the compounds were stored in a glove box. Chlorides and cobalt precursors were weighted and grinded in glove box. The mixture was put into a glassy carbon crucible and sealed in the heating set-up very quickly to avoid the interaction with water in the air. Then, the mixture was dried in the set-up at 150 °C for 24h to eliminate all the remaining water traces. Afterwards, the temperature of the bath was increased up to 405°C by step of 3 °C per minute. All the experiments were performed under Ar atmosphere with a flow of 38 mL min^{-1}. 50 mL of molten salts were used and a cobalt concentration of 1.10^{-5}, 2.5 10^{-5} and 5.10^{-5} mol. cm^{-3}. The density of the eutectic molten LiCl-KCl system is given by the following equation (Eq. 36) [94]:

$$\rho(T) = 2.0286 - (5.2676\ 10^{-4})T \qquad \text{(Eq. 36)}$$

Where: T is the temperature in K. At the working temperature of 405°C, ρ= 1.67 g cm^{-3} [94]. The heating period was of about 3 days for each experience.

2.2. Electrochemical measurements

The same electrochemical techniques and protocol used in chapter III are here applied. Regarding cyclic voltammetry the same theoretical approaches are used in this chapter while in the case of chronoamperometry, theoretical approaches have been applied for determining cobalt diffusion coefficient value.

Chronoamperometry

Chronoamperometry has been used for recovering cobalt by electrolysis and determining its diffusion coefficient. Gold, graphite and cobalt were used as working, counter and reference electrodes respectively, for the experiments to determine cobalt diffusion coefficient. For electrolysis, cobalt and Ag^{I}/Ag were used as reference electrodes and the same working and counter ones. For the experiments to determine the diffusion coefficient, the potential steps from 0.30 V to -0.25 vs. Co^{II}/Co^{0}. For the first electrolysis shown in this chapter, the potential steps from -0.10 V to -0.65 V vs. Ag^{I}/Ag^{0}., and for the second one from 0.50 V to -0.30 vs. Co^{II}/Co^{0}.

Electrodes

A three-electrode system has been used for all the electrochemical measurements.

- The reference electrodes:

  - The same pseudo-reference of cobalt used in Chapter III
  - A silver electrode named Ag^{I}/Ag^{0} that consists in an alumina tube closed by sintered 4 mm diameter alumina plug, from Radiometer analytical. Inside of the tube a 1 mm diameter silver wire was plunged in a mixture of eutectic LiCl-KCl and Ag_2SO_4. The optimal portion of 5% mol of Ag_2SO_4/ LiCl-KCl was decided by considering the literature[140].

- The working electrodes:

- A 1 mm diameter cobalt wire 99.99 % pure from Goodfellow
- A 1 cm^2 gold plate 99% pure from Goodfellow
- A 1mm diameter gold wire 99% pure from Goodfellow
-A 1 mm diameter tungsten wire
- A 4.5 mm diameter glassy carbon rod (HTW SIGRADUR)

- The same counter electrode described in Chapter III was used

The immersed length of the working electrodes was measured with a caliper at the end of the measurements. Then, all the electrodes were cleaned with distilled water and dried. Finally, all the metallic pieces composing the electrodes were polished with sandpaper (SiC paper #1200, from Struers), rinsed with ethanol and dried. The working and counter electrode wires were maintained in the molten system by the same alumina sheath used for electrodes in chapter III.

2.3. Other characterizations

Inductively Coupled Plasma- Atomic Emission Spectroscopy (ICP-AES) and Flame atomic absorption spectroscopy (F-AAS) were used with the same aim described in chapter III. The same equipment and protocol were also used. **X-ray Diffraction (XRD)** was used for analyzing the product of the thermal pretreatment of cathode materials with hydrogenosulfates and the deposit from electrolysis in molten chlorides. The deposit was rinsed with distilled water and dried before the XRD measurements. The same measurements conditions and equipment described in chapter III have been used. **Energy-dispersive X-ray spectroscopy (EDX)** was used to determine the composition of the deposit. The deposit was taken off from the working electrode at the end of the electrolysis with a spatula, rinsed with distilled water and dried before being analyzed. The equipment used was a Field effect gun Scanning Electron Microscope from HITACHI-SU-70. It has a detector X-Max from Oxford Instruments, with a surface of 50 mm^2. The measurements were done at room temperature and atmosphere. A conductor support of carbon was used for all the EDX measurements.

3. Results and discussion

In this chapter, the study of different cobalt compounds behavior in eutectic LiCl-KCl molten system is presented. First, the study of this melt without cobalt was done to define the electrochemical active window. Then $CoCl_2$ was studied as the reference compound. Finally, the behavior of cathode material $LiCoO_2$ (LCO) is presented and the optimization of cobalt solubility in this molten medium by using an additive is presented.

3.1. Electrochemical stability window of molten LiCl-KCl eutectic

Eutectic LiCl-KCl was studied by cyclic voltammetry in order to identify the electrochemical window of this solvent (see Figure 47). The measurement started from the anodic potential to the cathodic one and vice versa to complete the cycle. The electrochemical window is of about 3 V, which is slightly lower than the one reported in literature[135].

In Figure 47, the anodic limit is given by the oxidation of the gold working electrode according to the following reaction (Eq. 37)[135]:

$$Au \rightleftarrows Au^{+} + 1e^{-} \qquad \text{(Eq. 37)}$$

And the cathodic limit is given by the reduction of lithium cations from the molten solvent according to(Eq. 38)[135]:

$$Li^{+} + 1e^{-} \rightleftarrows Li \qquad \text{(Eq. 38)}$$

Six other peaks are present in curve (a): 4 anodic (A_1, A_2, A_3 and A_4) and 2 cathodic ones (C_1, C_2). The peak A_1 implies the oxidation of metallic lithium formed in (Eq. 38) and the peak C_1 implies the Au^+ reduction after its oxidation by (Eq. 37).

A_2, A_3, A_4 and C_2 can be attributed to the formation of alloys gold-lithium and gold-potassium[141]. Several gold-potassium alloys have been reported in literature: Au_2K, Au_4K, AuK, AuK_x with x= 1.28; 1.24; 1.17; 1.03; 0.54 and 0.52[141]. On the contrary lithium-gold alloys are not well known in literature[141].

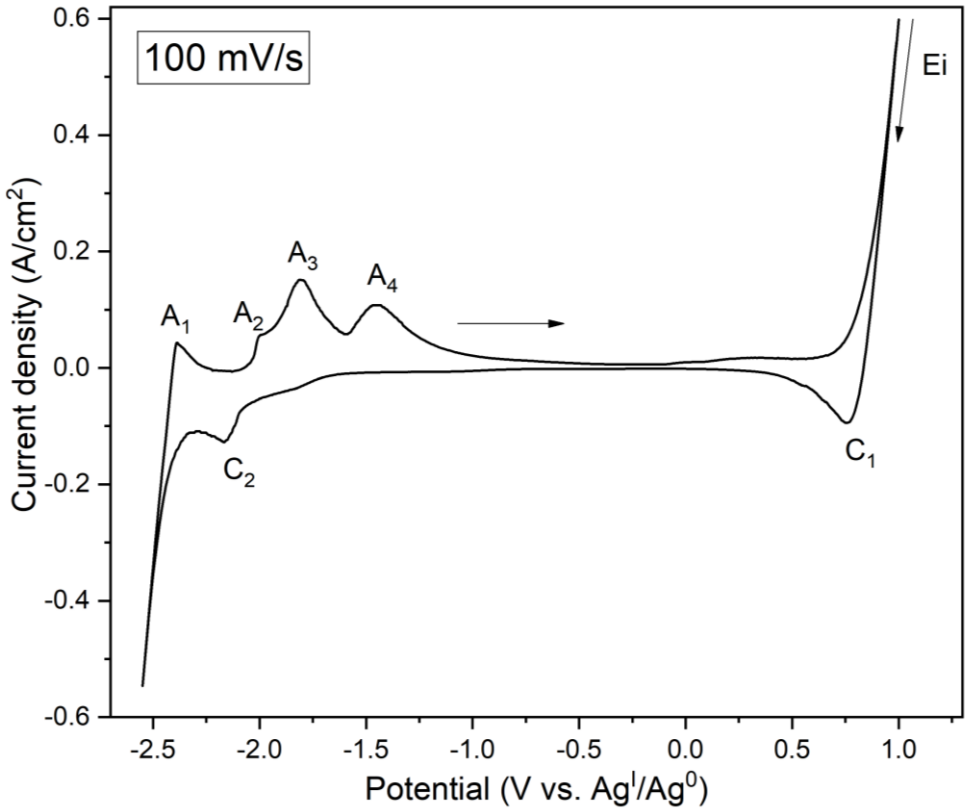

Figure 47 : Electrochemical window of eutectic LiCl-KCl on gold wire working electrode at 405°C, 1 atm Ar. Graphite and Ag^{I}/Ag^{0} have been used as counter and reference electrodes, respectively

3.2. Electrochemical study of $CoCl_2$ precursor in molten LiCl-KCl eutectic

Testing working electrodes

Several electrochemical configurations have been tested to identify the most suitable set-up for the electrochemical study of cobalt in this molten medium. In this way, gold, tungsten and cobalt were used as working electrodes. Figure 48 shows the voltammograms obtained for the three working electrodes.

The reactions observed correspond to the couple Co(II)/Co(0)[136,139].The voltammogram on cobalt electrode has only one cathodic peak which appears at -0.003V vs. Co^{II}/Co^{0}. The absence of anodic peak for this voltammogram may be explained by the dissolution of metallic cobalt from the working electrode after the oxidation of the deposited one. It was expected to observe the transition between the end of oxidation of the electrodeposited cobalt and the beginning of the electrode material oxidation, as it has already been observed in previous

studies for silver oxidation on a silver electrode[142]. This transition appears as a change on the slope during the anodic current density increase. From this statement, it would be delicated to study of electrochemical behavior of cobalt on a cobalt working electrode. Nevertheless, it is possible to electrodeposit cobalt over this substrate.

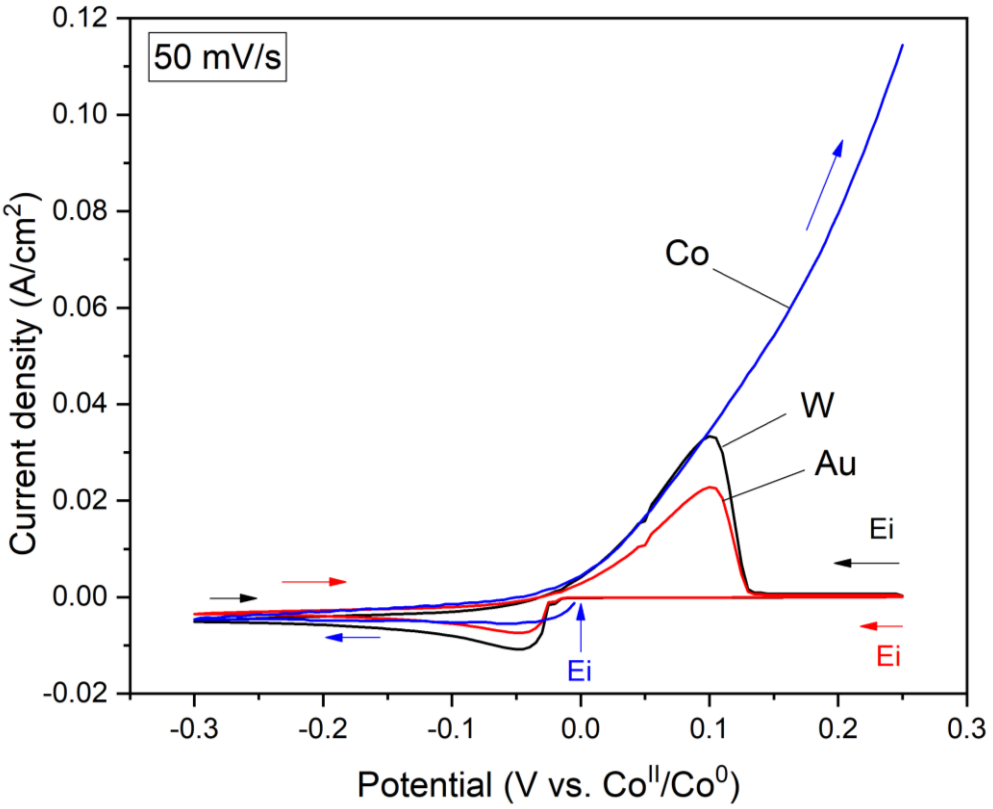

Figure 48 : Voltammograms of the solution containing $CoCl_2$ in eutectic molten LiCl-KCl, on tungsten (black curve), gold (red line) and cobalt (blue line) working electrodes, 1 atm Ar. Graphite and cobalt were counter and reference electrodes, respectively

Voltammograms on gold and tungsten working electrode has one cathodic and one anodic peak, with a position that varies slightly from one electrode to another. A small shift of cathodic peaks position towards the negative potentials (of about 0.011 V) is observed for both working electrodes. This may be explained by the important nucleation energy needed when depositing cobalt on a different material from itself[138]. The morphology of the voltammogram peaks is characteristic of an insoluble metal electrodeposition phenomenon, which confirms previous results of Behl works (on glassy carbon working electrode)[137].

Determining cobalt diffusion coefficient

To determine the concentration of dissolved cobalt in the molten medium it is necessary to know cobalt diffusion coefficient $D_{Co^{+II}}$. Chronoamperometry technique was used to quantify it. In the molten system, it can be considered that the migration phenomenon is negligible due to the presence of the chlorides that act as supporting electrolyte. By this way when a large and negative potential is applied to the electrode, the current at it is limited by the diffusion rate of the active species in the medium[143]. This current is known as limiting diffusion one and its expression is given by Cottrell's equation:

$$I_D = nSF(\frac{D}{\pi t})^{\frac{1}{2}}[M^{x+}] \quad \text{(Eq. 39)}$$

Where:

I_D : the chronoamperogramm limiting diffusion current in A

S: working electrode surface in cm^2

n: the number of exchanged electrons

F: Faraday constant 96485 in C. mol^{-1}

D: the diffusion coefficient of the active specie in $cm^2.s^{-1}$, in this case $D_{Co^{+II}}$

t: the time in s

$[M^{x+}]$: active specie M^{x+} concentration in the bulk, in $mol.cm^{-3}$, in this case $[Co^{+II}]$

The measurement's period of time that respects Cottrell's conditions depends on the equipment. In the best of the cases it includes a time period that goes from 20 µs to 200 s[131]. In fact, the current of the electrical double layer masks the limiting diffusion current at the very small-time intervals. By contrast, it is masked at the high time intervals by the convection current [144]. The interval of time between 0.1 and 3.8 s was chosen to apply the Cottrell's equation. Figure 49 (a) shows the corresponding chronoamperogramm. The current density evolution as function of $1/t^{1/2}$ for time interval chosen for applying this law is shown in Figure 49 (b).

The dissolved cobalt concentration in the medium $[Co^{+II}]$ is equal to the introduced concentration of $CoCl_2$ ($2.5\ 10^{-5}$ $mol.cm^{-3}$). With this value, a coefficient diffusion value of $D_{Co^{+II}} = 1.63\ 10^{-5}$ $cm^2.s^{-1}$ is calculated. This value is in agreement with the reported cobalt diffusion coefficient value obtained by electrochemical means in 58.2% mol LiCl- 41.8% mol KCl in similar temperature (400°C) [139].

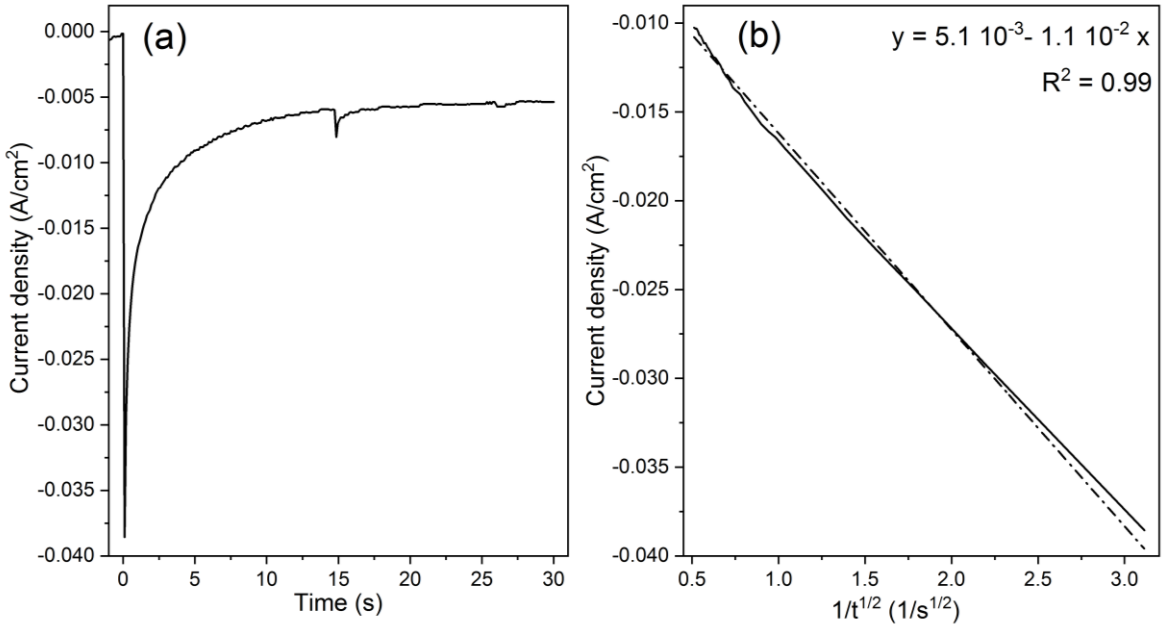

Figure 49 : Chronoamperogramm for the system $CoCl_2$ in molten eutectic ternary LiCl- KCl at 405 °C, 1 atm Ar (a). Current density evolution as function of $1/t^{1/2}$ for Cottrell's law application is shown on (b). Gold, graphite and cobalt were used as working, counter and reference electrodes. The potential step goes from 0.30 V to -0.25 vs. Co^{II}/Co^{0}.

3.3. Electrochemical study of $LiCoO_2$ in molten LiCl-KCl eutectic

Here the cathode material $LiCoO_2$ (LCO) behavior in this molten medium is presented. As mentioned in chapter III, it has been the first cathode material to be studied because it contains only cobalt as transition metal.

Quantifying dissolution

As in chapter III, Cyclic Voltammetry, Flame Atomic Absorption Spectroscopy (F-AAS) and Inductively Coupled Plasma- Atomic Emission Spectroscopy (ICP-AES) were used to quantify cobalt dissolution in the molten system. Figure 50 (a) shows the voltammogram of the solution of eutectic LiCl-KCl containing $LiCoO_2$. The presence of only one anodic and cathodic peak can be observed, which position varies slightly according to the scan rate set for the measurement. The measurement has been done from the open circuit potential (OCP) towards the cathodic one and backwards to complete the cycle.

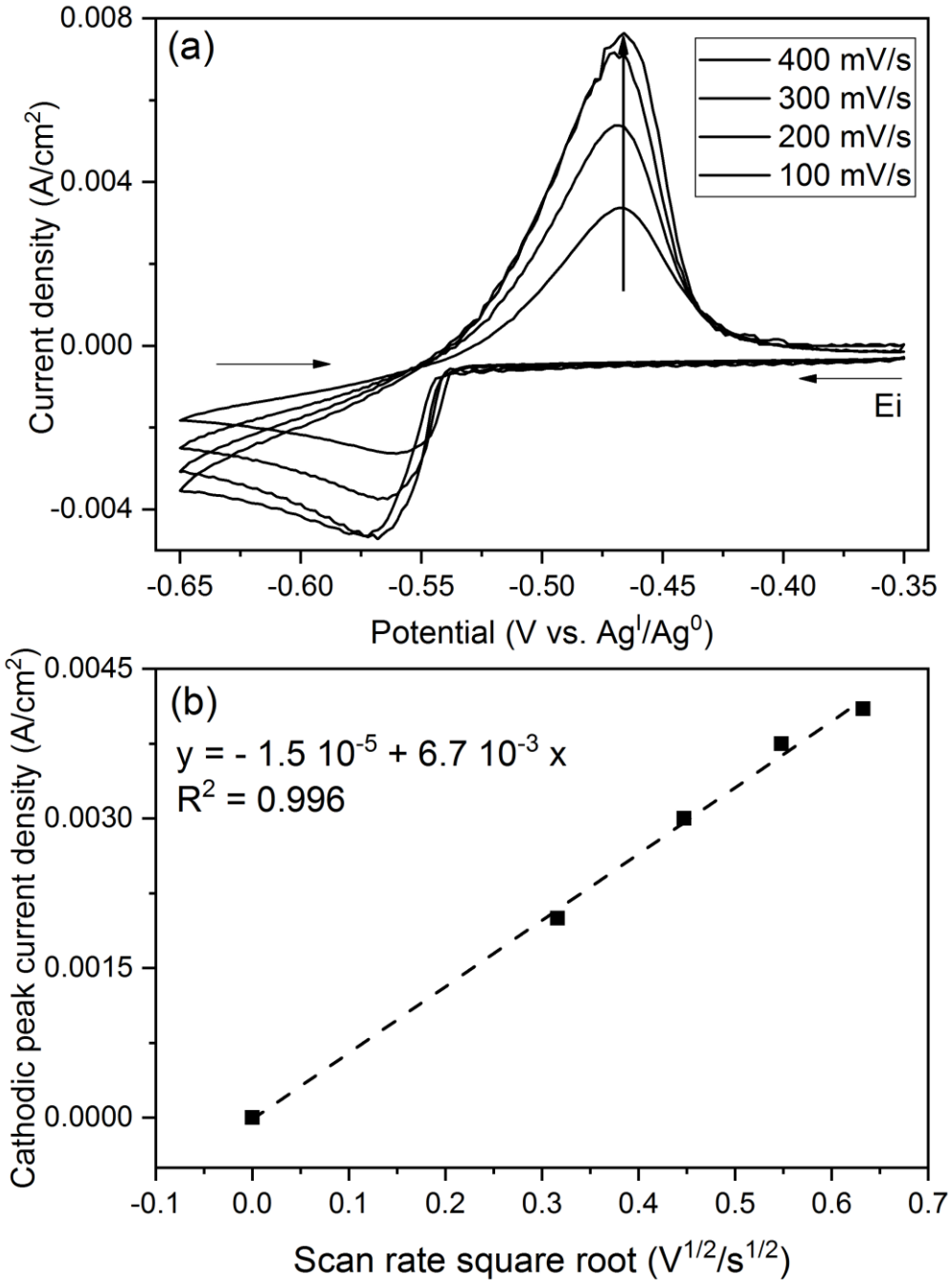

Figure 50 : Voltammograms of the solution containing LCO in eutectic molten LiCl-KCl on gold wire working electrode at 405°C (for 48h), 1 atm Ar (a). Its cathodic peak current density evolution in function of cyclic voltammetry scan rate square root (b). Graphite and Ag^I/Ag^0 were used as counter and reference electrodes, respectively. Cobalt concentration introduced equal to 5.10^{-5} mol.cm^{-3}

The voltammogram in Figure 50 (a), shows the presence of an anodic peak at -0.560 ± 0.010 V vs. Ag^I/Ag^0 and a cathodic peak at -0.467 ± 0.002 V vs. Ag^I/Ag^0 depending on the

measurement scan rate. In the literature, the couple Co(II)/Co(0) potential corresponds to -0.264 V vs. Ag^{I}/Ag^{0} [135]. As observed, the voltammogram peaks potential is shifted of about -0.2 V. This difference is due to the reference electrode, where we suspected a leak. This leak was confirmed later.

No standard potential has been reported for Co(III)/Co(II) in this medium. Furthermore, Delarue empirical studies concluded that Co^{+III} is too oxidant to exist in the melt[136]. To confirm that the couple observed does not correspond to Co(III)/Co(II), we compared as example the difference of standard potential of couples Co(II)/Co(0) and Co(III)/Co(II) in aqueous solutions. In this kind of system, Co(II)/Co(0) appears at -0.28 V and Co(III)/Co(II) at 1.82 V vs. standard hydrogen electrode. As observed, there is a difference of about 2V between both couple potentials. Assuming that a similar difference of potential exists for both couples in our system, Co(III)/Co(II) would appear after the anodic limit of the solvent. As a consequence, we can conclude that the observed redox reactions correspond to the couple Co(II)/Co(0) with a single two-electron exchange. Co^{+II}. This implies that a small portion of Co(III) from the cathode material is transformed into Co^{+II} in the medium, because the voltammogram peaks' current density is low compared to the added cobalt concentration. The maximal dissolution has been obtained in a shorter time (48h) compared to molten carbonates (about 160h). This leads to the conclusion that cobalt dissolution kinetics in molten chlorides is quicker than in molten carbonates.

Berzins and Delahay relation (Eq. 33) can be used for calculating the dissolved cobalt concentration $[Co^{+II}]$ (Figure 50 (b)). A value $[Co^{+II}] = 2.6\ 10^{-6}$ mol.cm^{-3} is obtained from calculations. This value was correlated with the results of Flame atomic absorption spectroscopy (F-AAS) and Inductively Coupled Plasma- Atomic Emission Spectroscopy (ICP-AES). For the preparation details see section 2.3 of this chapter. The dissolution values determined from measurements are shown in Table 18.

Table 18 : Results of dissolved cobalt concentration $[Co^{+II}]$ for $LiCoO_2$ in eutectic molten LiCl-KCl

Cathode material	**Slope ($A.cm^{-2}.V^{-1/2}.s^{1/2}$)**	**Measured by CV $[Co^{+II}]$ ($mol.cm^{-3}$)**	**Measured by F-AAS $[Co^{+II}]$ ($mol.cm^{-3}$)**	**Measured by ICP-AES $[Co^{+II}]$ ($mol.cm^{-3}$)**
LCO	$6.7\ 10^{-3} \pm 0.2\ 10^{-3}$	$2.4\ 10^{-6}$	$2.6\ 10^{-6}$	$0.5\ 10^{-6}$

Figure 51 : Appearance of the cooled bath $LiCoO_2$ in eutectic molten LiCl-KCl after the heating

The concentrations values obtained by electrochemistry are well in between the values determined by flame spectroscopy and ICP-AES. It confirms that the obtained value of cobalt self-diffusion coefficient by chronoamperometry is correct. This difference can be attributed to a matrix effect as for carbonates. The low solubility has been confirmed when recovering the cooled bath shown on Figure 51. As observed in this figure, there is not blue color characteristic of cobalt dissociation into Co^{+II}. The melt shows a white color corresponding to molten chlorides and LCO appears to precipitate to the bottom of it.

3.4. $NaHSO_4.H_2O$ addition influence on $LiCoO_2$ dissolution in molten LiCl-KCl eutectic

As seen in the previous section, LCO shows a low solubility in this molten system due to the presence of cobalt as Co (III). We have seen in chapter III, that cobalt soluble form corresponds to Co (II) in molten carbonates. Furthermore, we know from the literature that cobalt with the same oxidation state appears to be soluble in molten chlorides[136]. We look forward finding solutions for reducing Co(III) into Co(II) previously to its dissolution in molten chlorides.

Wang *et al.*, proposed recently a new approach to recycle cobalt and lithium by roasting $LiCoO_2$ with hydrogenosulfate $NaHSO_4.H_2O$ for 30 min at 600°C [145, 146].This method appears to show a total reduction of cobalt Co(III) into Co(II) depending of the molar ratio used between

both compounds. In fact from a molar ratio 1:3 $NaHSO_4.H_2O/LiCoO_2$ a total reduction of Co(III) into Co(II) takes place[145, 146].

Inspired by this approach, we used hydrogenosulfates to reduce cobalt from cathode materials. Three cathode materials LCO, NCA and NMC were pretreated with $NaHSO_4.H_2O$ for 12h at molar proportion of 3:1 hydrogenosulfates /cathode material. Our aim here was to go further than Wang *et al.* works and to determine the best protocol for the total reduction reaction. To do it, we varied and studied the influence of different parameters on this process:

-Temperature: 188 °C, 405°C and 500°C

-Atmosphere: Ar or air

-Alkali cation: sodium ($NaHSO_4.H_2O$) or potassium ($KHSO_4$)

Most of the experiments were carried out with $NaHSO_4.H_2O$. Figure 52 shows the pictures of some the different thermal treatments carried out with $NaHSO_4.H_2O$ as example.

As observed in Figure 52, the products obtained have a different appearance depending on the temperature and atmosphere conditions. LCO, NCA and NMC treated at 188°C lead to black or gray products more or less homogenous. As LCO, NCA and NMC are black powders, we can imagine that the reaction might not be total at this temperature. Nevertheless, this hypothesis must be verified by analytical techniques. The treatments done at 405°C seem to be more homogenous than the ones done at 188°C, especially when air atmosphere was used (most homogenous ones). In most of the cases there is an important difference of color compared to the LCO, NCA and NMC powders. For LCO, the product obtained at Ar atmosphere has a dull purple color while in air atmosphere it has a vivid purplish color. The same trend is observed for NCA, a vivid orange product is obtained in air atmosphere while a dull greyish-orange color in Ar atmosphere. In the case of NMC, a greyish product is obtained from the treatment in Ar atmosphere and a pink product in air atmosphere. We analyzed the product of these thermal treatments by XRD and XAS to determine the different products of the reaction and the cobalt oxidation state. Moreover, we monitored the evolution (kinetics) of the reaction in-situ by XAS.

Figure 52 : Picture of the cathodes LCO, NCA and NMC cathode materials thermal treatments with hydrogenosulfates at different temperatures (188°C, 405°C or 500°C) and atmosphere (Ar or air) conditions

3.4.1. X-ray characterizations

Figure 53 shows the different X-ray diffractograms for each LCO pretreatment done and at the bottom the diffractograms of both precursors used for the pretreatments.

As observed on Figure 53, there are important differences within the diffractograms as function of the treatment temperature. In fact, there are peaks between 24° and 31° which intensity increases from 188°C to 405°C. There are also new peaks that appears at 405°C around 50° and 55°. Atmosphere also influences on the products obtained.

As seen on Figure 53 for the treatments at 188°C, there are several peaks that disappear between 14° and 21°, and in the interval between 24° and 27°. Less significant differences are observed when changing the atmosphere at 405°C. Only few new peaks appear when the atmosphere is changed from Ar to air. As a consequence, we suspect that atmosphere plays an important role on the phases obtained, especially at 188 °C. Several phases are present in each diffractogram. In all the cases, no $LiCoO_2$ seems to remain after the treatment because all the principal peaks of $LiCoO_2$ are absent. As for $LiCoO_2$, $NaHSO_4.(H_2O)$ precursor, seems to be absent after each pretreatment.

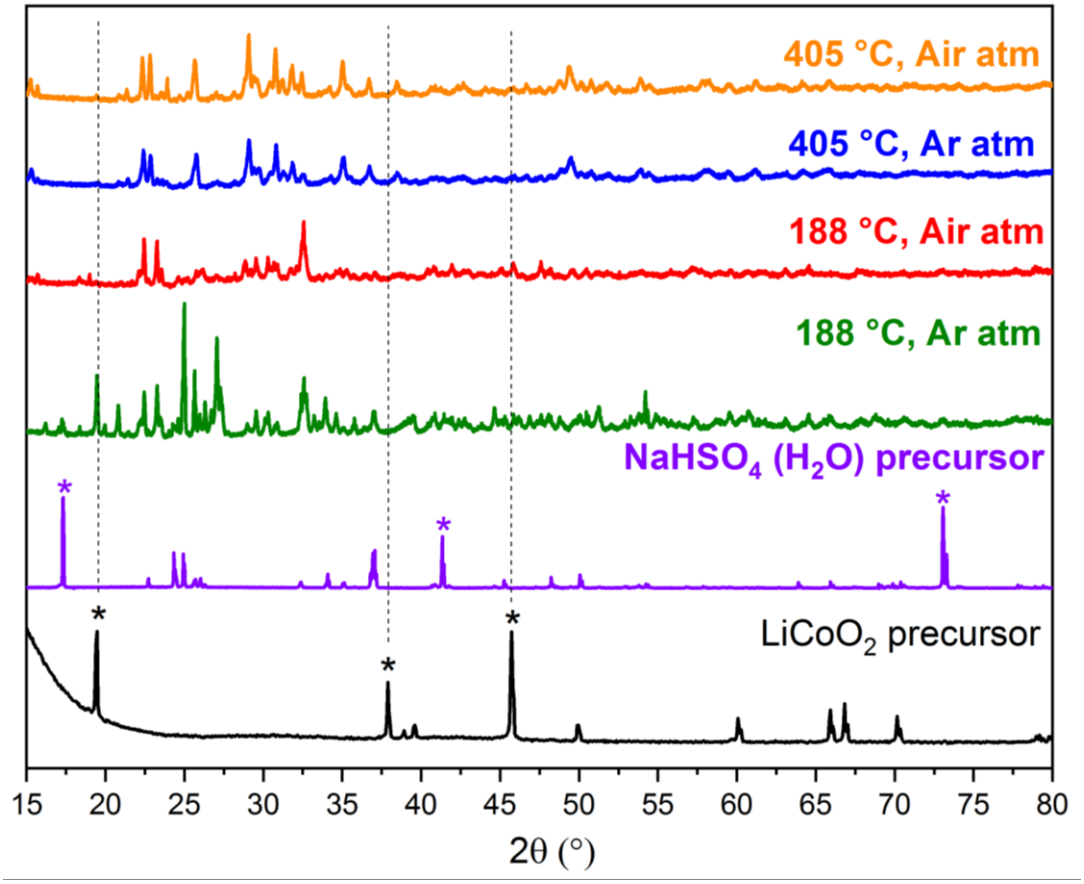

Figure 53 : X-ray diffractogram of $LiCoO_2$ pretreatment at different conditions of temperature and atmosphere. At the bottom, the diffractogram of the precursors used for the pretreatment step. X-ray scan step = 0.01 ° and total acquisition time= 3h

We did not achieve determining the phases present by the XRD measurements of Figure 53. As a consequence, we decided to start by using the pretreatment at 405°C in Ar atmosphere

for two reasons. First of all, the samples treated at a lower temperature seemed to be less homogeneous and they had a gray color, similar to $LiCoO_2$ one. The treatments carried out at 405°C and 500°C showed a purple color and they seemed to be homogenous and a total reaction taking place. Among both atmospheres, we chose Ar one because the product seemed to be homogenous and the XRD seemed to indicate less phases present compared to air treatment. We carry out new XRD measurements with a better resolution over 15h. We achieved determining most of the phases of the pretreatment product used for our electrochemical studies, as shown in Figure 54.

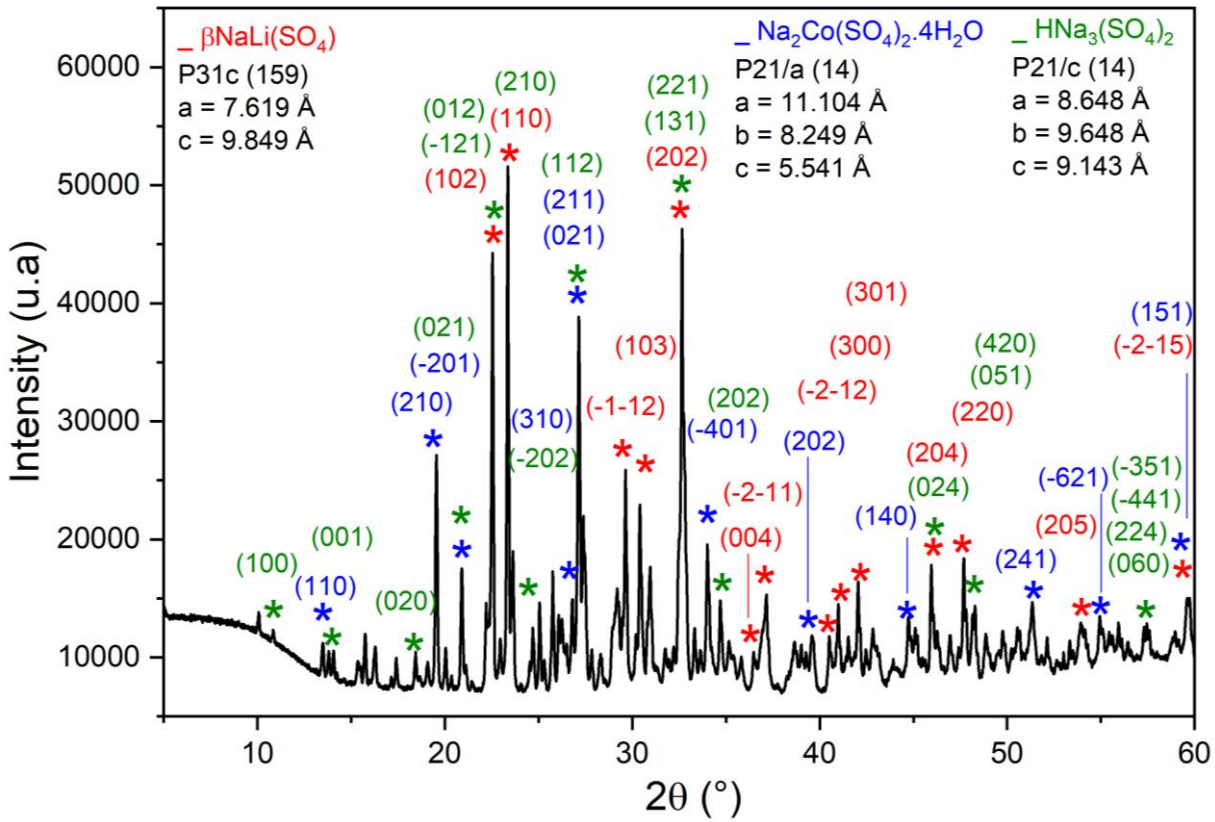

Figure 54 : X-ray diffractogram of $LiCoO_2$ treated with $NaHSO_4.H_2O$ at 405 °C, in Ar atmosphere. Scan step= 0.01° and total acquisition time= 15h

We suppose that 4 or 5 phases are present in the XRD measurement. We achieved to determine 3 phases which are: beta-$NaLi(SO_4)$, $Na_2Co(SO_4)_2.4H_2O$ and $HNa_3(SO_4)_2$. Figure 54 confirms that the precursors are not present anymore after the treatment. We can see that three sulfate phases are obtained. Furthermore, it confirms the reduction of cobalt from $LiCoO_2$ after the treatment, leading to the formation of a sulfate phase. We propose the following reduction reaction (Eq. 40):

$$4LiCoO_2 + 12(HSO_4)^- \rightarrow 4Li^+ + 4Co^{2+} + 12(SO_4)^{2-} + 6H_2O + O_2 \quad \text{(Eq. 40)}$$

3.4.2. Ex-situ XAS measurements

As complement to the XRD results, X-ray absorption spectroscopy (XAS) measurements were carried out. As detailed in chapter 2, XAS allow us to analyze the oxidation state and the local structure of cobalt. In a first step, we studied the samples prepared previously and analyzed by XRD. In a second step, we studied the reaction *in situ* (section 3.4.3).

The influence of hydrogenosulfate $NaHSO_4.H_2O$ in the oxidation state of cobalt within various conditions of temperature and atmosphere was studied. The solid product of the reaction of $LiCoO_2$ and hydrogenosulfate $NaHSO_4.H_2O$ or $KHSO_4$ was grinded and mixed with boron nitride. The mixture was pressed into a pellet to record the X-ray absorption spectrum.

Figure 55 shows XANES measurements at Co K-edge for all the pretreatment conditions tested and the reference compounds. After the treatment of $LiCoO_2$ with the hydrogenosulfate, the edge is clearly shifted toward lower energy value confirming the reduction of the cobalt in agreement with Wang *et al.* observations[145,146]. To go further, we applied the same method as described in chapter 2 to determine the averaged oxidation state of the sample. Though this method is sensitive to the choice of the integral value, it is helpful in the case of a mixture of compounds and provides more reliable results than the method using the maximum of the derivative of the spectrum. Co foil, $CoSO_4$ and $LiCoO_2$ were used as reference compounds for the calibration curve as observed in Figure 56. This figure also shows the average oxidation state determined for each sample. The edge shifts obtained for samples and references are listed in Table 19. The treatment with the hydrogenosulfate leads to an approximative oxidation state of 2.2. The sticking point is that the average oxidation state is very slightly modified by:

- the temperature: the higher leads to the better reduction
- the atmosphere: no effect
- the ion: sodium better than potassium

These microscopic results differ from the macroscopic observations, as the color changed from black-gray at 188°C to purple at 405°C, and under air the sample looks even more homogenous than under argon.

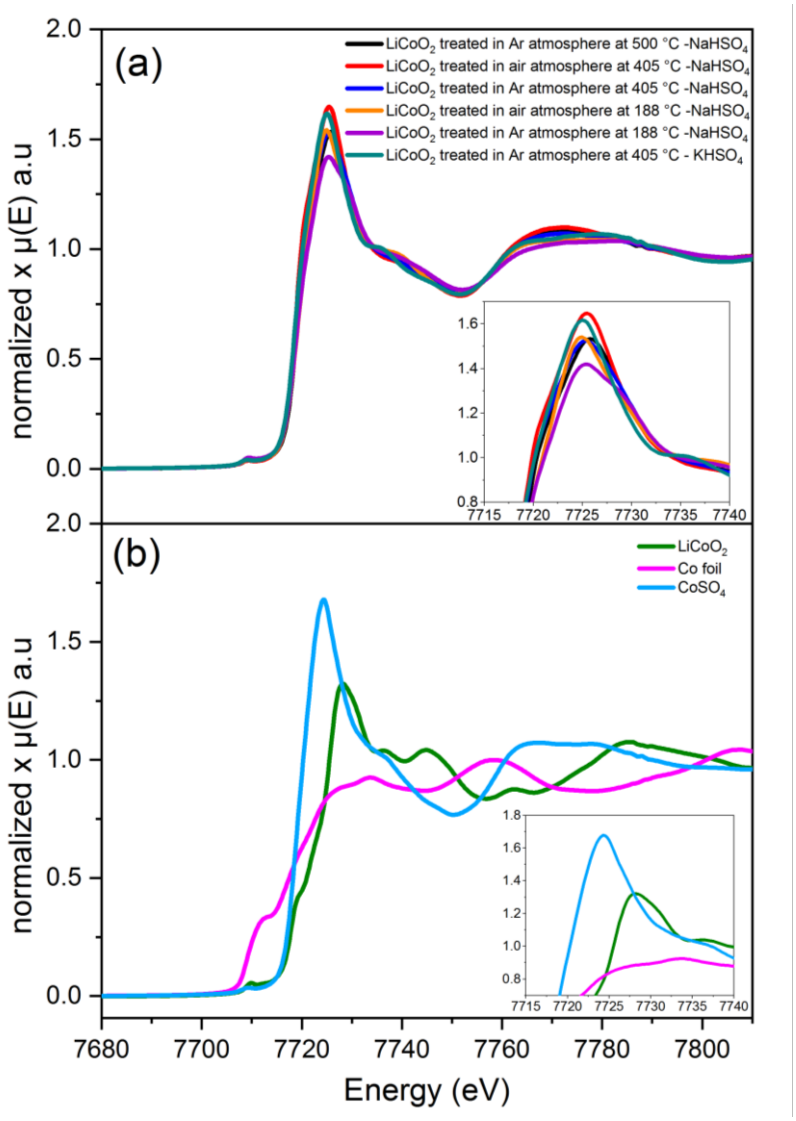

Figure 55 : Co K-edge XANES of $LiCoO_2$ pretreated with $NaHSO_4.H_2O$ or $KHSO_4$ at different temperature and atmosphere conditions (a) and 3 reference compounds (b)

Table 19 : List of reference compounds and samples measured by XAS

Compound	δE **(eV)**	**Oxidation state**
Co foil	0	0
$LiCoO_2$	6.49	3
$CoSO_4$	4.57	2
CoO	4.17	2
$LiCoO_2$ treated in Ar at 188 °C – $NaHSO_4$	4.69	2.2
$LiCoO_2$ treated in air at 188 °C – $NaHSO_4$	4.80	2.2
$LiCoO_2$ treated in Ar at 405 °C – $NaHSO_4$	4.54	2.1
$LiCoO_2$ treated in air at 405 °C – $NaHSO_4$	4.57	2.1
$LiCoO_2$ treated in Ar at 500 °C – $NaHSO_4$	4.50	2.1
$LiCoO_2$ treated in Ar at 405 °C – $KHSO_4$	4.65	2.2

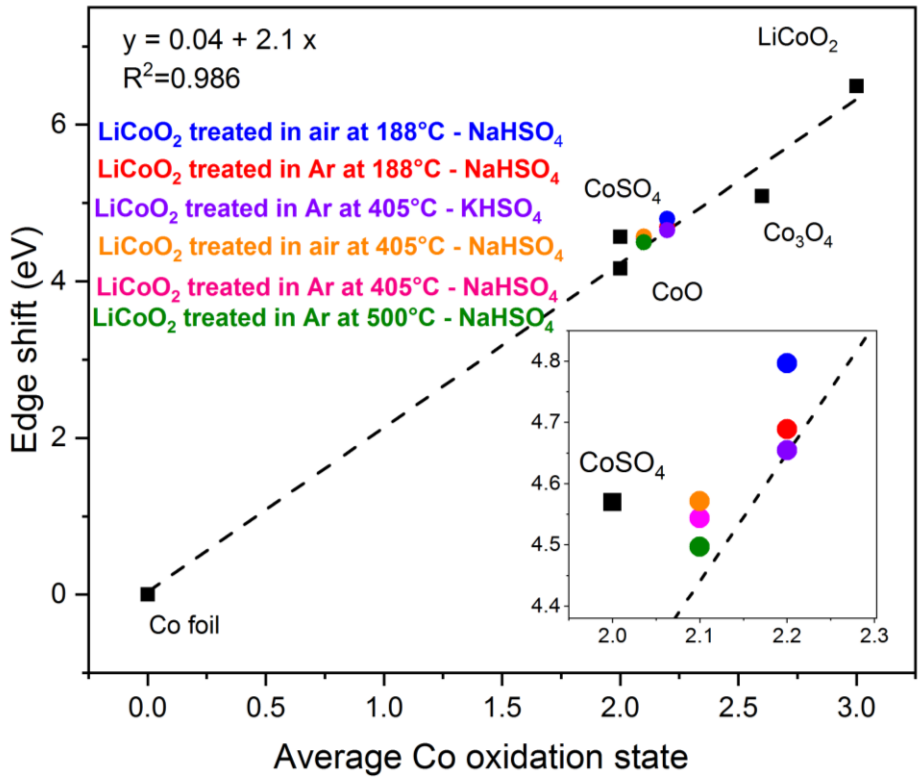

Figure 56 : Calibration curve employing different reference compounds (dash dots). Average oxidation state for $LiCoO_2$ pretreated with $NaHSO_4.H_2O$ at different temperature and atmosphere conditions

We also looked at the EXAFS part of the absorption spectra in Figure 57 (a) and (b). The EXAFS spectra for all the samples treated strongly differ from the $LiCoO_2$ one, Figure 57(a). A clear modification of the neighborhood of cobalt is observed for all the treatment conditions as compared to the native $LiCoO_2$ along with the reduction of the oxidation state. Contrary to the analysis performed in chapter 2 with the carbonate molten salt, it is not possible here to model the experimental spectra by a linear combination of solid reference compound EXAFS spectra.

We compared then the Fourier Transform (FT) of these contributions with those of $CoSO_4$ and $LiCoO_2$ to identify the speciation of cobalt, Figure 57 (c) and (d)). All the Fourier transforms show a first peak, with the maximum at about 1.5 Å, that corresponds to the cobalt-oxygen bond. This contribution is much wider for $CoSO_4$ and all the samples than for $LiCoO_2$. $LiCoO_2$ shows a very important second contribution, peak with a maximum at about 2.5 Å,

which corresponds to cobalt-cobalt bond. This contribution is absent for all the samples. It means that for all the samples only the sphere of oxygen is visible at proximity of cobalt. The highest contributions are always observed for the treatments in air atmosphere and at the highest temperature. This leads to the conclusion that the optimal reduction is obtained at least at 405°C in air atmosphere.

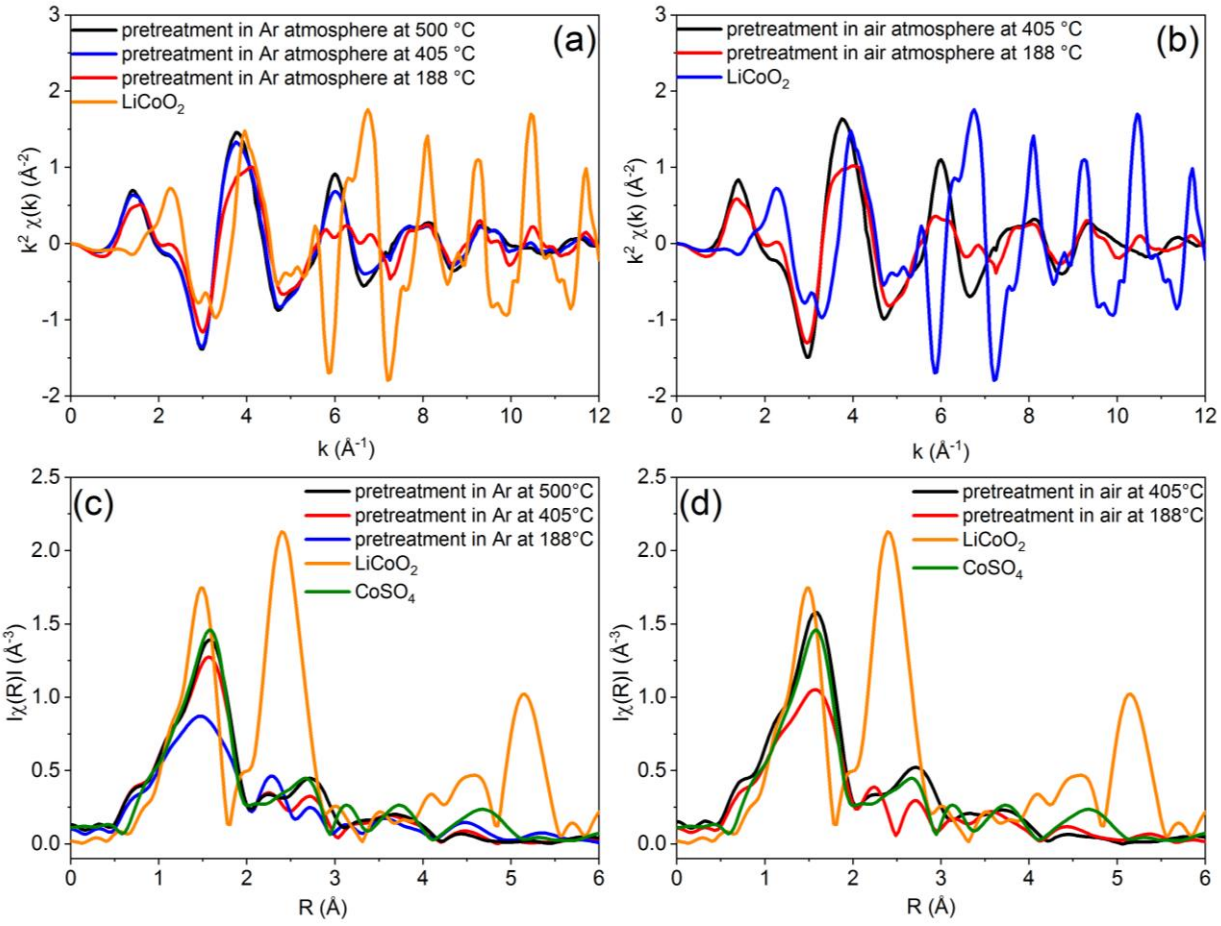

Figure 57 : Co K-edge EXAFS raw data for pretreatments of $LiCoO_2$ in: Ar atmosphere (a), air (b). EXAFS contributions of $LiCoO_2$ reference compound (a and b). Fourier transform (FT) of $LiCoO_2$ pretreated in Ar (c), air (d) and reference compounds $CoSO_4$ and $LiCoO_2$ (c and d)

Concerning the temperature effect, it can be seen that the structure for the 188°C treatment seems to be a combination of different structural environment, in contrast to the structure for 405 and 500°C treatments, as seen in Figure 57 (a). The analysis of the first neighborhood shell, i.e. the first peak of the RDF in Figure 57 (c), by back Fourier transform shows that the cobalt environment goes from the environment it has in $LiCoO_2$ crystal to the

environment it has in $CoSO_4$ crystal. At 188°C, the oscillation is intermediate between the two structures.

Concerning the atmosphere effect, we compared the oscillation of the back Fourier transform of the first peak as previously. It appears that the local environment of cobalt in the sample treated under air is closer to its environment in $CoSO_4$ than for the sample treated under Ar. This result is consistent with the macroscopic observation where the sample treated under air looks more homogenous.

In the same way, we compared the difference between $KHSO_4$ and $NaHSO_4$, and no significant effect was observed in the first shell of neighborhood.

3.4.3. In-situ XAS measurements

For this kind of measurements, we used the same device developed for *in situ* XAS described in chapter II. Here, we mixed $LiCoO_2$ with $NaHSO_4.H_2O$ in a molar proportion 1:3. We added a portion of boron nitride to this mixture to dilute the sample and to have a good beam transmission.

To determine the starting point of the reduction reaction of Co (III) from $LiCoO_2$ with $NaHSO_4.H_2O$ and its kinetics, we monitored the evolution of the reaction *in situ*. Figure 58 (a) shows the *in situ* XANES for $LiCoO_2$ mixture with $NaHSO_4.H_2O$ at different temperatures. The main peak and the pre-edge peak are shifted toward low energy value when the temperature is increased. A pre-edge peak is present in each case and it shifts as function of temperature. This is an indication of a change in the oxidation state. As previously, we determine the oxidation state and the results are listed in Table 20. The oxidation state of the samples is plotted as a function of the temperature in Figure 58 (b). A linear decrease is observed up to 400°C followed by a plateau. When cooling back to room temperature a slight increase occurs (Table 20). The reaction starts at low temperature (100°C).

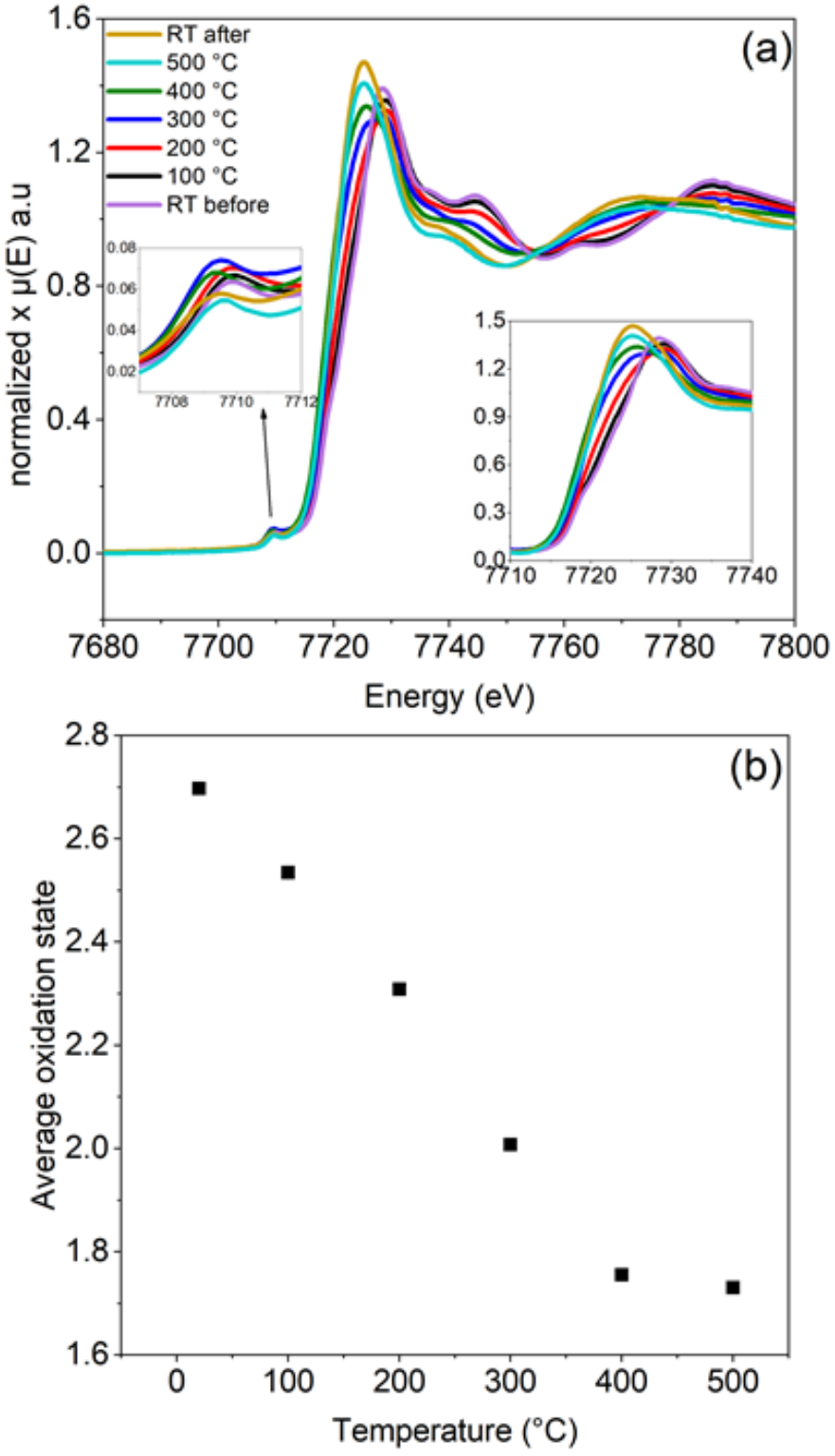

Figure 58 : In situ Co K-edge XANES of the mixture of $LiCoO_2$ with $NaHSO_4.H_2O$ at different temperatures (a). Average oxidation state of the mixture of $LiCoO_2$ with $NaHSO_4.H_2O$ evolution as function of temperature (b). RT before: at room temperature before the heating, RT after: at room temperature after the heating

Table 20 : List of samples obtained by in-situ XAS measurements and the reference compounds

Compound	δE **(eV)**	**Oxidation state**
$LiCoO_2$	6.49	3
Mixture $LiCoO_2$ with $NaHSO_4.H_2O$ at room temperature before the heating	5.76	2.8
Mixture $LiCoO_2$ with $NaHSO_4.H_2O$ at 100 °C	5.41	2.7
Mixture $LiCoO_2$ with $NaHSO_4.H_2O$ at 200 °C	4.93	2.4
Mixture $LiCoO_2$ with $NaHSO_4.H_2O$ at 300 °C	4.29	2.1
Mixture $LiCoO_2$ with $NaHSO_4.H_2O$ at 400 °C	3.75	1.9
Mixture $LiCoO_2$ with $NaHSO_4.H_2O$ at 500 °C	3.70	1.8
Mixture $LiCoO_2$ with $NaHSO_4.H_2O$ at room temperature after the heating	4.11	2.0

Figure 59 (a) and (b) show the in-situ and ex-situ EXAFS spectra for plateau temperatures of 200°C and 400°C. EXAFS oscillations for a given temperature does not superimpose indicating that the reaction is slow. Indeed, ex-situ samples have been heated for 12h while in-situ ones have been treated between 30 and 45 minutes at each temperature plateau. This is more clearly evidenced at 200°C, where the in-situ EXAFS oscillations are still characteristic of $LiCoO_2$ while the ex-situ oscillations are a combination of $LiCoO_2$ and final compound form.

We compared also the Fourier Transform of in-situ and ex-situ samples, as shown on Figure 59 (c) and (d). As it can be observed in Figure 59 (c), there is a difference between the magnitude of each sphere of neighbors between the different conditions of measurement and pretreatment. In fact, the treatment in air at 188°C has the highest contribution for the first sphere of cobalt neighbors (maximum at about 1.5 Å). This peak is assigned to the cobalt-oxygen bond. The sample at 188°C in Ar atmosphere and the in-situ measurement at 200°C show a similar magnitude for this contribution. Moreover, the in-situ measurement shows the characteristic of $LiCoO_2$ second sphere contribution of neighbors, which corresponds to cobalt one. This confirms that for the in-situ measurement at 200°C, the reduction reaction is incomplete. Figure 59 (d) also exhibits differences between the Fourier Transform of in-situ and ex-situ measurements. As before, the highest magnitude is observed for the pretreatment at 405°C in air atmosphere (ex-situ measurement). The lowest one is observed for the in-situ measurement at 400°C. This can be explained by the Debye Waller factor.

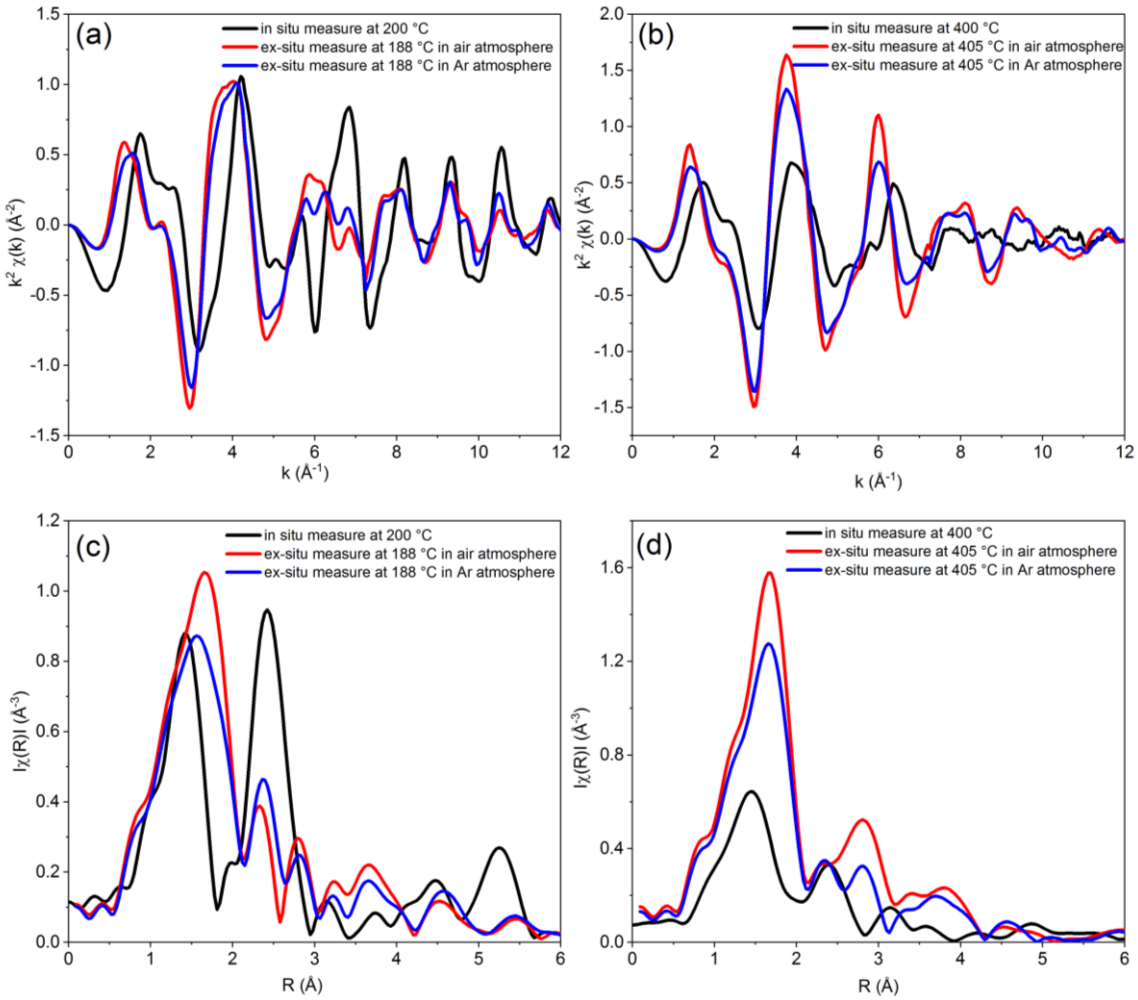

Figure 59 : Comparison of Co K-edge EXAFS raw data between in- situ measurements of mixture $LiCoO_2$ with $NaHSO_4.H_2O$ at 200°C and ex-situ measurements at 188°C (a). Their Fourier Transform comparison in (c). Comparison of Co K-edge EXAFS raw data between in- situ measurements of mixture $LiCoO_2$ with $NaHSO_4.H_2O$ at 400°C and ex-situ measurements at 405°C (b). Their Fourier Transform comparison in (d)

3.5. Influence of $NaHSO_4.H_2O$ on $LiCoO_2$ solubility in molten LiCl-KCl eutectic

Cobalt dissolution between LCO with and without being pretreated with $NaHSO_4.H_2O$ was compared (Figure 60). For both cases, the voltammogram shows the presence of an anodic and a cathodic peak. Their positions and current density can be seen in Table 21. For both measurements the starting point was 0.8 V vs Co^{II}/Co^0 and corresponds to the OCP of one of both systems. There is an important difference in the peaks' width for both voltammograms. Furthermore, the cathodic standard potentials show a difference of about 8. 10^{-2} V. Both aspects may be explained by a difference in cobalt Co(II) speciation in the medium.

As the current density of both cathodic peaks is compared, pretreated LCO peak shows a current density about 10 times higher than the one without the pretreatment. As peaks current density is linked to dissolved cobalt concentration (Eq. 33), it can be concluded that hydrogenosulfate $NaHSO_4.H_2O$ increases the solubility of cobalt from LCO in eutectic LiCl-KCl. This result is explained by the reduction of Co(III) in this compound into Co(II), which can be then dissolved in molten chloride as Co^{+II}. This is in accordance with the literature as Delarue has previously shown that Co(II) in cobalt oxide is dissociated into Co^{+II} in this medium[136].

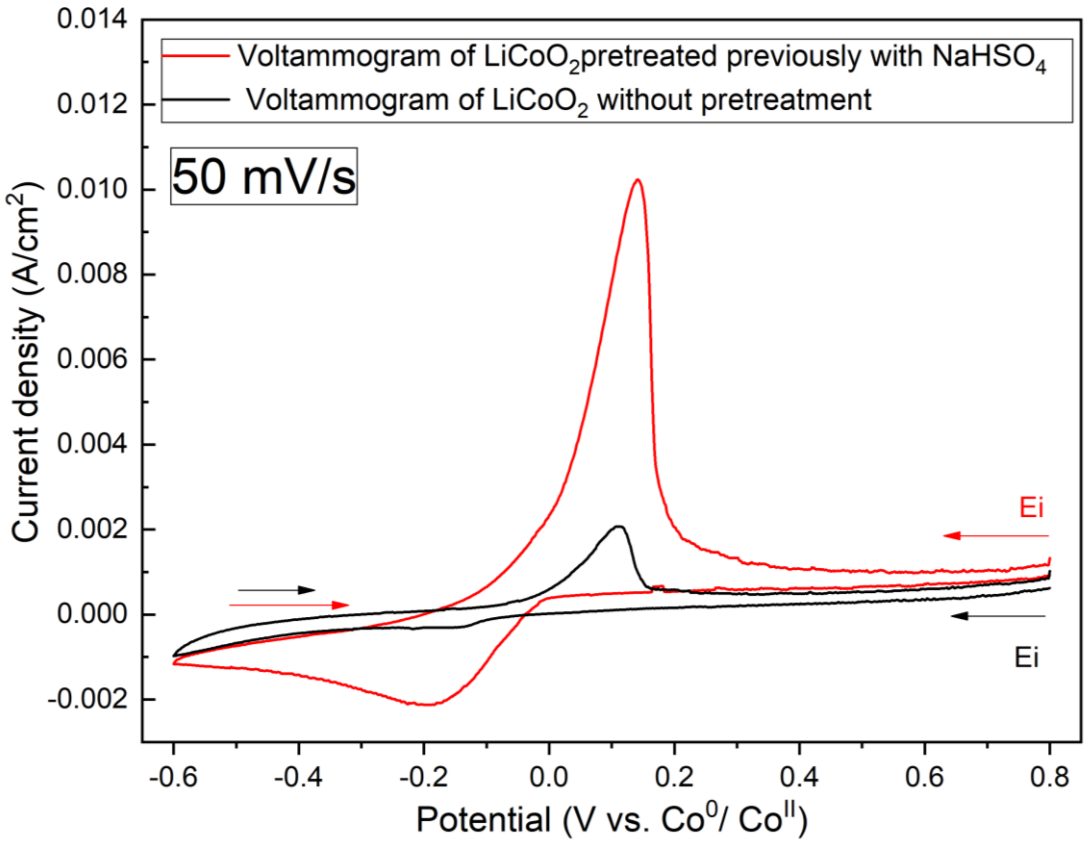

Figure 60 : Voltammogram comparison for $LiCoO_2$ (LCO) in molten eutectic LiCl-KCl on glassy carbon working electrode at 405°C (8h), 1 atm Ar with and without pretreatment. Graphite and cobalt used as counter and reference electrodes. Introduced cobalt concentration equal to 1.10^{-5} mol.cm^{-3}

Table 21 : Voltammogram parameters comparison between LCO with and without pretreatment (with $NaHSO_4.H_2O$ for 12h at 405°C) in molten eutectic LiCl-KCl

Compound	Anodic peak position (V vs. Co^{II}/Co^0)	Cathodic peak position (V vs. Co^{II}/Co^0)	Cathodic peak current density ($A.cm^{-2}$)	Measurement starting potential (V vs. Co^{II}/Co^0)
LCO in eutectic LiCl-KCl	0.11	-0.16	$3.12\ 10^{-4}$	0.8
Pretreated LCO in eutectic LiCl-KCl	0.14	-0.19	$2.7\ 10^{-3}$	0.8

In order to determine the necessity of a long thermal pretreatment (between $LiCoO_2$ and $NaHSO_4.H_2O$) and to define the best protocol, the impact of this one on cobalt dissolution was studied. In one case, $LiCoO_2$ was firstly mixed with eutectic chlorides LiCl-KCl and then melted. To this molten mixture, $NaHSO_4.H_2O$ was added (A on Figure 61). In the other case, $LiCoO_2$ was first mixed with $NaHSO_4.H_2O$ and heated during 12h at 405°C. This mixture was then added to molten eutectic LiCl-KCl (B on Figure 61). The details of peak positions for each voltammogram are found in Table 22.

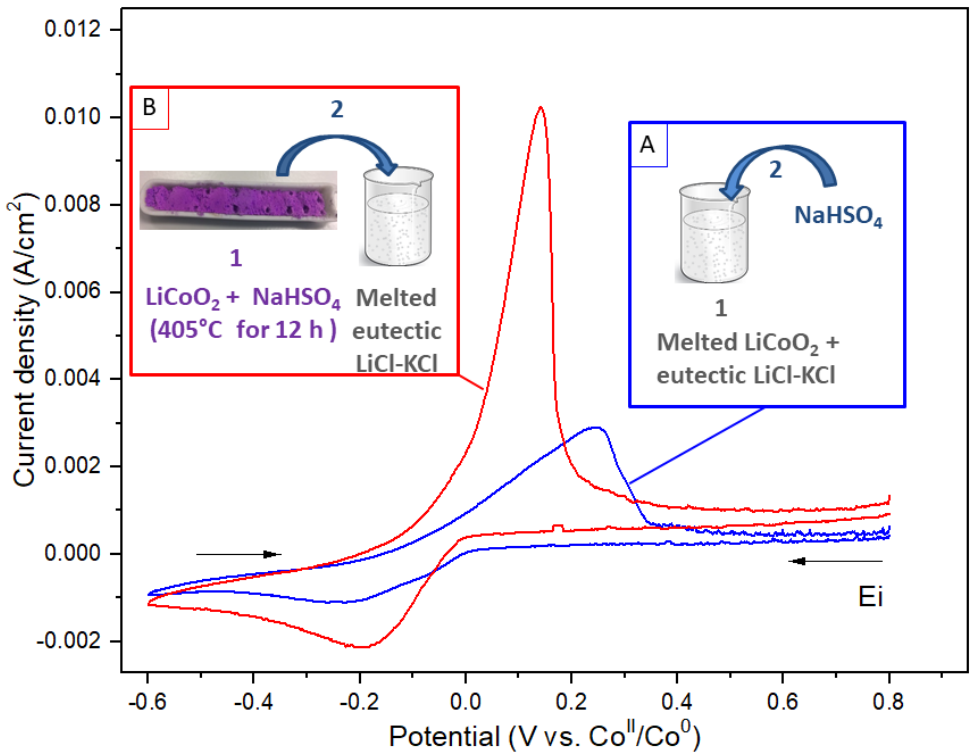

Figure 61 : Voltammogram comparison for $LiCoO_2$ (LCO) in molten eutectic LiCl-KCl according to the order of $NaHSO_4.H_2O$ addition on glassy carbon working electrode at 405°C (8h), 1 atm Ar. Graphite and cobalt used as counter and reference electrodes. Introduced cobalt concentration equal to 1.10^{-5} $mol.cm^{-3}$. Scan rate: 50mV/s

Table 22 : Voltammogram parameters comparison between both conditions of $NaHSO_4.H_2O$ addition shown on Figure 61

Voltammogram on figure 61	**Anodic peak position (V vs. Co^{II}/Co^0)**	**Cathodic peak position (V vs. Co^{II}/Co^0)**	**Cathodic peak current density ($A.cm^{-2}$)**	**Measurement starting potential (V vs. Co^{II}/Co^0)**
A	0.24	-0.22	$1.1\ 10^{-3}$	0.8
B	0.14	-0.21	$2.4\ 10^{-3}$	0.8

When comparing both voltammograms, we observed a difference in the shape of both cathodic and anodic peaks and the distance between them. In fact, A shows a wider anodic peak than B. Furthermore, a difference of 0.009 V appears between both cathodic potentials. Both variations may be explained by a difference of Co(II) speciation in the system. Regarding the distance between voltammograms cathodic and anodic peaks, it is higher in the case of A. This may imply that for A the redox reaction is limited by the charge transfer, while for B it is limited by the mass transport. This leads to the conclusion that cobalt cations are more available around the electrode in B.

When comparing both cathodic peaks, it can be seen that B shows a current density two times higher than A. It means, there is twice cobalt dissolution when the thermal pretreatment is present ($LiCoO_2$ mixed with $NaHSO_4.H_2O$ for 12h at 405°C), confirming its impact on $LiCoO_2$ dissolution in the melt. As a consequence, the protocol adopted for the next studies included this thermal step as the first one.

Hydrogenosulfates addition approach was also tested on molten carbonates. Here previously pretreated $LiCoO_2$ was mixed with molten carbonates before the heating (using method B in Figure 61). The results of both systems, with and without pretreatment, are shown in Figure 62. As observed, hydrogenosulfates pretreatment does not increase cobalt dissolution from $LiCoO_2$ in molten carbonates. Cathodic and anodic peaks are quite similar in both cases. This result was expected as cobalt dissolved in form of Co(II) in molten carbonates, as seen in chapter II from XANES results.

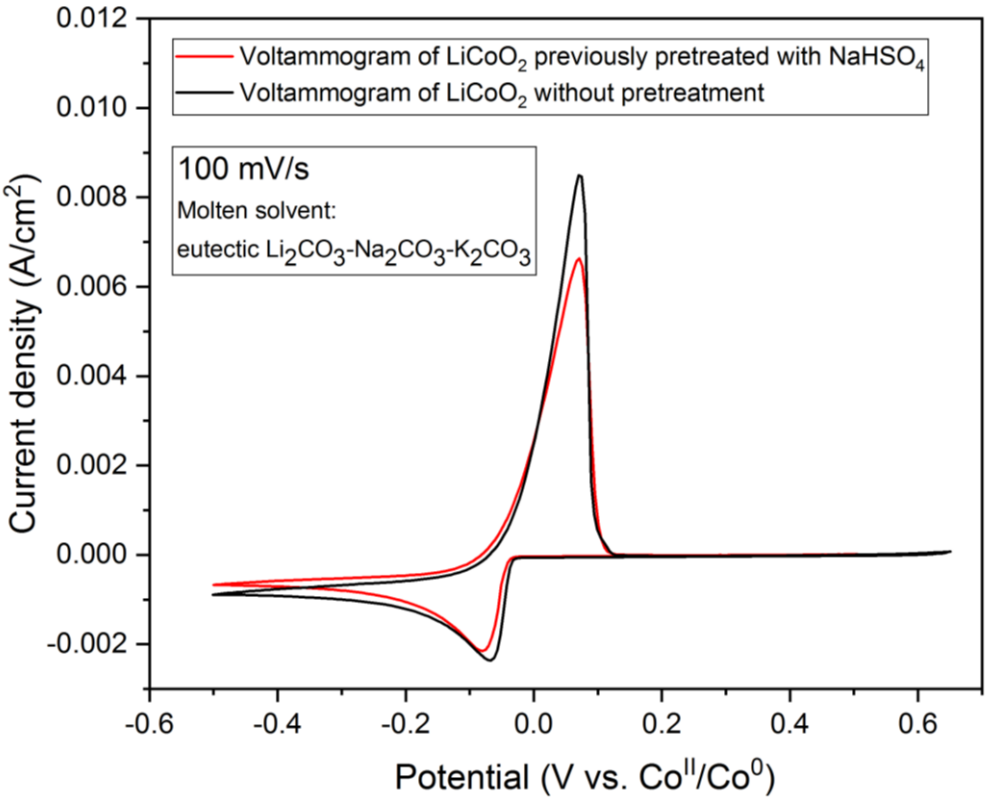

Figure 62 : Voltammogram comparison for $LiCoO_2$ (LCO) in molten eutectic Li_2CO_3-Na_2CO_3-K_2CO_3 on silver wire working electrode at 450°C (168h), 1 atm Ar with and without pretreatment. Graphite and cobalt used as counter and reference electrodes. Introduced cobalt concentration equal to 2.5 10^{-5} mol.cm^{-3}.

3.6. Electrochemical study of $LiCoO_2$ pretreated with $NaHSO_4.H_2O$ in molten LiCl-KCl eutectic

Quantifying dissolution

The voltammogram in Figure 63 shows the redox system observed in this case. For the details about electrode preparation, they are given in section 2.2 of this chapter. The cathodic and anodic peaks are present at -0,504 ± 0.005 and -0,371 ± 0,004 V. vs Ag^I/Ag^0 respectively. The measurement was done from the OCP (-0.1 V. vs Ag^I/Ag^0) towards the cathodic potentials and backwards. As before, there is the same negative potential shift, about 0.2V, compared to the literature. The same problems encountered with the reference electrode for $LiCoO_2$ (Figure 50) appeared in this case.

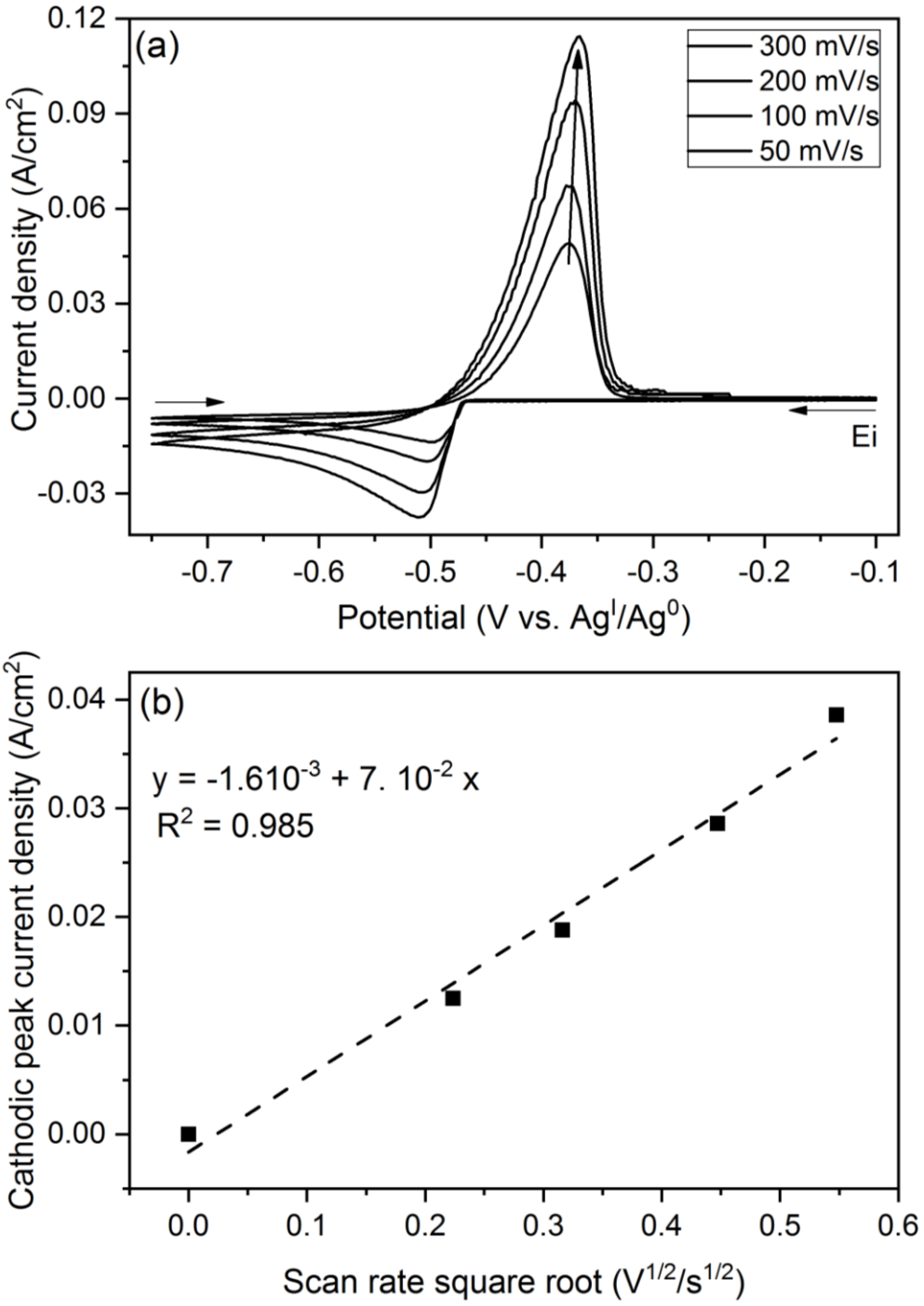

Figure 63 : Voltammograms of the solution containing LCO pretreated with $NaHSO_4.H_2O$ in eutectic molten LiCl-KCl on gold wire working electrode at 405°C (for 48h), 1 atm Ar (a). Its cathodic peak current density evolution in function of cyclic voltammetry scan rate square root (b). Graphite and Ag^I/Ag^0 were used as counter and reference electrodes, respectively. Cobalt concentration introduced equal to 5.10^{-5} mol.cm^{-3}

XANES results in section 3.4 of this chapter confirmed Wang *et al.* results[145,146] implying Co(III) from $LiCoO_2$ reduction into Co(II). This results leads to the conclusion that the observed redox reactions on Figure 63 correspond to Co (II)/Co(0) couple, with a single two-electron exchange for reduction and oxidation. The reduction of cobalt Co^{+III} into Co^{+II} was also confirmed by the physical aspect of the cooled bath (Figure 64), which shows a blue color characteristic of Co^{+II} in molten chlorides as reported in the literature [136].

Figure 64 : Appearance of the cooled bath $LiCoO_2$ pretreated with $NaHSO_4.H_2O$ in eutectic molten LiCl-KCl after the heating

The dissolved cobalt concentration $[Co^{+II}]$ was calculated by using Berzins and Delahay relation (Eq. 33). This concentration value was correlated with Flame atomic absorption spectroscopy (F-AAS) and Inductively Coupled Plasma- Atomic Emission Spectroscopy (ICP-AES) measurements, as shown on

Table 23. All the values obtained are quite similar (about 2. 10^{-5} mol.cm^{-3}). There is no the difference within the techniques observed in molten carbonates and LCO without pretreatment measurements. This is a surprising result as no matrix effect is observed, in particular due the presence of sodium.

Table 23 : Results of dissolved cobalt concentration $[Co^{+II}]$ for $LiCoO_2$ pretreated with $NaHSO_4.H_2O$ in eutectic molten LiCl-KCl obtained by electrochemistry and flame spectroscopy

Cathode material	**Slope ($A.cm^{-2}.V^{-1/2}.s^{1/2}$)**	**Measured by CV $[Co^{+II}]$ ($mol.cm^{-3}$)**	**Measured by F-AAS $[Co^{+II}]$ ($mol.cm^{-3}$)**	**Measured by ICP.$[Co^{+II}]$ ($mol.cm^{-3}$)**
LCO pretreated with $NaHSO_4.H_2O$	$7.\ 10^{-2} \pm 0.40\ 10^{-2}$	$2.5\ 10^{-5}$	2.10^{-5}	2.310^{-5}

When comparing both dissolution values obtained for LCO with (this section) and without pretreatment (section 3.3), we can conclude that dissolved cobalt concentration is about 10 times more important.

Cobalt electrodeposition from pretreated $LiCoO_2$ with $NaHSO_4.H_2O$ in molten chlorides LiCl-KCl eutectic

Once that pretreated $LiCoO_2$ with $NaHSO_4.H_2O$ was studied by cyclic voltammetry, the possibility of recovering metallic cobalt by electrolysis from this medium was investigated. The following section shows the results of the deposit obtained and the analysis of the electrodeposited product. Figure 65 (a) shows the chronoamperogramm obtained during the electrodeposition.

From the beginning of the electrolysis, there is a continuous increase in the current. It indicates that there is a constant rise of the electrode surface area, and leads to the conclusion that the deposit corresponds to a conductor material. The deposit is a solid with black and blue colors as observed in Figure 65 (b). The blue color can be attributed to the solvent (where Co(II) is dissolved). For this reason, we rinsed it with distilled water and dried the deposit before analyzing it.

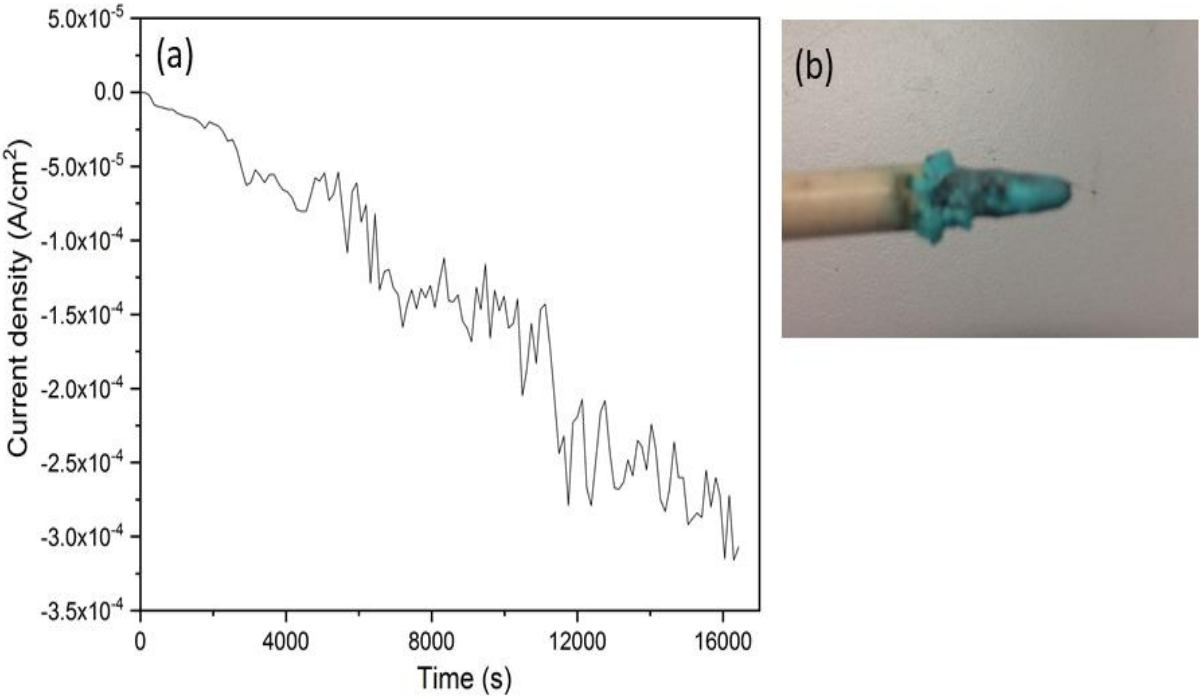

Figure 65 : Chronoamperogramm during the electrolysis on gold wire electrode (a). Photo of the deposit (b). Graphite and Ag^I/Ag^0 were used as counter and reference electrodes, respectively. The potential steps from -0.10 V to -0.65 V vs. Ag^I/Ag^0

Figure 66 shows the deposit X-ray diffraction (XRD) measurement, for the first electrode set-up tested. The X-ray diffraction measurement in Figure 66 confirms that the recovered matter is constituted of metallic cobalt by the presence of the two principal peaks of it at 41.54 and 47.41 °. This implies that the recovery of metallic cobalt in molten chlorides after pretreating it with $NaHSO_4.H_2O$ is possible by electrochemical means.

Other metals are also observed on the deposit. In fact, silver, gold and copper seem to be present. In order to confirm the presence of these impurities Energy-dispersive X-ray spectroscopy (EDX) was used.

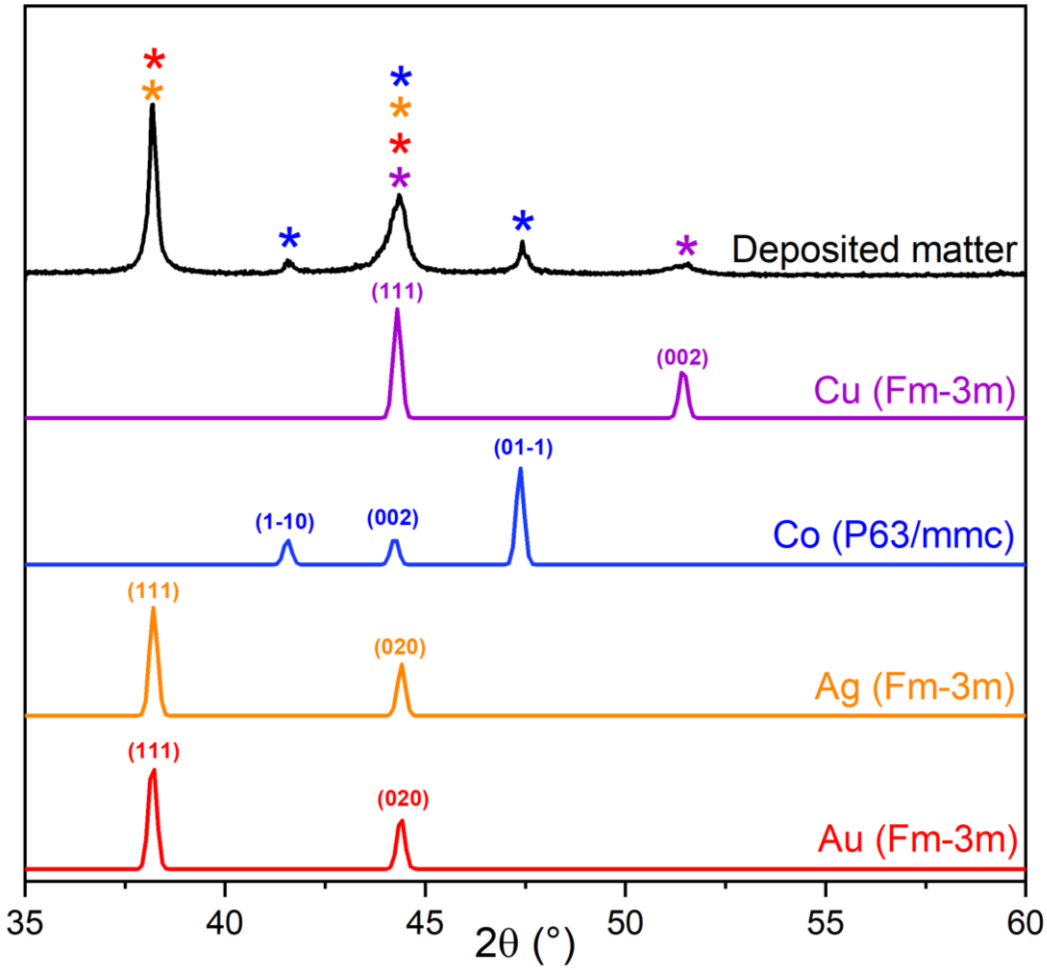

Figure 66 : XRD of deposited matter after washing, from $LiCoO_2$ pretreated with $NaHSO_4.H_2O$ in molten eutectic LiCl-KCl on gold wire working electrode. Graphite and Ag^I/Ag^0 were used as counter and reference electrodes, respectively

Figure 67 shows cartographies obtained for each deposit constituent by this technique. The cartographies confirm that the electrodeposited matter recovered is constituted by cobalt. Furthermore, they confirm the presence of silver, gold and cooper pollutions. The existence of chlorides and oxygen compounds are also identified by EDX measurement. The presence of silver can be explained by a leak of the reference electrode. The copper observed can be explained by the fall of the counter electrode which is constituted by a graphite rod connected to a copper wire. The gold presence can be attributed to an attack of the working electrode.

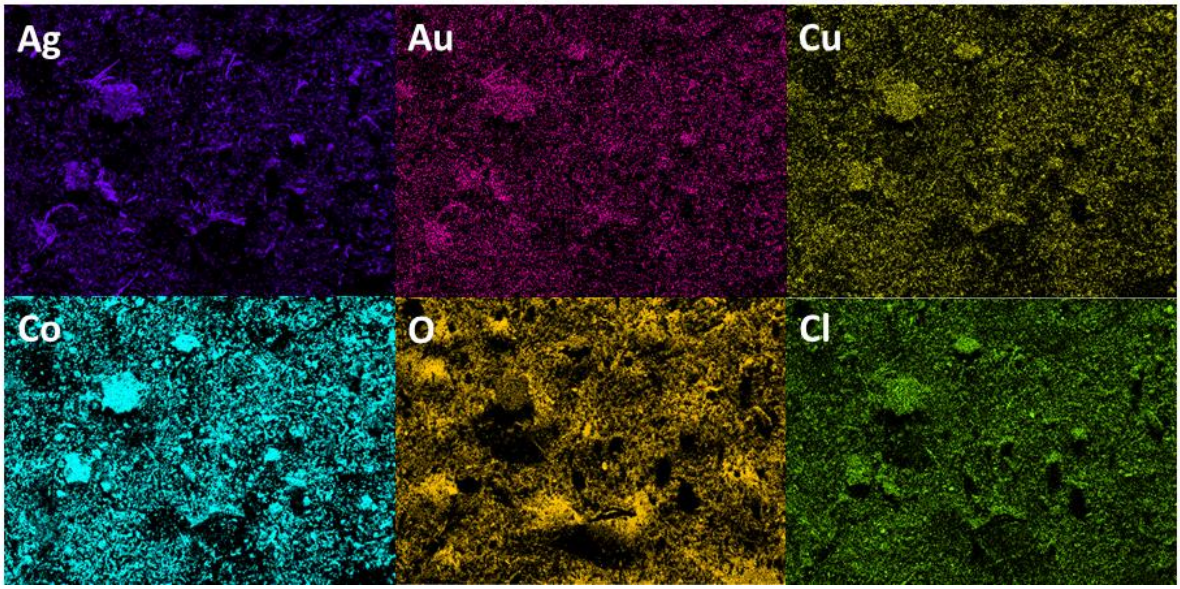

Figure 67 : Energy-dispersive X-ray spectroscopy (EDX) cartographies of the deposit, from $LiCoO_2$ pretreated with $NaHSO_4.H_2O$ in molten eutectic LiCl-KCl on gold wire working electrode. Measurements were done on a carbon support, at room atmosphere and temperature. Graphite and Ag^I/Ag^0 were used as counter and reference electrodes, respectively

The quantities of each element are shown in the Table 24 below. We do not consider the portion of carbon detected, as the support of the sample for EDX is made of it. As shown, the cobalt is the element present in the highest weight % in the sample. The presence of a non-depreciable quantity of copper and silver is also confirmed, which is respectively 6.9 and 15.4 weight %. Gold presence was also confirmed in a low percentage of 0.4 weight percent. Furthermore, the estimated quantity of oxygen in the electrodeposited matter may be explained by the fact that the measurement was done at room atmosphere and the deposit can be easily oxidized.

Table 24 : Weight composition of electrodeposited from $LiCoO_2$ pretreated with $NaHSO_4.H_2O$ in molten eutectic LiCl-KCl on gold wire working electrode. Graphite and Ag^I/Ag^0 were used as counter and reference electrodes, respectively

	O % weight	**Cl % weight**	**Co % weight**	**Cu % weight**	**Ag % weight**	**Au % weight**
Mean	30.2	0.1	**46.6**	**6.9**	**15.4**	0.4

From these results, it was concluded that several optimizations of the electrodes set-up were needed. Ag^{I}/Ag^{0} reference electrode was not the most suitable to obtain a deposit without pollutions. Furthermore, an optimization in the counter electrode conception was needed in order to prevent the counter electrode and its connecting wire from falling in the molten melt. Finally, it seemed to be necessary to test in the future other materials as working electrodes as gold was attacked during the electrolysis. First, the silver reference was changed by a cobalt bar as reference electrode and the counter electrode connector wire changed by a steel rod.

The Figure 68 (a) shows the chronoamperogramm obtained during the electrolysis, for the second electrode set-up tested. There is an abrupt increase in the current at the beginning of the electrolysis. Then, there is a continuous rise of the current due to the increase in the electrode surface. This trend is observed until about 4500 s, where a plateau is observed. This is a sticking result as the deposit is expected to be a conductor material.

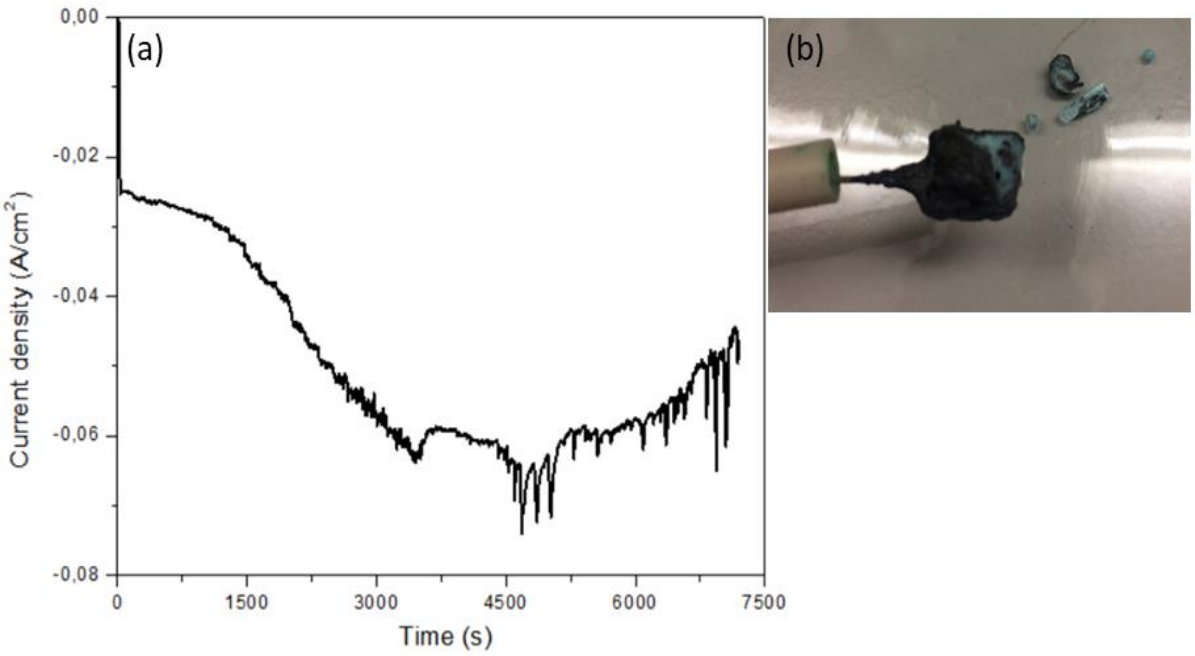

Figure 68 : Chronoamperogramm during the electrolysis on gold plate electrode (a). Photo of the recovered matter (b). Graphite and cobalt were used as counter and reference electrodes respectively. The potential steps from 0.50 V to -0.30 vs. Co^{II}/Co^{0}.

The recovered matter has the same aspect of the previous recovered matter (solid with black and blue colors), as seen in Figure 68 (b). The Figure 69 shows the XRD measurement obtained for the electrodeposited matter. As it is observed, the deposit is constituted by cobalt and gold essentially. As a consequence, it can be concluded that the optimization of electrodes

set-up was efficient because there are no more copper and silver pollutions observed. Furthermore, these results confirm once again that metallic cobalt can be recovered by electrodeposition from this system.

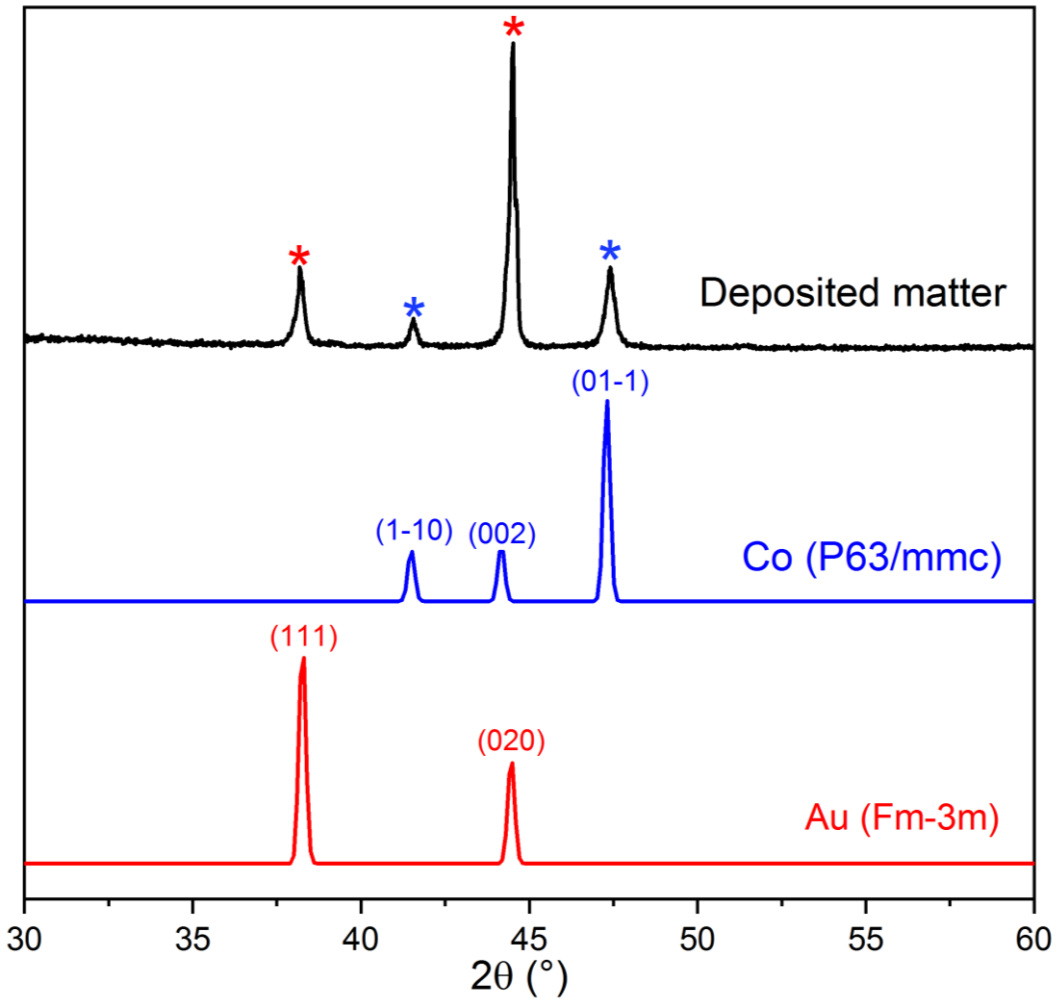

Figure 69 : XRD of deposited matter from $LiCoO_2$ pretreated with $NaHSO_4.H_2O$ in molten eutectic LiCl-KCl on gold plate working electrode. Graphite and cobalt were used as counter and reference electrodes, respectively

As before, we analyzed the deposited matter by EDX to determine the composition of it. Figure 70 exhibits the cartographies of each element present in the recovered matter. They confirmed the presence of gold and cobalt already detected by XRD measurement. The presence of gold confirms the attack of it during the electrolysis. As before, the presence of oxygen can be attributed to the possible oxidation of the deposit in room atmosphere. The quantities of each element were estimated by EDX as shown in Table 25.

Table 25 : Weight composition of electrodeposited from $LiCoO_2$ pretreated with $NaHSO_4.H_2O$ in molten eutectic LiCl-KCl on gold plate working electrode. Graphite and cobalt were used as counter and reference electrodes, respectively

	O % weight	**Cl % weight**	**K % weight**	**Co % weight**	**Au % weight**
Mean	16.2	0.6	0.1	**78.6**	**4.5**

Cobalt is the element with the highest ratio on the deposit, about 78.6 weight %. The presence of a non-depreciable quantity of gold, about 4.5 weight %, is also detected.

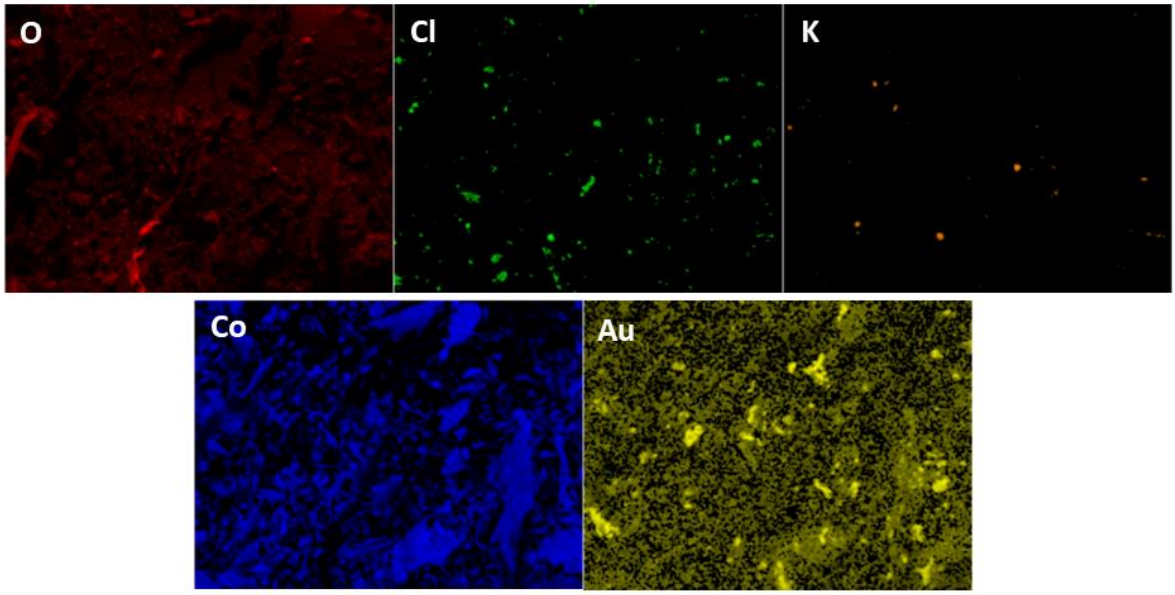

Figure 70 : Energy-dispersive X-ray spectroscopy (EDX) cartographies of the deposit, from $LiCoO_2$ pretreated with $NaHSO_4.H_2O$ in molten eutectic LiCl-KCl on gold plate working electrode. Measurements done on a carbon support and at room atmosphere and temperature. Graphite and cobalt were used as counter and reference electrodes, respectively

We also characterized the deposited matter by Scanning Electron Microscopy (SEM) as shown in Figure 71. The deposited matter appears to have the form of leaf trees of different sizes and forms. In some cases, they agglomerate to form larger particles. These leaves are not constituted of a single element but cobalt appears to be the preponderant constituent of them. Furthermore, the particles do not appear to be distributed uniformly.

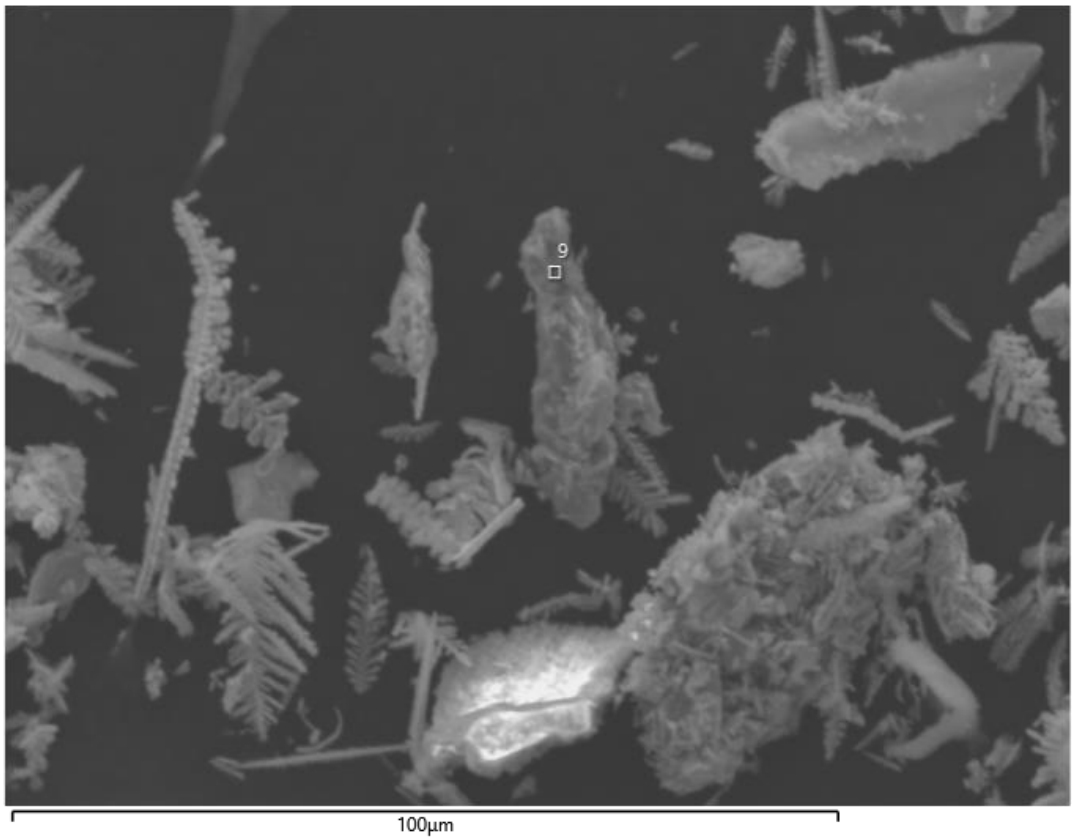

Figure 71 : Scanning Electron Microscopy (SEM) image of the of the deposit, from $LiCoO_2$ pretreated with $NaHSO_4.H_2O$ in molten eutectic LiCl-KCl on gold plate working electrode. Graphite and cobalt were used as counter and reference electrodes, respectively

4. Conclusions

In this chapter, it was proven that the cathode material $LiCoO_2$ shows a low dissolution in molten chlorides (LiCl-KCl). As a consequence, LiCl-KCl eutectic does not exhibit one of the key features for considering it as a "good" molten medium for cobalt recycling: solubilizing cathode materials such as LCO. Nevertheless, it was proven that thermal pretreatment of $LiCoO_2$ with $NaHSO_4.H_2O$ can enhance its dissolution about 10 times in molten eutectic LiCl-KCl because it reduces Co(III) into Co(II). Ex-situ XAS results confirms this reduction for all the thermal treatments. The thermal treatment at least at 405°C in air atmosphere appears to be the optimal protocol for the reduction of cobalt. Furthermore, in-situ measurements allow us to monitor the kinetics of the reaction. By this way, it has been demonstrated that the average oxidation state evolves slowly as function of temperature and stabilizes at +II at about 500°C.

Moreover, it was shown that when using this thermal pretreatment, it is possible to recover metallic cobalt by electrochemical means on gold working electrode, where cobalt constitutes 78.6 weight% of the deposit. Therefore, this approach is promising for the future. The pretreatment impact on other cathode materials NCA and NMC dissolution in molten LiCl-KCl appears to be one of the steps to follow.

Regarding the experimental set-up presented in this chapter, it can be concluded that cobalt pseudo-reference is more practical than Ag^{I}/Ag^{0} as it prevents the pollution of the deposit by silver. Looking for another working electrode material is necessary in the future, as gold electrode is attacked during the electrolysis. Tungsten can be suggested as a candidate to be tested. For matter of time, this electrode was not tested for electrolysis during this project.

It is important to note that regarding the recovery of metallic cobalt from Co_3O_4, new approaches have been developed recently by using non miscible molten mixtures, containing one alkali chlorides phase. Amietszajew *et al.* studied Co_3O_4 in this kind of system. The mixture was composed of a borate phase (Na_2O-$2B_2O_3$) and a chloride one (NaCl) [147]. In the oxide melt Co_3O_4 was dissolved and then transported to the oxide/chloride interface and finally transferred to the chloride phase. The results from this work showed that cobalt form Co_3O_4 is present in the molten media at two oxidation states +II and +III. Furthermore, it was proven that 99% pure metallic cobalt can be recovered by electrolysis from this medium. This kind of system could be another alternative to explore in the future.

General conclusions and perspectives

"Il faut faire de la vie un rêve et d'un rêve une réalité."

Marie Curie

Li-ion batteries are composed of organic and inorganic compounds. Molten salts systems are widely applied as solvents for different metals recovery and manufacturing, by electrolysis. Furthermore, some molten systems have the capacity of trapping and/or decomposing hazardous organic compounds. From these points of view, they seem promising candidates for Li-ion batteries recycling. The main objective of this work was to explore and analyze the feasibility of recycling Li-ion battery organic and inorganic compounds (cathode materials) in one molten system. Among the different inorganic compounds in Li-ion battery our aim was particularly to understand cobalt behavior in the molten media and exploring the possibility of recovering it by electrolysis. We selected two molten media during this project: molten carbonates (Li_2CO_3-Na_2CO_3-K_2CO_3) and molten chlorides (LiCl-KCl).

In this context, a good solvent should fulfill three main requirements. First of all, it must show a good dissolution of cathode oxides and particularly of cobalt oxide. Secondly, it should ensure the possibility of recovering cobalt by electrochemical means. Finally, the third condition consists in the good decomposition of Li-ion battery organic compounds such as: binders, separators.

Concerning cobalt speciation, XAS experiments in molten carbonates highlights that cobalt is reduced from +III to +II in molten Li_2CO_3-Na_2CO_3-K_2CO_3 for LCO, NCA and NMC cathode materials. Moreover, results show that for LCO, it is transformed into CoO, which remains stable during all the XAS experiment. If we consider the possibility of valorizing this compound, it would be difficult as industries generally use cobalt carbonate or sulfate as precursors for their applications.

Regarding cobalt dissolution, we establish that cobalt from cathode materials LCO, NCA and NMC dissolution kinetics in molten carbonates is slow. Cyclic voltammetry, flame spectroscopy and ICP-AES results reveal that its maximal dissolution in this medium is low. XRD results on the deposit from electrolysis in this medium, demonstrate that the dissolution of cobalt is too low for its recovery by electrochemical means. Indeed, no cobalt is detected in the recovered matter. With respect to organic compounds recycling, preliminary results show the decomposition of Li-ion battery binders CMC, PVDF and separator PP in different hydrocarbons. From all these results, the molten Li_2CO_3-Na_2CO_3-K_2CO_3 eutectic seems not to be the most suitable for cobalt recovery but a promising alternative to explore the future regarding organic compounds valorization.

The results in molten chlorides also reveal a low dissolution of cobalt from cathode material LCO, confirming that Co(III) form is very poorly soluble in this medium. Nevertheless, Cyclic voltammetry, flame spectroscopy and ICP-AES results demonstrate that a thermal pretreatment of cathode material LCO with $NaHSO_4.H_2O$ enhances cobalt solubility about 10 times in molten chlorides. XAS results confirm the reduction of Co(III) into Co(II) and the slow evolution of cobalt oxidation state as function of temperature. Cobalt electrodeposition success has been proven for LCO in molten chlorides when we apply a thermal pretreatment of cathode material with $NaHSO_4.H_2O$ previously. Indeed, EDX and XRD results highlight that cobalt is the predominant element in the deposit with at least 46% weight. For the study in molten chlorides, the choice of electrode and their fabrication was a challenge needed to be addressed. XRD and EDX results reveal that leaks are constantly observed for Ag^I/Ag^0 leading to the presence of pollution in the deposit. Results demonstrate that gold working electrode can be used for achieving cobalt recovering in this medium but no without been attacked.

During this work we developed a whole set-up for measuring the absorption spectrum of cobalt in molten salts. We demonstrate its reliability for performing measurements at 550°C for several hours.

This thesis work opens several routes for the future:

With respect to XAS results in molten carbonates, the need of new measurements in the same conditions of electrochemical measurements is necessary in the future, to confirm the formation of CoO small aggregates in the bath and the reduction of a portion of Co (II) into metallic cobalt in molten carbonates. Furthermore, the in-situ XAS measurements of electrolysis could be carried out in the same device developed during this project. The addition of electrodes can be done in this device design. Moreover, the cell design developed during this project could be manufactured in the future in boron nitride for in-situ studies in hydrogenosulfates, as we detected no interaction between it and the sample mixture (cobalt + hydrogenosulfates).

Regarding cobalt recovery by electrolysis, molten chlorides LiCl-KCl are a suitable system but only after pretreating the cathode material with hydrogenosulfates. The electrochemical characterization in molten LiCl-KCl of the other pretreated cathodes NCA and NMC should be continued in the future as the next step. Then, the whole Li-ion battery cathodes (cathode + current collector + binder) behavior in the salt could be tested. Furthermore, testing

Li-ion battery organic compounds (separators and binders) could be another aspect to be explored.

The pretreatment of cathode materials with hydrogenosulfates should be continued in at air atmosphere and at least at 405°C as it shows the best reduction of cobalt. Concerning the electrodes used for the recovery, other material should be tested because gold electrode is attacked during the electrolysis. Testing tungsten electrode in a first place could be one of the alternatives.

In what concerns the recycling of Li-ion battery compounds, new molten mixtures could be explored in the future. The solution for recycling organic and inorganic compounds might not include one molten salt system but at least two molten salts. From this point of view, exploring non miscible mixtures, containing one alkali chlorides phase could be another alternative to explore.

References

(1) Yoo, H. D.; Markevich, E.; Salitra, G.; Sharon, D.; Aurbach, D. On the Challenge of Developing Advanced Technologies for Electrochemical Energy Storage and Conversion. *Mater. Today* **2014**, *17* (3), 110–121. https://doi.org/10.1016/j.mattod.2014.02.014.

(2) Xianlai, Z.; Jinhui, L.; Narendra, S. Recycling of Spent Lithium-Ion Battery: A Critical Review. *Crit. Rev. Environ. Sci. Technol.* **2014**, *44*, 1129–1165. https://doi.org/10.1080/10643389.2013.763578.

(3) Gaines, L.; Richa, K.; Spangenberger, J. Key Issues for Li-Ion Battery Recycling. *MRS Energy Sustain.* **2018**, *5*, 1–14. https://doi.org/10.1557/mre.2018.13.

(4) Nelson, P. A.; Gallagher, K. G.; Bloom, I.; Dees, D. W. *Modeling the Performance and Cost of Lithium-Ion Batteries for Electric-Drive Vehicles,*; Illinois, 2011. https://doi.org/10.2172/1027714.

(5) McKinsey & Company. *Lithium and Cobalt- a Tale of Two Commodities*; 2018.

(6) Avicenne Energy. *Battery Market Development for Consumer Electronics, Automotive, and Industrial : Materials Requirements and Trends*; 2015.

(7) Berckmans, G.; Messagie, M.; Smekens, J.; Omar, N.; Vanhaverbeke, L.; Mierlo, J. *Cost Projection of State of the Art Lithium-Ion Batteries for Electric Vehicles up to 2030*; 2017; Vol. 10. https://doi.org/10.3390/en10091314.

(8) Gaines, L.; Sullivan, J.; Burnham, A. *Life-Cycle Analysis for Lithium-Ion Battery Production and Recycling*; 2011.

(9) Nitta, N.; Wu, F.; Lee, J. T.; Yushin, G. Li-Ion Battery Materials: Present and Future. *J. Mater. today* **2015**, *18*, 252–264.

(10) Freitas, M. B. J. G.; Garcia, E. M. Electrochemical Recycling of Cobalt from Cathodes of Spent Lithium-Ion Batteries. *J. Power Sources* **2007**, *171* (2), 953–959. https://doi.org/10.1016/j.jpowsour.2007.07.002.

(11) Natarajan, S.; Aravindan, V. Recycling Strategies for Spent Li-Ion Battery Mixed Cathodes. *ACS Energy Lett.* **2018**, *3* (9), 2101–2103. https://doi.org/10.1021/acsenergylett.8b01233.

(12) ALBERMARLE. *Global Lithium Market Outlook*; 2016.

(13) Avicenne Energy. *Lithium-Ion Battery Raw Material Supply and Demand 2017-2025*; 2018.

(14) Statista. Countries with the largest Nickel reserves Worldwide in 2017, by country (in million metric tons) https://www.statista.com/statistics/273634/nickel-reserves-worldwide-by-country/.

(15) Statista. Countries with the largest Cobalt reserves Worldwide in 2017, by country (in metric tons) https://www.statista.com/statistics/264930/global-cobalt-reserves/.

(16) Statista. Countries with the largest Lithium reserves worldwide in 2017 (in metric tons) https://www.statista.com/statistics/268790/countries-with-the-largest-lithium-reserves-worldwide/%0A.

(17) European Commission. *Methodology for Establishing the EU List of Critical Raw Materials*. https://doi.org/10.2873/769526.

(18) European Commission. *Report on Critical Raw Materials and the Circular Economy*; 2018. https://doi.org/10.1097/PPO.0b013e3181b9c5d5.

(19) U.S. Department of the Interior. Draft List of 35 Minerals Deemed Critical to U.S. National Security and the Economy https://www.doi.gov/pressreleases/interior-seeks-public-

comment-draft-list-35-minerals-deemed-critical-us-national.

(20) Lubaba, C.; Banza, N.; Nawrot, T. S.; Al., E. High Human Exposure to Cobalt and Other Metals in Katanga, a Mining Area of the Democratic Republic of Congo. *Environ. Res.* **2009**, *109* (6), 745–752. https://doi.org/10.1016/j.envres.2009.04.012.

(21) Petroff, A. Carmakers and big tech struggle to keep batteries free from child labor http://money.cnn.com/2018/05/01/technology/cobalt-congo-child-labor-car-smartphone-batteries/index.html.

(22) Kim, J. H.; Gibbs, J.; Howe, P. D.; Wood, M. Concise International Chemical Assessment Document 69: Cobalt and Inorganic Cobalt Compounds. *World Heal. Organ.* **2006**, 1–93.

(23) Bonhoure, J.; Mahy, G.; Lange, B.; Colinet, G.; Séleck, M.; Shutcha, M.; Faucon, M.-P.; Decrée, S.; Pourret, O. Assessment of Soil Metal Distribution and Environmental Impact of Mining in Katanga (Democratic Republic of Congo). *Appl. Geochemistry* **2016**, *64*, 43–55. https://doi.org/10.1016/j.apgeochem.2015.07.012.

(24) Chemical properties of cobalt - Health effects of cobalt - Environmental effects of cobalt http://www.lenntech.com/periodic/elements/co.htm.

(25) Cobalt price evolution https://www.lme.com/Metals/Minor-metals/Cobalt. Consulted on January 2019.

(26) Avicenne Energy. *The Rechargeable Battery Market and Main Trends 2012-2025*; 2017.

(27) Gaines, L. To Recycle, or Not to Recycle, That Is the Question: Insights from Life-Cycle Analysis. *MRS Bull.* **2012**, *37* (4), 333–338. https://doi.org/10.1557/mrs.2012.40.

(28) Kong, L.; Li, C.; Jiang, J.; Pecht, M. G. Li-Ion Battery Fire Hazards and Safety Strategies. *Energies* **2018**, *11* (9), 1–11. https://doi.org/10.3390/en11092191.

(29) Tanong, K.; Coudert, L.; Mercier, G.; Blais, J. F. Recovery of Metals from a Mixture of Various Spent Batteries by a Hydrometallurgical Process. *J. Environ. Manage.* **2016**, *181*, 95–107. https://doi.org/10.1016/j.jenvman.2016.05.084.

(30) Chagnes, A.; Pospiech, B. A Brief Review on Hydrometallurgical Technologies for Recycling Spent Lithium-Ion Batteries. *J. Chem. Technol. Biotechnol.* **2013**, *88* (7), 1191–1199. https://doi.org/10.1002/jctb.4053.

(31) Kang, J.; Senanayake, G.; Sohn, J.; Shin, S. M. Recovery of Cobalt Sulfate from Spent Lithium Ion Batteries by Reductive Leaching and Solvent Extraction with Cyanex 272. *Hydrometallurgy* **2010**, *100* (3–4), 168–171. https://doi.org/10.1016/j.hydromet.2009.10.010.

(32) Bernades, A. M.; Espinosa, D. C. R.; Ténorio, J. Recycling of Batteries: A Review of Current Processes and Technologies. *J. Power Sources* **2004**, *130*, 291–298.

(33) Sun, F.; Liu, J.; Li, L.; Chen, R.; Wu, F. Preparation of LiCoO2 Films from Spent Lithium-Ion Batteries by a Combined Recycling Process. *Hydrometallurgy* **2011**, *108* (3–4), 220–225. https://doi.org/10.1016/j.hydromet.2011.04.013.

(34) Schaeffer, N.; Gras, M.; Passos, H.; Mogilireddy, V.; Mendonça, C.; Pereira, E.; Chainet, E.; Billard, I.; Coutinho, J.; Papaiconomou, N. Synergistic Aqueous Biphasic Systems: A New Paradigm for the "One-Pot" Hydrometallurgical Recovery of Critical Metals. *ACS Sustain. Chem. Eng.* **2018**, 1–33. https://doi.org/10.1021/acssuschemeng.8b05754.

(35) Gras, M.; Papaiconomou, N.; Schaeffer, N.; Chainet, E.; Tedjar, F.; Coutinho, J.; Billard, I. Ionic-Liquid-Based Acidic Aqueous Biphasic Systems for Simultaneous Leaching and Extraction of Metallic Ions. *Angew. Chemie - Int. Ed.* **2018**, *57* (6), 1563–1566. https://doi.org/10.1002/anie.201711068.

(36) Chen, X.; Ma, H.; Luo, C.; Zhou, T. Recovery of Valuable Metals from Waste Cathode

Materials of Spent Lithium-Ion Batteries Using Mild Phosphoric Acid. *J. Hazard. Mater.* **2017**, *326*, 77–86. https://doi.org/10.1016/j.jhazmat.2016.12.021.

(37) Zeng, X.; Li, J.; Shen, B. Novel Approach to Recover Cobalt and Lithium from Spent Lithium-Ion Battery Using Oxalic Acid. *J. Hazard. Mater.* **2015**, *295* (2015), 112–118. https://doi.org/10.1016/j.jhazmat.2015.02.064.

(38) Li, L.; Ge, J.; Wu, F.; Chen, R.; Chen, S.; Wu, B. Recovery of Cobalt and Lithium from Spent Lithium Ion Batteries Using Organic Citric Acid as Leachant. *J. Hazard. Mater.* **2010**, *176* (1–3), 288–293. https://doi.org/10.1016/j.jhazmat.2009.11.026.

(39) Zeng, G.; Deng, X.; Luo, S.; Luo, X.; Zou, J. A Copper-Catalyzed Bioleaching Process for Enhancement of Cobalt Dissolution from Spent Lithium-Ion Batteries. *J. Hazard. Mater.* **2012**, *199–200*, 164–169. https://doi.org/10.1016/j.jhazmat.2011.10.063.

(40) Chen, S.; Wang, J.; Xin, B.; Huang, Q.; Niu, Z.; Yang, Y. Metallic Ions Catalysis for Improving Bioleaching Yield of Zn and Mn from Spent Zn-Mn Batteries at High Pulp Density of 10%. *J. Hazard. Mater.* **2015**, *298*, 170–177. https://doi.org/10.1016/j.jhazmat.2015.05.038.

(41) Gratz, E.; Sa, Q.; Apelian, D.; Wang, Y. A Closed Loop Process for Recycling Spent Lithium Ion Batteries. *J. Power Sources* **2014**, *262*, 255–262. https://doi.org/10.1016/j.jpowsour.2014.03.126.

(42) Heelan, J.; Gratz, E.; Zheng, Z.; Wang, Q.; Chen, M.; Apelian, D.; Wang, Y. Current and Prospective Li-Ion Battery Recycling and Recovery Processes. *Jom* **2016**, *68* (10), 2632–2638. https://doi.org/10.1007/s11837-016-1994-y.

(43) Shi, Y.; Chen, G.; Chen, Z. Effective Regeneration of LiCoO2 from Spent Lithium-Ion Batteries: A Direct Approach towards High-Performance Active Particles. *Green Chem.* **2018**, *20* (4), 851–862. https://doi.org/10.1039/c7gc02831h.

(44) Zhu, S.; Qin, Y.; Zhang, J. Renovation of Lithium Cobalt Oxide from Spent Lithium Ion Batteries by an Aqueous Pulsed Discharge Plasma. *Int. J. Electrochem. Sci.* **2016**, *11* (7), 6403–6411. https://doi.org/10.20964/2016.07.103.

(45) Zhang, Z.; He, W.; Li, G.; Xia, J.; Hu, H.; Huang, J. Ultrasound-Assisted Hydrothermal Renovation of LiCoO2 from the Cathode of Spent Lithium-Ion Batteries. *Int. J. Electrochem. Sci.* **2014**, *9* (7), 3691–3700.

(46) Nie, H.; Xu, L.; Song, D.; Song, J.; Shi, X.; Wang, X.; Zhang, L.; Yuan, Z. LiCoO2: Recycling from Spent Batteries and Regeneration with Solid State Synthesis. **2014**, 1–5. https://doi.org/10.1039/b000000x.

(47) Circular Energy Storage. The lithium-ion battery end-of-life market 2018-2025 https://circularenergystorage.com/buy/report-the-lithium-ion-battery-end-of-life-market-2018-2025 (accessed May 14, 2019).

(48) SAE International. *SAE Battery Recycling Committee : What Is the Mission*.

(49) Battery Association of Japan. Recycling Portable Rechargeable Batteries http://www.baj.or.jp/e/recycle/recycle04.html.

(50) Cassir, M.; Belhomme, C. Technological Applications of Molten Salts: The Case of the Molten Carbonate Fuel Cell. *Plasmas Ions* **1999**, *2* (1), 3–15. https://doi.org/10.1016/S1288-3255(99)80006-9.

(51) Rollet, A.-L.; Salanne, M. Studies of the Local Structures of Molten Metal Halides. *Annu. reports Prog. Chem. Sect. C* **2011**, *107*, 88–123.

(52) Volkov, S. V. Chemical Reactions in Molten Salts and Their Classification. *Chem. Soc. Rev.* **1990**, *19*, 21–28. https://doi.org/10.1039/CS9901900021.

(53) Lantelme, F.; Groult, H. *Molten Salts Chemistry from Lab to Applications*, First edit.; Elsevier: Burlington, 2013.

(54) Janz, G. *Molten Salts Handbook*; A. Press: New York, 1967.

(55) Yao, Z.; Li, J.; Zhao, X. Molten Salt Oxidation: A Versatile and Promising Technology for the Destruction of Organic-Containing Wastes. *Chemosphere* **2011**, *84* (9), 1167–1174. https://doi.org/10.1016/j.chemosphere.2011.05.061.

(56) Lovering, D. *Molten Salt Technology*; Springer: Boston, 2014.

(57) Perkin, F. M. *The Discovery of the Alkali Metals by Humphry Davy : The Bearing of the Discovery upon Industry*; 1907.

(58) Runge, J. M. *The Metallurgy of Anodizing Aluminum: Connecting Science to Practice*; Springer US, 2018.

(59) Beck, T. R. Hall and Héroult and the Discovery of Aluminum Electrolysis. *Electrochem. Soc. Interface* **2014**, *23* (2), 36–37. https://doi.org/10.1149/2.F01142if.

(60) MacPherson, H. G. The Molten Salt Reactor Adventure. *Nucl. Sci. Eng.* **1985**, *90* (4), 374–380. https://doi.org/10.13182/NSE90-374.

(61) Le Van, K.; Groult, H.; Lantelme, F.; Dubois, M.; Avignant, D.; Tressaud, A.; Komaba, S.; Kumagai, N.; Sigrist, S. Electrochemical Formation of Carbon Nano-Powders with Various Porosities in Molten Alkali Carbonates. *Electrochim. Acta* **2009**, *54* (19), 4566–4573. https://doi.org/10.1016/j.electacta.2009.03.049.

(62) Massot, L.; Chamelot, P.; Bouyer, F.; Taxil, P. Electrodeposition of Carbon Films from Molten Alkaline Fluoride Media. *Electrochim. Acta* **2002**, *47* (12), 1949–1957. https://doi.org/10.1016/S0013-4686(02)00047-6.

(63) Massot, L.; Chamelot, P.; Bouyer, F.; Taxil, P. Studies of Carbon Nucleation Phenomena in Molten Alkaline Fluoride Media. *Electrochim. Acta* **2003**, *48* (5), 465–471. https://doi.org/10.1016/S0013-4686(02)00646-1.

(64) Devilliers, D.; Teisseyre, B.; Vogler, M.; Chemla, M. Polished Carbon Electrodes for Improving the Fluorine Production Process. *J. Appl. Electrochem.* **1990**, *20* (1), 91–96. https://doi.org/10.1007/BF01012476.

(65) Groult, H.; Kaplan, B.; Lantelme, F.; Komaba, S.; Kumagai, N.; Yashiro, H.; Nakajima, T.; Simon, B.; Barhoun, A. Preparation of Carbon Nanoparticles from Electrolysis of Molten Carbonates and Use as Anode Materials in Lithium-Ion Batteries. *Solid State Ionics* **2006**, *177* (9–10), 869–875. https://doi.org/10.1016/j.ssi.2006.01.051.

(66) Wulandari, W.; Brooks, G.; Rhamdhani, M.; Monaghan, B. Magnesium: Current and Alternative Production Routes. In *Chemeca 2010: Australasian Conference on Chemical Engineering*; 2010. https://doi.org/10.1002/hrdq.1020.

(67) Dandapani, K. S.; Srinivasan, L. K. Production of Magnesium in 30 kA Cells. *Electrometall. Thermics* **1987**, *3* (2), 127–129.

(68) Senderoff, S.; Mellors, G. W. Coherent Coatings of Refractory Metals. *Science (80-.).* **1966**, *153* (3743), 1475–1481.

(69) Taxil, P.; Chamelot, P.; Massot, L.; Hamel, C. Electrodeposition of Alloys or Compounds in Molten Salts and Applications. *J. Min. Metall.* **2003**, *39* ((1-2)B), 177–200. https://doi.org/10.2298/JMMB0302177T.

(70) Sethi, R. S. Electrocoating from Molten Salts. *J. Appl. Electrochem.* **1979**, *9*, 411–426.

(71) Taxil, P. Formation Des Alliages Nickel-Tantale Par Voie Électrochimique. *J. Less-Common Met.* **1985**, *113*, 89–101.

(72) Galopin, M.; Daniel, J. S. Molten Salts in Metal Treatment: Present Uses and Future Trends. *Electrodepos. Surf. Treat.* **1975**, *3*, 1–31.

(73) Sadoway, D. R. The Electrochemical Processing of Refractory Metals. *J. Miner. Met. Mater. Soc.* **1991**, *overview*, 15–19.

(74) Mansfeld, F.; Pérez, F. J. Surface Modification of Aluminum Alloys in Molten Salts Containing CeCl3. *Thin Solid Films* **1995**, *270* (1–2), 417–421. https://doi.org/10.1016/0040-6090(95)06932-1.

(75) Forsberg, C. W.; Peterson, P. F.; Pickard, P. S. Molten-Salt-Cooled Advanced High-Temperature Reactor for Production of Hydrogen and Electricity. *Nucl. Technol.* **2003**, *144* (3), 289–302. https://doi.org/10.13182/NT03-1.

(76) Haubenreich, P. N.; Engel, J. R. Experience with the Molten-Salt Reactor Experiment. *Nucl. Appl. Technol.* **1970**, *8* (2), 118–136. https://doi.org/10.13182/NT8-2-118.

(77) Serp, J.; Allibert, M.; Beneš, O.; Delpech, S.; Al., E. The Molten Salt Reactor (MSR) in Generation IV: Overview and Perspectives. *Prog. Nucl. Energy* **2014**, *77*, 308–319. https://doi.org/10.1016/j.pnucene.2014.02.014.

(78) Mendoza Blanco, L. Revêtements Protecteurs à Base d'oxyde de Cobalt , de Titane Ou de Cérium Pour La Cathode de Nickel Des Piles à Combustible à Carbonates Fondus, University Paris VI, 2003.

(79) Sudworth, J. L. The Sodium / Nickel Chloride (ZEBRA) Battery. *J. Power Sources* **2001**, *100*, 149–163.

(80) Alam, M.; Kamath, S. Cyanide Destruction in Molten Carbonate Bath: Melt and Gas Analyses. *Environ. Sci Technol.* **1998**, *32*, 3986–3992. https://doi.org/10.1021/es9710969.

(81) Wartena, R.; Winnick, J.; Pfromm, P. H. Recycling Kraft Pulping Chemicals with Molten Salt Electrolysis. *J. Electrochem. Soc.* **2002**, *149*, D125–D131. https://doi.org/10.1149/1.1495907.

(82) Flandinet, L.; Tedjar, F.; Ghetta, V.; Fouletier, J. Metals Recovering from Waste Printed Circuit Boards (WPCBs) Using Molten Salts. *J. Hazard. Mater.* **2012**, *213–214*, 485–490. https://doi.org/10.1016/j.jhazmat.2012.02.037.

(83) Organisation for economic co-operation and development. *Pyrochemical Separations in Nuclear Applications*; 2014.

(84) Laider, J. J.; Battles, J. E.; Miller, W. E.; Ackerman, J. P.; E.L., C. Development of Pyroprocessing Technology. *Prog. Nucl. Energy* **1997**, *31* (1/2), 131–140. https://doi.org/10.1038/nsmb0204-117.

(85) Nourry, C.; Souček, P.; Massot, L.; Malmbeck, R.; Chamelot, P.; Glatz, J. P. Electrochemistry of Uranium in Molten LiF-CaF2. *J. Nucl. Mater.* **2012**, *430* (1–3), 58–63. https://doi.org/10.1016/j.jnucmat.2012.06.028.

(86) Griffiths, T. R.; Volkovich, V. A.; Yakimov, S. M.; May, I.; Sharrad, C. A.; Charnock, J. M. Reprocessing Spent Nuclear Fuel Using Molten Carbonates and Subsequent Precipitation of Rare Earth Fission Products Using Phosphate. *J. Alloys Compd.* **2006**, *418* (1–2), 116–121. https://doi.org/10.1016/j.jallcom.2005.10.060.

(87) Griffiths, T. R.; Volkovich, V. A New Technology for the Nuclear Industry for the Complete and Continuous Pyrochemical Reprocessing of Spent Nuclear Fuel: Catalyst Enhanced Molten Salt Oxidation. *Nucl. Technol.* **2008**, *163*, 382–400.

(88) Nourry, C.; Massot, L.; Chamelot, P.; Taxil, P. Neodymium and Gadolinium Extraction from Molten Fluorides by Reduction on a Reactive Electrode. *J. Appl. Electrochem.* **2009**, *39* (12), 2359–2367. https://doi.org/10.1007/s10800-009-9922-2.

(89) Gale, R.; Lovering, D. *Molten Salt Techniques*, first edit.; Springer Science+ Business: New York, 1984.

(90) Moutiers, G. Propriétés Electrochimiques Dans Les Carbonates Alcalins Fondus, Université Paris VI, 1992.

(91) Trémillon, B. *Electrochimie Analytique et Réactions En Solution*; Masson S.A: Paris, 1993.

(92) Chery, D. Approche Prévisionnelle de La Valorisation Électrochimique Du CO 2 Dans Les Carbonates Fondus, Université Pierre et Marie Curie, 2015.

(93) Lair, V.; Ringuedé, A.; Cassir, M.; Albin, V. Theoretical Predictions vs. Experimental Measurements of the Electrical Conductivity of Molten Li2CO3-K2CO3 Modified by Additives. *Int. J. Hydrogen Energy* **2012**, *37*, 19357–19364. https://doi.org/10.1016/j.ijhydene.2011.09.153.

(94) Sridharan, K.; Allen, T.; Anderson, M.; Simpson, M.; Olson, L.; Mohammadian, M.; Martin, S. *Thermal Properties of LiCl-KCl Molten Salt for Nuclear Waste Separation*; 2012.

(95) Gomez-Vidal, J.; Tirawat, R. Corrosion of Alloys in a Chloride Molten Salt (NaCl-LiCl) for Solar Thermal Technologies. *Sol. Energy Mater. Sol. Cells* **2016**, *157*, 234–244. https://doi.org/10.1016/j.solmat.2016.05.052.

(96) Ghetta, V.; Fouletier, J.; Taxil, P. *Sels Fondus à Haute Température*; presse polytechniques et universitaires romandes: Lausanne, 2009.

(97) Chen, G.; Fray, D. J.; Farthing, T. Direct Electrochemical Reduction of Titanium Dioxide to Titanium in Molten Calcium Chloride. *Nature* **2000**, *407*, 361–364. https://doi.org/10.1177/019459988209000413.

(98) Baba, M.; Ono, Y.; Suzuki, R. O. Tantalum and Niobium Powder Preparation from Their Oxides by Calciothermic Reduction in the Molten CaCl2. *J. Phys. Chem. Solids* **2005**, *66* (2–4), 466–470. https://doi.org/10.1016/j.jpcs.2004.06.042.

(99) Claux, B.; Serp, J.; Fouletier, J. Electrochemical Reduction of Cerium Oxide into Metal. *Electrochim. Acta* **2011**, *56* (7), 2771–2780. https://doi.org/10.1016/j.electacta.2010.12.040.

(100) Ono, K.; Suzuki, R. O. A New Concept for Producing Ti Sponge: Calciothermic Reduction. *J. Miner.* **2002**, *54* (2), 59–61. https://doi.org/10.1007/BF02701078.

(101) Fontaine, A. Spectroscopie d'absorption X (EXAFS et XANES) Application Du Rayonnement Synchrotron. *Techniques de l'ingénieur*. 2014.

(102) Boon K, T. *EXAFS: Basic Principles and Data Analysis*; Springer: Berlin, 1985.

(103) Koningsberger, D. C.; Prins, R. *X-Ray Absorption : Principles, Applications, Techniques of EXAFS, SEXAFS, and XANES*; Wiley: New York, 1988.

(104) Ellis, P. J. Structural Studies of Metalloproteins Using X-Ray Absorption Spectroscopy and X-Ray Diffraction, University of Sydney, 1995.

(105) Mikkelsen, J. C.; Boyce, J. B.; Allen, R. Sample Cell for EXAFS Measurements on Molten Materials at Elevated Temperatures. *Rev. Sci. Instrum.* **1980**, *51* (3), 388–389. https://doi.org/10.1063/1.1136190.

(106) Filipponi, A.; Di Cicco, A. Development of an Oven for X-Ray Absorption Measurements under Extremely High Temperature Conditions. *Nucl. Instruments Methods Phys. Res. B* **1994**, *93*, 302–310.

(107) Di Cicco, A.; Berrettoni, M.; Marassi, R.; Tossici, R.; Filipponi, A. X-Ray Absorption Study on Solid and Molten Alkali Halides. *Electrochem. Soc.* **1994**, *94–13*, 77–82. https://doi.org/10.1149/199413.0077PV.

(108) Launay, X.; Gautier, N.; Ruffler, D.; Landron, C.; Coutures, J.; Bazin, D. Etude sans Contact

Par EXAFS Haute Temperature Aux Seuils K de Ga et Y. *Comptes Rendus l'Académie des Sci. - Ser. IIB - Mech.* **1997**, *012*, 527–535.

(109) Okamoto, Y.; Akabori, M.; Motohashi, H.; Itoh, A.; Ogawa, T. High-Temperature XAFS Measurement of Molten Salt Systems. *Nucl. Instruments Methods Phys. Res. A* **2002**, *487*, 605–611.

(110) Rollet, A. L.; Bessada, C.; Auger, Y.; Melin, P.; Gailhanou, M.; Thiaudiere, D. A New Cell for High Temperature EXAFS Measurements in Molten Rare Earth Fluorides. *Nucl. Instruments Methods Phys. Res. Sect. B Beam Interact. with Mater. Atoms* **2004**. https://doi.org/10.1016/j.nimb.2004.06.034.

(111) Briois, V.; La Fontaine, C.; Belin, S.; Barthe, L.; Moreno, T.; Pinty, V.; Carcy, A.; Girardot, R.; Fonda, E. ROCK: The New Quick-EXAFS Beamline at SOLEIL. *J. Phys. Conf. Ser.* **2016**, *712* (1). https://doi.org/10.1088/1742-6596/712/1/012149.

(112) Capehart, T. W.; Herbst, J. F.; Mishra, R. K.; Pinkerton, F. E. X-Ray Absorption Edge Shifts in Rare-Earth - Transition-Metal Compounds. *Phys. Rev. B* **1995**, *52* (11), 7907–7915.

(113) Krylova, G.; Giovanetti, L. J.; Requejo, F. G.; Dimitrijevic, N. M.; Prakapenka, A.; Shevchenko, E. V. Study of Nucleation and Growth Mechanism of the Metallic Nanodumbbells. *J. Am. Chem. Soc.* **2012**, *134* (9), 4384–4392. https://doi.org/10.1021/ja211459p.

(114) Huck-Iriart, C.; Soler, L.; Casanovas, A.; Marini, C.; Prat, J.; Llorca, J.; Escudero, C. Unraveling the Chemical State of Cobalt in Co-Based Catalysts during Ethanol Steam Reforming: An in Situ Study by Near Ambient Pressure XPS and XANES. *ACS Catal.* **2018**, *8* (10), 9625–9636. https://doi.org/10.1021/acscatal.8b02666.

(115) Dos Santos, D. M.; Breda, M. M. High-temperature Reduction of Iron Oxides by Solid Carbon or Carbon Dissolved in Liquid Iron–Carbon Alloy. *Scand. J. Metall.* **2004**, *33* (4), 229–235. https://doi.org/10.1111/j.1600-0692.2004.00689.x.

(116) Pauvert, O.; Zanghi, D.; Bessada, C.; Salanne, M.; Simon, C.; Reguer, S.; Thiaudière, D.; Okamoto, Y.; Matsuura, H. Ion Specific Effects on the Structure of Molten AF-ZrF4 Systems (A+ = Li+, Na+, and K+). *J. Phys. Chem. B* **2011**, *115* (29), 9160–9167. https://doi.org/10.1021/jp203137h.

(117) Mendoza, L.; Baddour-Hadjean, R.; Cassir, M.; Pereira-Ramos, J. P. Raman Evidence of the Formation of LT-LiCoO 2 Thin Layers on NiO in Molten Carbonate at 650°C. *Appl. Surf. Sci.* **2004**, *225* (1–4), 356–361. https://doi.org/10.1016/j.apsusc.2003.10.026.

(118) Mendoza, L.; Ringuedé, A.; Cassir, M.; Galtayries, A. II. Structural, Morphological, Chemical and Electrochemical Analysis of Nickel Covered by Electrochemically Deposited Co3O4 in Molten Li2CO3-Na2CO3 at 650 °C. *J. Electroanal. Chem.* **2005**, *576* (1), 147–160. https://doi.org/10.1016/j.jelechem.2004.09.033.

(119) Escudero, M. J.; Ringuedé, A.; Cassir, M.; González-Ayuso, T.; Daza, L. Porous Nickel MCFC Cathode Coated by Potentiostatically Deposited Cobalt Oxide. III. Electrochemical Behaviour in Molten Carbonate. *J. Power Sources* **2007**, *160*, 775–781. https://doi.org/10.1016/j.jpowsour.2007.06.013.

(120) Veldhuis, J. B. J.; Eckes, F. C.; Plomb, L. The Dissolution Properties of LiCoO2 in Molten 62:38 Mol% Li:K Carbonate. **1992**, *139* (1), L6.

(121) Ota, K.; Takeishi, Y.; Shibata, S.; Yoshitake, H.; Kamiya, N. Solubility of Cobalt Oxide in Molten Carbonate. *J. Electrochem. Soc.* **1995**, *142*, 3322–3326. https://doi.org/10.1149/1.2049982.

(122) Ward, A. T.; Janz, G. J. Molten Carbonate Electrolytes: Electrical Conductance, Density and Surface Tension of Binary and Ternary Mixtures. *Electrochim. Acta* **1965**, *10* (8), 849–857.

https://doi.org/10.1016/0013-4686(65)80048-2.

(123) Pelton, A. D.; Bale, C. W.; Lin, P. L. Calculation of Phase Diagrams and Thermodynamic Properties of 14 Additives and Reciprocal Ternary Systems Containing Li2CO3 , Na2CO3 , K2CO3 , Li2SO4 , Na2SO4 , K2SO4 , LiOH, NaOH, and KOH. *Can. J. Chem.* **1984**, *62*, 457–474. https://doi.org/10.1139/v84-078.

(124) Chen, C.; Tran, T.; Olivares, R.; Wright, S.; Sun, S. Coupled Experimental Study and Thermodynamic Modeling of Melting Point and Thermal Stability of Li2CO3-Na2CO3-K2CO3 Based Salts. *J. Sol. Energy Eng.* **2014**, *136* (3), 031017. https://doi.org/10.1115/1.4027264.

(125) Sato, H.; Nishina, T.; Yamada, K.; Uchida, I.; Tomczyk, P. Oxide Electrodes in Molten Carbonates Part 2. Electrochemical Behaviour of Cobalt in Molten Li + K and Na + K Carbonate Eutectics. *J. Electroanal. Chem.* **2003**, *391* (1–2), 133–139. https://doi.org/10.1016/0022-0728(95)03943-b.

(126) Yang, B. Y.; Kim, K. Y. Electrochemical Study of the Oxidation Behaviors of Ni and Ni-Co Alloy Electrodes in Molten Li + K Carbonate Eutectic. *Electrochim. Acta* **1998**, *43* (21–22), 3343–3352. https://doi.org/10.1016/S0013-4686(98)00003-6.

(127) Yang, B. Y.; Kim, K. Y. The Oxidation Behavior of Ni-50%Co Alloy Electrode in Molten Li+K Carbonate Eutectic. *Electrochim. Acta* **1999**, *44* (13), 2227–2234. https://doi.org/10.1016/S0013-4686(98)00333-8.

(128) Kim, S. W.; Uematsu, K.; Toda, K.; Sato, M. Viscosity Analysis of Alkali Metal Carbonate Molten Salts at High Temperature. *J. Ceram. Soc. Japan* **2015**, *123* (1437), 355–358. https://doi.org/10.2109/jcersj2.123.355.

(129) Shannon, R. D. Revised Effective Ionic Radii and Systematic Studies of Interatomic Distances in Halides and Chaleogenides. *Acta Crystallogr.* **1976**, *32*, 751–767.

(130) Kirillov, S. A.; Pavlatou, E. A.; Papatheodorou, G. N. Instantaneous Collision Complexes in Molten Alkali Halides: Picosecond Dynamics from Low-Frequency Raman Data. *J. Chem. Phys.* **2002**, *116* (21), 9341–9351. https://doi.org/10.1063/1.1473810.

(131) Bard, A. J.; Faulkner, L. R. Electrochimie Principes, Méthodes et Applications; Masson: Paris, 1983; pp 239–271.

(132) Claux, B. Etude de La Réduction Électrochimique d'Oxydes d'Actinides En Milieu Sels Fondus, 2012.

(133) Fabre, S. Comportement de Métaux et Alliages En Milieux Fluorures Fondus, Université Toulouse III-Paul Sabatier, 2009.

(134) Fukui, T.; Okawa, H.; Tsunooka, T. Solubility and Deposition of LiCoO2 in a Molten Carbonate. *J. Power Sources* **1998**, *71* (1–2), 239–243. https://doi.org/10.1016/S0378-7753(97)02729-8.

(135) Plambeck, J. A. *Encyclopedia of Electrochemistry of the Elements*; Bard, A. J., Ed.; Marcel Dekker.Inc: New York, 1976; Vol. X.

(136) Delarue, G. Propriétés Chimiques Dans l'eutectique LiCl-KCl Fondu. *J. Electroanal. Chem.* **1960**, *1* (4), 285–300. https://doi.org/10.1016/0022-0728(60)85029-2.

(137) Behl, W. K. Linear Sweep Voltammetry of Ni(II), Co(II), Cd(II), and Pb(II) at Glassy Carbon Electrodes in Molten Lithium Chloride-Potassium Chloride Eutectic. *J. Electrochem. Soc.* **1971**, *118* (6), 889–894. https://doi.org/10.1149/1.2408212.

(138) Lantelme, F.; Hanselin, J.-P.; Chemla, M. Electrocrystallisation and Diffusion Process in the Electroreduction of Cu+ and Co2+ Ions in Fused LiCl+KCl. *J. Electroanal. Chem.* **1979**, *97*, 49–61.

(139) Groult, H.; El Ghallali, H.; Barhoun, A.; Briot, E.; Perrigaud, L.; Hernandorena, S.; Lantelme, F. Preparation of Co-Sn Alloys by Electroreduction of Co(II) and Sn(II) in Molten LiCl-KCl. *Electrochim. Acta* **2010**, *55* (6), 1926–1932. https://doi.org/10.1016/j.electacta.2009.11.010.

(140) Shirai, O.; Nagai, T.; Uehara, A.; Yamana, H. Electrochemical Properties of the Ag+|Ag and Other Reference Electrodes in the LiCl-KCl Eutectic Melts. *J. Alloys Compd.* **2008**, *456* (1–2), 498–502. https://doi.org/10.1016/j.jallcom.2007.02.104.

(141) Pascal, P. *Nouveau Traité de Chimie Minérale*; Masson et Cie: Paris, 1963.

(142) Liu, D. Analyse Des Méthodes à Potentiel et à Courant Imposé Pour Des Réactions Avec Dépôt Métallique Rapides et Lentes - Dépôt d'argent Sur or Dans HNO3 1 M, KNO3 1M et Dans Le Liquide Ionique [EMIM][NTf2] Anhydre Ou Humide, Université Pierre et Marie Curie, 2014.

(143) Rieger, P. H. Electrochemistry; Chapman and Hall: London, 1994; pp 155–158.

(144) H.H.Girault. Electrochimie Physique et Analytique; presse polytechniques et universitaires romandes, 2001; pp 311–350.

(145) Wang, D.; Wen, H.; Chen, H.; Yang, Y.; Liang, H. Chemical Evolution of LiCoO2 and NaHSO4.H2O Mixtures with Different Mixing Ratios during Roasting Process. *Chem. Res. Chinese Univ.* **2016**, *32* (4), 674–677. https://doi.org/10.1007/s40242-016-5490-2.

(146) Wang, D.; Zhang, X.; Chen, H.; Sun, J. Separation of Li and Co from the Active Mass of Spent Li-Ion Batteries by Selective Sulfating Roasting with Sodium Bisulfate and Water Leaching. *Miner. Eng.* **2018**, *126*, 28–35. https://doi.org/10.1016/j.mineng.2018.06.023.

(147) Amietszajew, T.; Sridhar, S.; Bhagat, R. Metal Recovery by Electrodeposition from a Molten Salt Two-Phase Cell System. *J. Electrochem. Soc.* **2016**, *163* (9), D515–D521. https://doi.org/10.1149/2.0991609jes.

List of figures

List of tables